NASA TECHNICAL MEMORANDUM

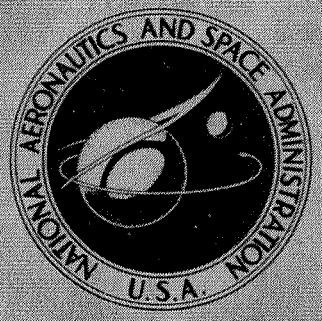

NASA TM X-2310

NASA TM X-2310

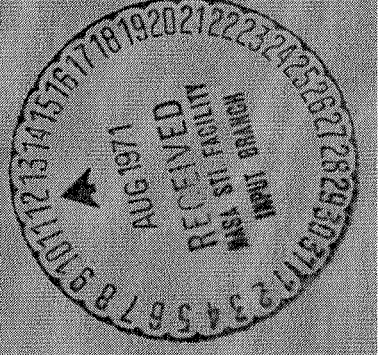

SHEAR-STRESS, EDDY-VISCOSITY, AND MIXING-LENGTH DISTRIBUTIONS IN HYPERSONIC TURBULENT BOUNDARY LAYERS

by Dennis M. Bushnell and Dana J. Morris

Langley Research Center
Hampton, Va. 23365

NATIONAL AERONAUTICS AND SPACE ADMINISTRATION • WASHINGTON, D. C. • AUGUST 1971

1. Report No.	2. Government Accession No.	3. Recipient's Catalog No.
NASA TM X-2310		

4. Title and Subtitle	5. Report Date
SHEAR-STRESS, EDDY-VISCOSITY, AND MIXING-LENGTH DISTRIBUTIONS IN HYPERSONIC TURBULENT BOUNDARY LAYERS	August 1971
	6. Performing Organization Code

7. Author(s)	8. Performing Organization Report No.
Dennis M. Bushnell and Dana J. Morris	L-7731
	10. Work Unit No. 136-13-01-11

9. Performing Organization Name and Address	11. Contract or Grant No.
NASA Langley Research Center Hampton, Va. 23365	
	13. Type of Report and Period Covered
12. Sponsoring Agency Name and Address	Technical Memorandum
National Aeronautics and Space Administration Washington, D.C. 20546	14. Sponsoring Agency Code

15. Supplementary Notes

16. Abstract

A method is developed to obtain shear-stress, eddy-viscosity, and mixing-length distributions from hypersonic turbulent boundary-layer profile data by using the assumption of local similarity. Application of the method to published profile data indicates an increase in the maximum value of mixing length and eddy viscosity as the Reynolds number decreases. The level and trend of this low Reynolds number effect agrees with similar results previously obtained at low speeds when wall conditions are used in the correlating parameter. Examination of the wall-damping effect on the mixing length indicates more validity for evaluating the Van Driest damping scale by using wall conditions than by using local sublayer properties and that the impermeable-wall damping constant may be somewhat greater at hypersonic conditions than the usual low-speed value of 26. In several instances, areas of disagreement occurred between the expected and observed behavior of the data, usually concerning the shape of the published velocity profiles. Indications are that the total-temperature data obtained in hypersonic, low Reynolds number, cold-wall boundary layers may not be suitably corrected for conditions near the wall.

17. Key Words (Suggested by Author(s))	18. Distribution Statement
Eddy viscosity Mixing length Hypersonic or compressible turbulent boundary layer	Unclassified – Unlimited

19. Security Classif. (of this report)	20. Security Classif. (of this page)	21. No. of Pages	22. Price*
Unclassified	Unclassified	72	$3.00

*For sale by the National Technical Information Service, Springfield, Virginia 22151

SHEAR-STRESS, EDDY-VISCOSITY, AND MIXING-LENGTH DISTRIBUTIONS IN HYPERSONIC TURBULENT BOUNDARY LAYERS

By Dennis M. Bushnell and Dana J. Morris
Langley Research Center

SUMMARY

A method is developed to obtain shear-stress, eddy-viscosity, and mixing-length distributions from hypersonic turbulent boundary-layer profile data by using the assumption of local similarity. Application of the method to published profile data indicates an increase in the maximum value of mixing length and eddy viscosity as the Reynolds number decreases. The level and trend of this low Reynolds number effect agree with similar results previously obtained at low speeds when wall conditions are used in the correlating parameter. Examination of the wall-damping effect on the mixing length indicates more validity for evaluating the Van Driest damping scale by using wall conditions than by using local sublayer properties and that the impermeable-wall damping constant may be somewhat greater at hypersonic conditions than the usual low-speed value of 26. In several instances, areas of disagreement occurred between the expected and observed behavior of the data, usually concerning the shape of the published velocity profiles. Indications are that the total-temperature data obtained in hypersonic, low Reynolds number, cold-wall boundary layers may not be suitably corrected for conditions near the wall.

INTRODUCTION

Of the several finite-difference and sophisticated integral methods available (refs. 1 to 11) which compute the development of compressible turbulent boundary layers, all of these methods except that in reference 3 utilize either a mixing-length (refs. 1, 2, 4, and 5) or eddy-viscosity (refs. 6 to 11) model for the turbulence-shear term. Most of the shear-stress models employed in these calculation procedures were developed from data obtained in low-speed flow studies. The application of these low-speed models to compressible boundary layers was investigated in reference 12, where a set of "universal" velocity profiles were derived and used to obtain the turbulent shear-stress distribution from the momentum equation. These results indicated that the low-speed mixing-length models were directly applicable to adiabatic flows up to a Mach number of 5 and that the

eddy-viscosity expression of reference 13 could be used by retaining the incompressible or kinematic definition of displacement thickness.

The validity of these low-speed turbulence-shear models for supersonic turbulent flows at high Reynolds number was established by comparisons of profile calculations with experimental data. (See refs. 1 to 2 and 4 to 11.) Also, work in reference 14 and private communication with the author of that reference indicate that the mixing-length and "Clauser" (ref. 13) eddy-viscosity models in the outer region are not significantly affected by moderate rates of blowing, at least up to a Mach number of 3.5. However, a significant increase in the outer-region eddy-viscosity model was found necessary in order to successfully compute low Reynolds number supersonic turbulent flows. (See ref. 6.) Furthermore, reference 6 points out that as Mach number increases, the low Reynolds number type of turbulent flows is more often encountered because of the decrease in density and increase in viscosity close to the wall. A similar type of low Reynolds number effect (increasing eddy viscosity with decreasing Reynolds number) was found for low speeds in references 15 and 16. In addition to this low Reynolds number effect, both low and supersonic speed boundary layers show an effect of nonequilibrium pressure gradients and high rates of blowing upon the turbulence models. This latter effect was pointed out in reference 1, which shows a correlation of the effect of blowing and nonequilibrium pressure gradient on the mixing-length model as a function of the incompressible or kinematic form factor. The data of reference 17 indicate the existence of a nonequilibrium pressure-gradient effect upon the Clauser eddy-viscosity model. For supersonic flows, no satisfactory turbulence-shear model exists which includes the combined effects of low Reynolds number and nonequilibrium pressure gradient.

Since generally good results were obtained by using essentially incompressible turbulent shear-stress models at supersonic conditions, several calculations for hypersonic conditions have been compared with experimental data. (See refs. 1, 4, 5, 7, 10, 11, 18, 19, 20, and 21.) These comparisons indicate that the "incompressible" turbulent shear-stress models usually give reasonable agreement at hypersonic conditions for surface phenomena such as heat transfer. However, there are disagreements with the actual profile shapes and thicknesses. (See refs. 1, 18, 19, and 21.)

An alternate method of validating a turbulent shear model (beside comparing computed and experimental profiles) uses the experimental profile data or correlations thereof in the momentum equation and extracts the turbulent shear-stress variation. This shear-stress variation in conjunction with the various turbulent-shear-model definitions gives the "constants" for a particular model. The shear-stress distribution has been obtained by using this method (usually employing velocity-profile correlations) for compressible speeds up to a Mach number of 7. (See refs. 12, 14, 22, 23, and 24.) The basic method of obtaining mixing-length distributions in this manner was validated for low-speed flows

in reference 25. The present work reports on a method to obtain shear-stress, eddy-viscosity, and mixing-length distributions directly from hypersonic profile data (Mach numbers from 5 to 20) by using the assumption of local similarity and compares results by this method with values and trends of turbulent shear-stress models successfully employed at low and supersonic speeds.

SYMBOLS

Values are given in both SI and U.S. Customary Units. The measurements and calculations were made in U.S. Customary Units.

A	damping scale, $\frac{A^+\mu}{\rho u_\tau}$
A^+	Van Driest damping constant (see eq. (9))
C_f	skin-friction coefficient, $\frac{\tau_w}{\frac{1}{2}\rho_e u_e^2}$
K	"Prandtl wall slope," slope of mixing-length variation with y in region $\frac{y}{\delta} \approx 0.1$ and passing through the origin
l	mixing length
M	Mach number
N	exponent of power-law velocity profile, $\frac{u}{u_e} = \left(\frac{y}{\delta}\right)^{1/N}$
n	integer
p	pressure
R	Reynolds number
R_{sl}	Reynolds number based on sublayer thickness, $\frac{\rho_w u_e y_{sl}}{\mu_w}$
R_θ	Reynolds number based on momentum thickness, $\frac{\rho_e u_e \theta}{\mu_e}$
r	radius
T	temperature

u,v longitudinal and normal velocity component, respectively

u_τ friction velocity, $\sqrt{\frac{\tau}{\rho}}$

u' velocity fluctuation

x,y longitudinal and normal Cartesian coordinate, respectively

y_{sl} sublayer thickness, $\frac{10\mu_w}{u_{\tau,w}\rho_w}$

$y^+ = \frac{yu_{\tau,w}\rho_w}{\mu_w}$

δ density thickness of boundary layer, value of y where $\frac{\rho}{\rho_e} = 0.995$

δ^+ boundary-layer thickness in law of the wall coordinates, $\frac{u_{\tau,w}\rho_w\delta}{\mu_w}$

δ^* displacement thickness

δ_i^* incompressible or "kinematic" displacement thickness

ϵ kinematic eddy viscosity

θ momentum thickness

μ molecular viscosity

ρ density

τ total shear stress, $(\mu + \rho\epsilon)\frac{\partial u}{\partial y}$, unless otherwise noted

Subscripts:

e local external to boundary layer

max average maximum value

o stagnation condition

t turbulent

w wall

ANALYTICAL APPROACH

Basic Equation

The equations for the conservation of mass and momentum in axisymmetric or two-dimensional compressible turbulent boundary-layer flows (see ref. 8, for example) are

Continuity:

$$\frac{\partial(\rho u r)}{\partial x} + \frac{\partial(\rho v r)}{\partial y} = 0 \tag{1}$$

Momentum:

$$\frac{\partial\left(\rho u^2 r\right)}{\partial x} + \frac{\partial(\rho u v r)}{\partial y} = -r\frac{\partial p}{\partial x} + \frac{\partial}{\partial y}(r\tau) \tag{2}$$

where, for internal or nozzle-wall flows (the usual case of available hypersonic data, ref. 26) $r \approx r_w - y$. The shear stress includes the turbulent component and is defined herein as $\tau = (\mu + \rho\epsilon)\frac{\partial u}{\partial y}$. Note that the boundary-layer thickness can be the order of the transverse radius of curvature.

An expression for $\rho v r$ is obtained by integrating equation (1) once with respect to y. By assuming an impermeable wall, the following equation is obtained:

$$\rho v r = -\int_0^y \frac{\partial(\rho u r)}{\partial x}\, dy \tag{3}$$

The usual assumption is next made that u/u_e, p/p_e, and ρ/ρ_e are all functions of only y/δ in the neighborhood of the profile under consideration. (See ref. 22.) The δ value used herein is the density thickness, which is perhaps more meaningful at hypersonic conditions than a velocity thickness. The velocity profiles of reference 21 at $M_e = 20$ are shown for various stations along the nozzle in figure 1 and indicate that for these data the assumption of a "local similarity" in y/δ coordinates is acceptable, even at $M_e = 20$. Obviously, in severe nonequilibrium flows, the assumption of y/δ similarity would not be valid, even locally. Therefore, the data examined will be restricted to hypersonic flows where the local pressure gradient is small or zero (although the nozzle-wall boundary layers have a favorable pressure-gradient history). It should be noted that the nonsimilar terms could still be important in the near-wall region, as the sublayer thins in comparison with δ with increasing Reynolds number.

By using this assumption $\left(u/u_e,\ p/p_e,\ \rho/\rho_e \text{ are all functions of } y/\delta\right)$, inserting equation (3) into equation (2), and integrating equation (2) out from the wall, the following equation is obtained $\left(\text{with } v_w = 0 \text{ and noting at high Mach number that pressure is a function of } y/\delta \text{ even for } \left(\frac{dp}{dx}\right)_e = 0, \text{ ref. 21}\right)$:

$$\frac{\tau}{\rho_e u_e^2}\left(1 - \frac{y}{r_w}\right) = \frac{C_f}{2} + \left[\int_0^{y/\delta} \frac{\rho}{\rho_e}\left(\frac{u}{u_e}\right)^2 d\left(\frac{y}{\delta}\right)\right]\left[\frac{\delta}{\rho_e u_e^2}\frac{d\left(\rho_e u_e^2\right)}{dx} + \frac{d\delta}{dx} + \frac{\delta}{r_w}\frac{dr_w}{dx}\right]$$

$$- \left[\int_0^{y/\delta} \frac{y}{\delta}\frac{\rho}{\rho_e}\left(\frac{u}{u_e}\right)^2 d\left(\frac{y}{\delta}\right)\right]\left[\frac{\delta^2}{r_w \rho_e u_e^2}\frac{d\left(\rho_e u_e^2\right)}{dx} + \frac{2\delta}{r_w}\frac{d\delta}{dx}\right]$$

$$- \left[\int_0^{y/\delta} \frac{\rho}{\rho_e}\frac{u}{u_e} d\left(\frac{y}{\delta}\right)\right]\left[\frac{u}{u_e}\frac{\delta}{\rho_e u_e}\frac{d\left(\rho_e u_e\right)}{dx} + \frac{u}{u_e}\frac{d\delta}{dx} + \frac{u}{u_e}\frac{\delta}{r_w}\frac{dr_w}{dx}\right]$$

$$+ \left[\int_0^{y/\delta} \frac{y}{\delta}\frac{\rho}{\rho_e}\frac{u}{u_e} d\left(\frac{y}{\delta}\right)\right]\left[\frac{u}{u_e}\frac{\delta^2}{r_w \rho_e u_e}\frac{d\left(\rho_e u_e\right)}{dx} + \frac{u}{u_e}\frac{\delta}{r_w}\frac{2\,d\delta}{dx}\right]$$

$$+ \frac{\delta}{\rho_e u_e^2}\frac{dp_e}{dx}\left[\int_0^{y/\delta} \frac{p}{p_e} d\left(\frac{y}{\delta}\right)\right] - \frac{\delta^2}{r_w}\frac{dp_e}{dx}\left[\int_0^{y/\delta} \frac{y}{\delta}\frac{p}{p_e} d\left(\frac{y}{\delta}\right)\right]\frac{1}{\rho_e u_e^2}$$

$$- \frac{p_e}{\rho_e u_e^2}\frac{d\delta}{dx}\frac{p}{p_e}\frac{y}{\delta} + \frac{p_e}{\rho_e u_e^2}\frac{d\delta}{dx}\left[\int_0^{y/\delta} \frac{p}{p_e} d\left(\frac{y}{\delta}\right)\right]$$

$$+ \frac{\delta}{r_w}\frac{p_e}{\rho_e u_e^2}\frac{d\delta}{dx}\left(\frac{y}{\delta}\right)^2\frac{p}{p_e} - \frac{\delta}{r_w}\frac{p_e}{\rho_e u_e^2}\frac{d\delta}{dx}\left[\int_0^{y/\delta} \frac{p}{p_e}\frac{2y}{\delta} d\left(\frac{y}{\delta}\right)\right] \qquad (4)$$

Except for reference 21, the data considered herein were reduced by assuming $\frac{p}{p_e} = 1$ for all y; therefore, the sum of the last four terms in equation (4) would not appear. As stated previously, this equation includes transverse curvature effects for internal or nozzle-wall flows as well as pressure-gradient effects. Two-dimensional flow is recovered by letting $r_w \to \infty$ and $\frac{dr_w}{dx} \to 0$. Equation (4) constitutes a relation for $\tau/\rho_e u_e^2$ once the profiles of u/u_e, p/p_e, and ρ/ρ_e as functions of y/δ and the various

x-derivatives are known. In the present work, these profiles and derivatives are taken from experimental data. Therefore, accurate profiles and values of ρ_e and u_e at several longitudinal stations are necessary for determination of the x-derivatives.

Because of the form of the basic equations (eqs. (1) and (2)), equation (4) cannot be used for flows with significant longitudinal curvature. The pertinent equations for this case are available in reference 27, and these would have to be integrated in a manner similar to that used herein to handle flows with significant longitudinal curvature (where $\frac{\delta}{r_w} > \frac{1}{300}$ for the turbulence models, ref. 28). With the shear-stress distribution calculated from equation (4), shear stress is obtained from the relation

$$\frac{\tau_t}{\rho_e u_e^2} = \frac{\tau}{\rho_e u_e^2} - \frac{\mu}{\rho_e u_e \delta} \frac{\partial(u/u_e)}{\partial(y/\delta)} \tag{5}$$

The definitions of the various turbulent shear-stress models are used with $\tau_t/\rho_e u_e^2$ to determine the eddy-viscosity and mixing-length distributions; that is,

$$\frac{\epsilon}{u_e \delta_i^*} = \frac{\tau_t}{\rho_e u_e^2} \frac{\delta}{\delta_i^*} \frac{1}{\partial\left(\frac{u}{u_e}\right) \Big/ \partial\left(\frac{y}{\delta}\right)} \frac{1}{\rho/\rho_e} \tag{6}$$

and

$$\frac{l}{\delta} = \frac{\sqrt{\frac{\tau_t}{\rho_e u_e^2} \frac{1}{\rho/\rho_e}}}{\partial\left(\frac{u}{u_e}\right) \Big/ \partial\left(\frac{y}{\delta}\right)} \tag{7}$$

which were obtained from the definitions

$$\tau_t = \rho \epsilon \frac{\partial u}{\partial y} \quad \text{and} \quad \tau_t = \rho l^2 \left| \frac{\partial u}{\partial y} \right| \frac{\partial u}{\partial y}$$

The derivatives of the experimental velocity profile $\frac{\partial(u/u_e)}{\partial(y/\delta)}$ are needed to obtain ϵ and l variations with y/δ. Also, when the near-wall data are sufficiently detailed to allow an examination of wall-damping effects, the expression from reference 29 (Van Driest damping function) will be employed:

$$\frac{l}{\delta} = \frac{Ky}{\delta}\left(1 - e^{-y/A}\right) \tag{8}$$

where

$$A = \frac{A^+ \mu}{\rho u_\tau} \tag{9}$$

and A^+ is the usual "damping constant" $(A^+ = 26)$. At the present time, no clear choice exists as to whether the ρ, μ, and τ in equation (9) should be evaluated at the wall or locally as a function of y. This question is investigated in the present paper.

In the present method, equation (4) is used to obtain shear-stress, eddy-viscosity, and mixing-length distributions from experimental data with the following restrictions:

(1) Impermeable wall

(2) Small or zero streamwise pressure gradient

(3) Accurate profile data at several longitudinal stations

(4) Small longitudinal curvature

(5) Mach numbers greater than approximately 5 (hypersonic)

Unfortunately, the amount and, to a certain extent, the accuracy of the published data decrease significantly from low-speed to supersonic and then hypersonic conditions. The data currently available which fulfill the restrictions noted are basic hypersonic turbulent boundary-layer information, and such data are not plentiful; however, the data presented in references 21 and 30 to 36 will be used herein to exercise the present method, and the results should give some indication of what shear-stress models might be used in hypersonic flow.

Method of Solution

Profiles of u/u_e and ρ/ρ_e as functions of y/δ were plotted for the data from references 21 and 30 to 36. Curves faired through each data point (except as noted in the discussion of the individual cases) were used to obtain detailed ρ/ρ_e and u/u_e distributions for the integrals in equation (4). In order to achieve a high degree of accuracy, 200 points were read from each curve and used as input to a computer program in tabular form. The trapezoid rule was used to evaluate the integrals in equation (4) with the program interpolating four points between each pair of points in the input table; this interpolation gave a 1000-point integration for the entire boundary layer. This integration allowed the determination of $\tau/\rho_e u_e^2$ as a function of y/δ. The necessary local streamwise derivatives were obtained graphically from fairings of the quoted variations of δ, r_w, $\rho_e u_e^2$, $\rho_e u_e$, and p_e.

The derivatives of u/u_e with respect to y/δ, necessary to obtain eddy-viscosity and mixing-length values from the shear-stress profile, were computed by using a least-squares method with an overlapping series of curve fits for six consecutive points in the input u/u_e table. Each curve fit was differentiated, and the derivatives of the third and fourth points in the curve fit were computed from this differentiation. The third and fourth points used in the first curve fit were then taken to be the first two points in the

next curve fit and so on. The derivatives obtained by this method were plotted and faired. The resultant derivatives are believed accurate to within approximately 15 percent (assuming the experimental data are exactly correct, which may not be true in all instances). The velocity derivatives in the outer region were successfully checked by comparison with results from an "N-power" approach; that is, a velocity distribution $\frac{u}{u_e} = \left(\frac{y}{\delta}\right)^{1/N}$ was assumed and differentiated. By using the experimental N value, a local derivative in the outer region was obtained to check the results from the curve-fit procedure.

SHEAR-STRESS, EDDY-VISCOSITY, AND MIXING-LENGTH DISTRIBUTIONS

The results of evaluating equation (4) along with the $\epsilon/u_e\delta_i^*$ and l/δ distributions for typical profiles from references 21 and 30 to 36 will now be presented. The various x or longitudinal derivatives and other input and output quantities used in the solution are given in table I. The skin-friction values used were obtained wherever possible from values quoted in the reference from which the data were taken. Exceptions to this procedure are noted in the discussion of the individual profiles considered. It should be noted that because of the incomplete nature of much of the published hypersonic data, the results presented herein of applying the present method should be considered as indicating trends rather than true absolute levels.

Mixing-length and eddy-viscosity distributions from reference 12 will be shown for comparison with the present computed hypersonic results. The curves shown from reference 12 are for supersonic flows over a fairly wide range of Reynolds numbers and are typical of variations currently employed in prediction methods.

Axisymmetric-Nozzle-Wall Data at a Mach Number of 20.8

Profile data are available from reference 21 for several stations along an axisymmetric nozzle wall at $M_e \approx 20$ in helium. The wall-to-total temperature ratio was near 1.0, and the data were reduced by assuming T_o was constant. The large density ratio across the boundary layer $\frac{\rho_e}{\rho_w} = 140$ provided a severe test case of compressibility or high Mach number effects. A re-reduction of the data by using $\frac{T_o - T_w}{T_{o,e} - T_w} = \left(\frac{u}{u_e}\right)^2$, with the lowest possible T_w/T_o being 0.96, indicated negligible change on the velocity profile for $\frac{y}{\delta} > 0.1$. Results are shown in figure 2 for both total-temperature distributions.

The profile chosen was from station 108 with a local Mach number of 20.8 and a small local favorable pressure gradient. (See table I.) The profile is given in table 2 of reference 21. The p/p_e profile used in equation (4) was the same one used to reduce

the profile data in reference 21. The R_θ was 6.90×10^3, which at supersonic speeds is usually large enough to insure a fairly well-developed turbulent flow. (See ref. 37.) The shear-stress results are shown in figure 2(a). As stated previously, the δ used in the present work is the pitot or density thickness. The nominal velocity thickness is less $\left(\frac{u}{u_e} = 0.995 \text{ corresponds to } \frac{y}{\delta} \approx 0.5\right)$. The computed shear stress goes to the laminar value when $\frac{u}{u_e} = 0.9983$ and $\frac{y}{\delta} = 0.695$. The fact that $\tau_t \to 0$ at $\frac{y}{\delta} < 1$ may be reasonable in this case because of the extreme fullness of the velocity profile $\left(\frac{\partial(u/u_e)}{\partial(y/\delta)} \to 0 \text{ when } \frac{y}{\delta} < 1\right)$. Also, the hot-wire data of reference 21 for total-temperature fluctuations may be interpreted in the outer region as twice the velocity-fluctuation level because of the high Mach number, and these results indicate a u'/u_e level less than 0.5 percent for $\frac{y}{\delta} > 0.7$ (low vorticity level).

At high Mach numbers, the energy equation reduces to $u \propto \sqrt{T_o}$; thus, for a hot- or near-adiabatic-wall turbulent boundary layer at high Mach number, the u/u_e profile is extremely full because T_o is nearly constant. However, at the same Mach number and a cold-wall case, where T_o may decrease in the outer high Mach number portion of the boundary layer, the velocity profile would be considerably less full. (See refs. 37 and 38.) Therefore, at hypersonic speeds, another mechanism besides the turbulence field is available which can have a first-order effect upon the mean velocity profile. This discussion implies that at hypersonic speeds correlations of pressure gradient and wall-blowing effects which are based on velocity-profile shape alone (such as those given in reference 1) may not be reliable because the correlations are based upon low-speed data where the turbulence is the dominating factor on the profile shape.

The eddy-viscosity and mixing-length distributions are shown in figure 2(b) and 2(c), respectively. In the outer region, the $\epsilon/u_e\delta_i^*$ and l/δ values are significantly larger than the usual adiabatic equilibrium value of 0.018 and 0.09, respectively. (See ref. 12.) A later portion of the present paper shows that these higher values may be expected and are a logical extension of the low Reynolds number effect noted in references 15 and 16 at low speeds. As indicated in the figure, the wall-region $\left(\frac{y}{\delta} < 0.3\right)$ results in figure 2(c) indicate a Prandtl wall slope of approximately 0.65 rather than the more usual value of 0.4 (ref. 12). This increased value of the slope again is shown later to be an expected result of the low Reynolds number trend noted in reference 39. Further calculations using the method of reference 1 indicate that the larger Prandtl slope at the wall constitutes the major reason for the disagreement shown in reference 21 between these profile data and predictions using the method of reference 1, which originally employed $K = 0.4$.

The mixing-length distribution shown in figure 2(c) indicates a region $\left(\frac{y}{\delta} < 0.1\right)$ where the Prandtl wall variation ($l = Ky$) is damped by the wall. This damping effect will be considered in a later section.

Turbulent Boundary-Layer Development Inside a Circular Duct at a Mach Number of 6

Profile data for the development of a turbulent boundary layer inside a constant-area circular duct at a Mach number of 6 are presented in reference 30. The duct was connected to the exit of a contoured axisymmetric nozzle, and the measurements were made during the subsequent development of the nozzle-wall boundary layer. Because of the δ^* increase in the duct, there is a small positive pressure gradient, whose strength is a function of Reynolds number. Two profiles which are typical of the low and high Reynolds number range of the tests were analyzed. The first profile examined was obtained at station 124, $p_o = 0.45$ MN/m^2 (65.3 psia), $\frac{T_w}{T_o} = 0.73$, and $M_e = 5.76$. The profile is given in table III(a) of reference 30. These results are typical of the low Reynolds number range of these data $\left(R_\theta = 8 \times 10^3\right)$.

The shear-stress distribution is shown in figure 3(a). Here the shear does not fall monotonically from the wall value but peaks at $\frac{y}{\delta} \approx 0.2$ before falling off toward the outer edge. Typically, this peaking away from the wall occurs for boundary layers in the presence of adverse pressure gradients or wall blowing. (See ref. 40.) Note that the velocity profile is much less full than for the Mach 20 helium case (shown in fig. 1) and exhibits a more usual shape (N = 7.7). The eddy-viscosity and mixing-length variations shown in figure 3(b) and 3(c), respectively, are fairly similar to those observed at $M_e \leqq 5$ and high Reynolds number. (See ref. 12.) Therefore, since the R_θ for this profile (8.00×10^3) is fairly close to the value for the Mach 20.8 profile $\left(6.90 \times 10^3\right)$ and the l/δ and $\epsilon/u_e\delta_i^*$ profiles are quite different (compare figs. 2(b) and 2(c) with figs. 3(b) and 3(c)), it appears that the magnitude of R_θ is no longer a valid representation of the "relative turbulent state" of a boundary layer at hypersonic speeds but the turbulent state is a function of R_θ, M_e, and T_w/T_o. For the Mach 20.8 profile, the wall-to-edge density ratio $\left(\frac{\rho_w}{\rho_e} = 0.007\right)$ is much less than that for the Mach 6 profile $\left(\frac{\rho_w}{\rho_e} = 0.18\right)$. This difference in the ρ_w/ρ_e ratio represents a probable explanation for the discrepancy. Also, the u_τ value is less at Mach 20.8 because of the much lower C_f value. Therefore, at hypersonic speeds a Reynolds number based on wall rather than edge conditions probably better characterizes the structure of the boundary layer. It is shown later in the present paper that the use of wall parameters allows a reasonable correlation of the available low Reynolds number eddy-viscosity and mixing-length data to be made from low speeds up to a Mach number of 20, at least for near-adiabatic flows.

The other profile examined from reference 30 was at station 172 and $p_o = 2.17$ MN/m^2 (315 psia), $\frac{T_w}{T_o} = 0.7$, $R_\theta = 47 \times 10^3$, and $M_e = 5.75$. The profile was taken from table IV(c) of reference 30. The shear-stress profiles are shown in figure 4(a). For this profile, the shear did not reach zero at the edge but deviated at

$\frac{y}{\delta} \approx 0.75$. The reason for this deviation is not known, but probable explanations are (1) y/δ similarity assumption erroneous or, perhaps more probable, (2) incorrect values of dp/dx and $d\delta/dx$. The profile measuring stations are fairly far apart, which makes the evaluation of accurate local x-derivatives difficult. A curve has been shown drawn to zero at the edge, and results will be shown for both computed and assumed outer-shear distributions. Again, the peaking away from the wall is apparent. A comparison of figures 3(a) and 4(a) indicates that the near-wall region (where significant laminar shear occurs) constitutes an appreciably smaller fraction of y/δ in figure 4(a) as would be expected because of the higher Reynolds number. The eddy-viscosity and mixing-length distributions are shown in figures 4(b) and (c). At this higher Reynolds number, the values are still in reasonable agreement (although somewhat higher than those at lower Mach numbers) with the results from reference 12 for $M_e \leqq 5$. This agreement corresponds to the finding in references 15, 16, and 39 that at high Reynolds number the l/δ, $\epsilon/u_e\delta_i^*$, and K values are nearly invariant with Reynolds number (the cornerstone of most finite-difference calculation methods).

Conical-Nozzle-Wall Data at a Mach Number of 10.65

Profile data for the development of a turbulent boundary layer on a conical nozzle wall (favorable pressure gradient) are available in reference 31. The nozzle had a total conical expansion angle of 7.5^o and was attached to a hypersonic gun tunnel facility. In the data region, the nominal test-section diameter was 0.102 meter (4 inches). Over a distance of 0.204 meter (8 inches), the Mach number increased from 10.2 to 11.6. The ratio of wall to total temperature was low (0.26); therefore, especially accurate total-temperature profiles are necessary in order to correctly reduce the pitot data to velocity profiles. (The static pressure was assumed constant.) The data analyzed herein correspond to $x = 0.665$ meter (26.2 inches), $M_e = 10.65$, and $p_o = 30.7$ MN/m^2 (4450 psia). The profiles were not tabulated and hence had to be obtained from figures 5.10c and 5.11b of reference 31. The R_θ was 12.8×10^3. This profile is typical of the high Mach number, high Reynolds number (comparatively speaking) portion of the data in reference 31.

The shear-stress results are shown in figure 5(a). The lower set of curves correspond to using a C_f obtained from table 5.1 of reference 31. A value of 5.2×10^{-4} was taken as a mean of the "measured" results, which varied from 5.49×10^{-4} to 4.89×10^{-4}. This value gives a shear stress which approaches zero at $\frac{y}{\delta} = 0.5$, clearly not correct for a velocity profile which has an N power of 6.2 (ref. 31). Solutions for shear stress obtained by varying the input parameters over a reasonable range of uncertainty yielded shear-stress distribution not very different from that shown. The only perturbation on the inputs which would give a reasonable shear-stress distribution was to increase the C_f value. Results are indicated by the upper set of curves for an arbitrary

increase of 100 percent in C_f. These results do not imply that the actual C_f for the profile was as high as 1.04×10^{-3}, but rather that something is wrong with either the present approach and/or the profile data. The validity of the local similarity assumption $\left(u/u_e \text{ and } \rho/\rho_e \text{ are functions of } y/\delta\right)$ can be questioned; however, the large effect shown in figure 5(a) indicates that there may be some problems with the data, particularly with the total-temperature profiles.

Reference 1 indicates that to compute this profile in terms of a total-temperature—velocity relation, the total turbulent Prandtl number (see ref. 1) would have to be increased to 2 in the outer region of the boundary layer. (See fig. 6 of ref. 1.) This value is considerably above the usual values of total turbulent Prandtl number (near 1); therefore, the total-temperature data for $\frac{u}{u_e} < 0.8$ $\left(\text{near the wall, } \frac{y}{\delta} < 0.2\right)$ may be too low. This assumption may be reasonable in light of the short running time of the facility (10 to 20 msec), the existence of a low Reynolds number region near the wall where the T_o probe corrections are presumably different from those obtained in the free stream (see ref. 38), and the fact that numerous runs with slightly varying conditions were necessary to obtain a single T_o profile. Consequently, the extreme difficulty of obtaining accurate T_o measurements near the wall in such a facility suggests that for $\frac{y}{\delta} < 0.2$ the T_o measurements may be low. This inaccuracy could explain part of the problem with the shear stress approaching the laminar value at $\frac{y}{\delta} = 0.5$. If the T_o values near the wall were higher, the u/u_e profile would necessarily be fuller (higher N value); therefore, the integrals in equation (4) would be affected. Also, the indicated C_f would probably increase. The net result of higher T_o values would be some increase in C_f and a change in slope of the curve of $\tau/\rho_e u_e^2$ as a function of y/δ.

Eddy-viscosity and mixing-length distributions are shown in figure 5(b) and (c), respectively, for the two $\tau/\rho_e u_e^2$ variations of figure 5(a). Using the upper shear-stress curve from figure 5(a) results in more conventional values of l/δ and $\epsilon/u_e\delta_i^*$ for this fairly high Reynolds number boundary layer. However, if the T_o profile was fuller, thus increasing the N power on the velocity profile, the $\frac{\partial(u/u_e)}{\partial(y/\delta)}$ values would be lower in the inner region of the boundary layer; therefore, the increase of l with y would be greater for $\frac{y}{\delta} < 0.2$. This discussion would explain the low Prandtl slope for this case (0.26 versus usual values of 0.4 or greater).

Axisymmetric-Nozzle-Wall Data at a Mach Number of 12

Profile data for the development of a turbulent boundary layer on a contoured axisymmetric nozzle wall with a mild favorable pressure gradient are given in reference 32; tabulations of the profiles were supplied by the author of that reference. The profile examined herein was taken at station -0.026 meter (-1.023 inches) (measured from the

nozzle exit) on a contoured steel nozzle with $p_o = 6.9$ MN/m^2 (1000 psia). The local Mach number was 12.0 and $\frac{T_w}{T_o} = 0.295$.

The scale of the facility is similar to that used in reference 31, with a nominal test-section diameter of 0.102 meter (4 inches). However, the Mach number is higher (12 versus 10.6) and the total pressure lower (6.9 MN/m^2 (1000 psia) versus 30.7 MN/m^2 (4450 psia)); therefore, the R_θ value of 1.12×10^3 is considerably below the value for the profile examined from reference 31. In fact, an R_θ value of 1×10^3 is low even for a supersonic boundary layer. (See ref. 37.) It should be noted that this profile constitutes some of the highest Reynolds number data taken in the investigation of reference 32. The possibility that this represents an "overdamped" boundary layer will be discussed in a later section.

The shear-stress profiles are shown in figure 6(a). Again, as in figure 5(a), the C_f value had to be increased by a factor of nearly 2 in order for the shear stress to approach zero in the outer region of the boundary layer. However, such a higher C_f value is perhaps defensible from the velocity-profile data shown in figure 6(b). These profile data raise an interesting point, one brought out in reference 33, as well as elsewhere. The data points near the wall in figure 6(b) exhibit a deviation from the general trend of the data. This deviation might be attributed to probe-interaction effects with the wall. However, another possible cause for at least some of this deviation is indicated in figure 16 of reference 33. In the very-near-wall region, especially for this low Reynolds number, turbulent boundary layer with a thick sublayer $\left(\frac{y_{sl}}{\delta} = 25 \text{ percent}\right)$, the laminar shear stress dominates a significant portion of the inner profile (out to y/δ from 0.05 to 0.2 from fig. 6(a) depending upon the C_f value). Therefore, the shear stress, which is nearly constant, is given by $\mu \frac{\partial u}{\partial y}$.

Because of the heat transfer to the wall, the static temperature (and consequently μ) increases to a peak $\left(\text{at } \frac{y}{\delta} \approx 0.12, \text{ ref. } 32\right)$ before decreasing to the edge value. The requirements of τ being constant and μ peaking imply that $\partial u/\partial y$ must first decrease and then increase again as the distance from the wall increases. Therefore, the velocity profile should exhibit a "kink" as illustrated in figure 16 of reference 33. The direction of such a kink is consistent with the deviation of the first data point in figure 6(b) from the rest of the profile. The consequence of this discussion is that the available data near the wall may not be sufficient to define a true C_f value; therefore, a higher C_f (such as used in fig. 6(a)) may be reasonable for this boundary layer. Further research is obviously needed to clarify the phenomena in the wall region of a low Reynolds number, hypersonic turbulent boundary layer, especially under cold-wall conditions.

The eddy-viscosity and mixing-length results are shown in figure 6(c) and 6(d), respectively. The values of both l/δ and $\epsilon/u_e\delta_i^*$ are rather low; this result will be discussed more fully in a later section.

Data Obtained in a Two-Dimensional Boundary-Layer Channel at a Mach Number of 5

Profile data are available from reference 33 for the development of a turbulent boundary layer at a Mach number of 5 in a two-dimensional boundary-layer "channel" with essentially zero pressure gradient locally. The channel wall is a continuation of a Mach 5 two-dimensional nozzle; therefore, the data were essentially from a two-dimensional nozzle-wall boundary layer, which is allowed to "relax" in a zero pressure gradient. Two profiles corresponding to runs 6211 and 12091 are examined. (See table 1(r) and 1(d), respectively, from ref. 33.) The local Mach number is 4.7 and $\frac{T_w}{T_o} = 0.7$.

The first profile examined (run 6211) corresponds to an $R_\theta = 57 \times 10^3$ and, therefore, should constitute a high Reynolds number flow. The shear-stress, eddy-viscosity, and mixing-length distributions are shown in figure 7. The shear-stress distribution looks fairly reasonable; however, the eddy-viscosity and mixing-length distributions show a "trough" region for $0.1 < \frac{y}{\delta} < 0.6$ approximately. In this region, both eddy-viscosity and mixing-length profiles are not as full as one would expect, especially for this Mach number and Reynolds number. (Note comparison with $M_e \leq 5$ results from ref. 12.)

A possible reason for the disagreement with the reference 12 results is readily available from the velocity profile for this case (shown plotted in log-log form in fig. 5c(2) of ref. 33). The N-power quoted in reference 33 for this profile is 8.3. Figure 5c(2) of reference 33 indicates that this N-power is valid for y/δ between 0.02 and 0.1 and also between 0.6 and 0.98. However, for y/δ from 0.1 to 0.6, the indicated N-power is significantly lower ($N \approx 5$). Therefore, there is an increase in $\frac{\partial(u/u_e)}{\partial(y/\delta)}$ in the midregion of this boundary layer which is not normally expected and which causes "less full" eddy-viscosity and mixing-length profiles in this region.

This apparent abnormal behavior of the variation of u with y may be due to (1) residual nonequilibrium effects of the nozzle expansion upon the boundary layer (see ref. 26), (2) nozzle sidewall effects, or (3) inaccurate total-temperature profiles. However, how these could cause this anomalous behavior in the velocity-profile data is not clear. The eddy-viscosity and mixing-length values which will be used in a later section of the paper will correspond to the more "normal" sections of the profile $\left(\frac{y}{\delta} < 0.1 \text{ and } \frac{y}{\delta} > 0.6\right)$.

Results from the second profile (run 12091) are shown in figure 8. The R_θ for this profile is 5×10^3, which is still comparatively high but an order of magnitude less than for the previous profile. Again, the shear-stress results are reasonable and the l/δ and $\epsilon/u_e\delta_i^*$ distributions have the same odd-looking trough as the higher Reynolds number data. This region has roughly the extent $0.1 < \frac{y}{\delta} < 0.65$. In figure 5b(1) of reference 33 (a log-log plot of velocity as a function of y/δ of this profile), there is again a corresponding "low N" region for $0.1 < \frac{y}{\delta} < 0.65$. Therefore, at an order of magnitude lower Reynolds number, the same anomalous phenomenon has occurred at roughly the same location.

To check the validity of the "local similarity" assumption for this case (u/u_e and ρ/ρ_e are functions of y/δ), a simple form of the integral momentum equation can be used:

$$\frac{C_f}{2} = \frac{d\left(\frac{\theta}{\delta}\,\delta\right)}{dx} = \frac{\theta}{\delta}\frac{d\delta}{dx} + \delta\frac{d\left(\frac{\theta}{\delta}\right)}{dx} \tag{10}$$

For a flow in local similarity, the ratio θ/δ should be invariant with x; therefore, the second term in equation (10) represents a nonsimilar correction. For the first profile considered (fig. 7), the terms in equation (10) are $\frac{C_f}{2} = 3.6 \times 10^{-4}$ and $\frac{\theta}{\delta}\frac{d\delta}{dx} = 3.86 \times 10^{-4}$; therefore, the second or nonsimilar term in equation (10) constitutes only about a 7-percent correction, and this flow is indeed near a local similarity, at least for the profile taken as a whole.

Measurements on a Hollow Cylinder at a Mach Number of 6

References 34 and 35 provide profile data for a boundary layer grown on a hollow cylinder at a Mach number of 6. Reference 34 presents an adiabatic-wall case, whereas reference 35 shows a cooled-wall condition on the same configuration in the same facility. The pressure gradient remains close to zero throughout the entire history of the boundary-layer development; therefore, these data should be "clean"; that is, there are no questions concerning possible effects of upstream pressure-gradient history, as was the case for the nozzle-wall results considered previously (figs. 2 to 8). However, as was shown in reference 37, the presence of a transition region provides a perturbation in the profile shape which requires a hundred or so boundary-layer thicknesses for relaxation. The profile examined from reference 34 is tabulated in table I(g) of that reference and corresponds to station 0.15 meter (6 inches), $M_e = 6.02$, $\frac{T_w}{T_o} = 0.895$, and $R_\theta = 1.4 \times 10^4$.

The shear-stress distribution is shown in figure 9(a), and the eddy-viscosity and mixing-length distributions in figure 9(b) and 9(c), respectively. The eddy-viscosity distribution peaks somewhat inboard, as indicated by comparison with the reference 12

results. The mixing-length distribution exhibits a high K value near the wall but a modest level in the outer region. Generally, a high K value is accompanied by a rather high level of $\left(\frac{l}{\delta}\right)_{max}$. A possible reason for this behavior was reported in reference 37, which shows that these profiles have a rather high N-power (9) for this Reynolds number. The profile evidently has not relaxed completely from the "N-power overshoot" (extreme profile fullness) that seems to dominate regions immediately downstream of transition at hypersonic speeds. (See ref. 37.)

The second profile examined was from reference 35, where $\frac{T_w}{T_o} = 0.45$, $R_\theta = 1.28 \times 10^4$, and $M_e = 5.98$. The profile is from station 4 and is shown in table 1(d) of reference 35. The shear-stress, eddy-viscosity, and mixing-length distributions for this profile are shown in figure 10. The eddy-viscosity (fig. 10(b)) and mixing-length (fig. 10(c)) distributions are somewhat lower than those of reference 12.

Measurements on a Flat Plate at a Mach Number of 6.5

Reference 36 provides data for a boundary layer developed on a sharp flat plate at $M_e = 6.5$. The profile examined herein corresponded to $\frac{T_w}{T_o} = 0.48$, $R_\theta = 2.53 \times 10^3$, and zero blowing with the test designated as run 3 and the profile given in table 5 of reference 36.

The shear-stress, eddy-viscosity, and mixing-length distributions are shown in figure 11. The shear-stress profile was computed by using a value of $C_f/2$ of 9.5×10^{-4} for this case, as used in reference 24 instead of 7.23×10^{-4}, as used in reference 36. The eddy-viscosity values are somewhat above the results from reference 12. As discussed in connection with previous profiles, this result is perhaps reasonable because of the low Reynolds number involved. The wall-damping region seems to extend out to $\frac{y}{\delta} \approx 0.15$. Therefore, the conventional region of the Prandtl wall slope is rather abbreviated, and the mixing levels off at a reasonable value. (See fig. 11(c).)

COMPARISON OF HYPERSONIC AND LOW-SPEED EDDY-VISCOSITY AND MIXING-LENGTH LEVELS

As stated previously in the present report, a definite low Reynolds number effect was noted in references 15 and 16 on the $\left(\frac{\epsilon}{u_e \delta_i^*}\right)_{max}$ and $\left(\frac{l}{\delta}\right)_{max}$ levels in low-speed flows. A similar effect was observed for K (increase with decreasing R) in reference 39 for low-speed flows. All of these investigations (refs. 15, 16, and 39) utilize R_θ as the correlating parameter for low Reynolds number effects at low speeds. At hypersonic conditions, one expects a similar low Reynolds number effect. However,

comments in the present paper in connection with the first two cases considered indicate that at hypersonic conditions (where generally $\rho_w \ll \rho_e$ and $\mu_w \gg \mu_e$) R_θ, which is based on edge conditions, would not be expected to correlate low Reynolds number effects. This disagreement between low-speed and high-speed data when R_θ is used as the basis for comparison is indicated in the inserted figure from reference 39 in figure 12(a). Reference 41 obtained good results in correlating high Mach number (M_e = 20 to 43) profiles by using wall conditions and a wall-friction velocity. Therefore, in an attempt to correlate low Reynolds number effects at both low and hypersonic speeds, a Reynolds number based on wall conditions is used. The form chosen was $\delta^+ = \frac{\rho_w u_{\tau,w} \delta}{\mu_w}$. Another kinematic scale factor, such as δ_i^*, could perhaps have been used; however, the use of δ^+ allows the ready identification of extremely low Reynolds number flows which may be "overdamped," since the wall-damping function (eqs. (8) and (9)) contains a damping constant A^+ which is defined in terms of law of the wall coordinates as $\frac{A\rho_w u_{\tau,w}}{\mu_w} = 26 = A^+$ (for impermeable-wall condition).

Generally, when $y^+ \gg A^+$, the profile data are in agreement with some form of the logarithmic (or "wall") law; the logarithmic region is considered the fully turbulent portion of the profile. For $y^+ \leqq A^+$ the wall damping affects the profile directly. As δ^+ approaches A^+, the wall damping will affect more and more of the profile and eventually reduces the turbulence in what is usually considered the outer region of the boundary layer $\left(\frac{y}{\delta} > 0.2\right)$. (See also reverse transition discussion in ref. 42.)

The low-speed results of references 15, 16, and 39 for K, $\left(\frac{l}{\delta}\right)_{max}$, and $\left(\frac{\epsilon}{u_e \delta_i^*}\right)_{max}$ have been plotted as a function of δ^+ (the tabulation of ref. 43 was used to convert from R_θ to δ^+ for the ref. 16 and 39 results) and are shown in figure 12. Also shown are the results presented herein (figs. 2 to 11) and those from references 12 and 13. Where anomalies have been found in the data (these are discussed in connection with the individual cases), the results have not been shown. The values shown from the results presented herein are tabulated in table I.

The variation of Prandtl wall slope K with δ^+ is shown in figure 12(a). The K values are only quoted for profiles where the damping does not extend beyond $\frac{y}{\delta} \approx 0.15$; that is, where a definite Prandtl wall region is present. If damping persists out farther than $\frac{y}{\delta} \approx 0.15$, a true law of the wall region probably does not occur and the profile goes almost directly from a sublayer to a wake region. Because of possible inaccuracies in the present analysis procedure (such as the similarity assumption) and the incompleteness of some of the data, considerable scatter exists. (This scatter is shown in all parts of figs. 12 and 13.) However, the present hypersonic values (especially the data at near-adiabatic-wall conditions) do tend to exhibit the same trend as the incompressible values of reference 39; that is, the values increase as Reynolds number decreases. Interestingly,

these K values at low δ^+ are appreciably above the usual accepted values of 0.4 to 0.44. These higher K values have an appreciable effect upon profile shape and predicted C_f when employed in a finite-difference procedure.

The outer mixing-length levels are shown in figure 12(b), and again the present hypersonic results are in fair agreement with the level and trends of the low-speed data. However, at very low values of δ^+ (66), where $\delta^+ \Rightarrow A^+$, the $\left(\frac{l}{\delta}\right)_{max}$ from reference 32 has reversed the trend of the values at higher δ^+. This reversal in trend may be due to excessive wall damping, since δ^+/A^+ has a value of only 2.5.

Obviously, with δ^+ sufficiently reduced the flow will revert to a laminar condition. (This relaminarization occurred in ref. 44.) Therefore, somewhere the upward trend of the low-speed data has to reverse, and the $\left(\frac{l}{\delta}\right)_{max}$ values decrease toward zero. The actual value of δ^+ where this reversion occurs is probably a function of the flow history, local conditions, and wall-to-total-temperature ratio and, therefore cannot be correlated on a plot such as figure 12(b).

It should be noted that the bulk of the published hypersonic turbulent profile data (such as refs. 21, 30, 31, 32, and 33) was obtained on nozzle walls (see also ref. 26) primarily because of the difficulty of obtaining turbulent boundary layers on basic configurations in hypersonic flows. This difficulty can be attributed to the trend toward high transition Reynolds number at high Mach numbers and the low unit Reynolds number and fairly small size of most hypersonic facilities. The nozzle-wall boundary layer is, in most instances, a thick, readily accessible, turbulent shear flow. However, a number of problem areas arise when the genesis of this type of boundary layer is considered. The original turbulence structure is formed in a low-speed settling-chamber-wall flow. The boundary layer is next expanded to the throat region where high heat transfer is present and partial relaminarization often occurs. Farther down the nozzle, the main effect is a drop in external density until the final Mach number is reached.

If a corresponding boundary layer had grown on a basic model in zero-pressure gradient, constant wall temperature, and at the same final Mach number, the flow would probably not be turbulent, at least for some of the available data (Reynolds number too low, see ref. 45). At low δ^+, probably the only reason the nozzle-wall boundary layers appear turbulent is the existence of a turbulent history in the low-speed settling-chamber region. Also, calculations carried out during the investigation reported in reference 1 indicate that, from the throat to the exit of a Mach 19 hypersonic nozzle (assuming a fairly hot throat and a cooled test-section wall), the wall boundary layer thickens appreciably but does not entrain a significant amount of mass. Therefore, history effects in terms of distorted temperature profiles tend to remain with the flow rather than be "washed out" or relaxed. (See ref. 26.)

Therefore, on an actual vehicle where transition occurs naturally and in a high Mach number region, turbulent flow would probably only exist at fairly high δ^+ values, and it would not be necessary to account for the increases in $\left(\frac{l}{\delta}\right)_{max}$ and K which occur at low δ^+ (figs. 12(a) and 12(b)), except perhaps in a method such as presented in references 5 and 11 which compute through transition. During transition, natural or tripped, a turbulence model should probably be corrected for low Reynolds number effects as well as intermittency.

The $\left(\frac{\epsilon}{u_e \delta_i^*}\right)_{max}$ values for the outer region are shown in figure 12(c). These results behave in a manner similar to the $\left(\frac{l}{\delta}\right)_{max}$ values in figure 12(b). Most of the values at low δ^+ are above the 0.016 to 0.018 eddy-viscosity range generally used in computational techniques. (See refs. 6, 7, 10, and 11.)

As a possible alternate method of correlating the low- and high-speed "low Reynolds number effect," a Reynolds number was used based on sublayer thickness, wall density, viscosity, and free-stream velocity; that is, $R_{sl} = \frac{u_e y_{sl} \rho_w}{\mu_w}$, where $\frac{y_{sl} u_{\tau,w} \rho_w}{\mu_w} = 10$ was used to determine y_{sl}. The K, $\left(\frac{l}{\delta}\right)_{max}$, and $\left(\frac{\epsilon}{u_e \delta_i^*}\right)_{max}$ values are shown in figure 13 as a function of R_{sl}. Again, considerable scatter appears in the data, but the trends do not seem to be as well matched between the low- and high-speed data as in figure 12 (except for K, fig. 13(a)); therefore, the use of δ^+ as a correlating factor is favored.

It should be noted that the nature of the variation of $\left(\frac{l}{\delta}\right)_{max}$, $\left(\frac{\epsilon}{u_e \delta_i^*}\right)_{max}$, or K with δ^+ or R_{sl} is probably a function of wall cooling. At the present time, insufficient data exist to attempt to settle this question, and the possibility of wall-cooling effects is raised as a cautionary note in the use of the results shown in figure 12 or 13. More data at hypersonic conditions, especially with cold walls, are obviously needed before any definite conclusions can be made as to the correct scaling parameters for low Reynolds number effects at hypersonic cold-wall conditions.

EVALUATION OF WALL-DAMPING EXPRESSION

Hypersonic turbulent boundary layers generally have fairly thick sublayer regions because of the low density near the wall. In this near-wall region, turbulence damping occurs and the mixing-length distributions deviate from the usual $l = Ky$ variation. The most commonly employed expression to account for this effect is equation (8), the Van Driest damping function (ref. 29). For compressible flows, there are several possible methods to use in evaluating τ, μ, and ρ appearing in equation (9), which is the

damping-scale expression. The most straightforward method is to evaluate all of these quantities at wall conditions. Based on the successful use of wall properties in reference 41 to correlate the entire profile even where the density change across the boundary layer is a factor of several hundred, the use of wall conditions seems a reasonable approach. However, other suggestions, such as using sublayer averaged or local conditions (ref. 20) on μ and ρ or using local shear (ref. 46), have been made. In the present case, the shear is approximately constant in the near-wall region (no large pressure gradient, wall blowing, or suction); therefore, the question of whether or not to use local shear cannot be investigated. However, especially for the Mach 20.8 investigation (fig. 2) where a sizable change in density exists across the sublayer, the question of whether to use wall or local ρ and μ in equation (9) can be examined. Note that there are several other wall-damping expressions which could be used. (See refs. 7 and 16, for example.)

Several of the profiles examined herein exhibit fairly extensive regions of wall-damping effects upon the l distribution. As an extreme case, the results shown in figure 6 indicate an extensive region near the wall with completely damped turbulence, a clue that the boundary layer may be "overdamped" as indicated in the previous section.

By using the K values given in table I (obtained from figs. 2 to 11), several of the computed l/δ distributions have been used in equation (8) to compute a variation of A^+ with y/δ for the cases where (1) μ and ρ are evaluated at the wall temperature and (2) μ and ρ are evaluated as functions of y. If the damping expression is correct and the l/δ variation accurate, A^+ should be a constant with y/δ. In addition, if the method of evaluation for ρ and μ is correct, the value of A^+ should be close to 26, which is the incompressible level generally used in an impermeable-wall situation. (See refs. 1 and 29.)

The resulting A^+ variations are shown in figure 14. The values exhibit large deviations from the expected value of 26, probably due more to inaccuracies in the l/δ variations reported herein than in the form of the damping function. By treating the deviation from the 26 value of A^+ as a random error, the root-mean-square deviation and average error were obtained for both methods of evaluating ρ and μ in equation (9). The resulting errors are shown in figure 15 as averages for all the cases of figure 14. From this figure, it is evident that (1) the value of 26 is somewhat too low, and (2) the method which provides the least error results from an evaluation of ρ and μ at wall conditions.

CONCLUDING REMARKS

A method is developed to obtain shear-stress, eddy-viscosity, and mixing-length distributions from hypersonic turbulent boundary-layer profile data by using the

assumption of local similarity. Application of the method to published profile data indicates an increase in the maximum value of mixing length and eddy viscosity as the Reynolds number decreases. The level and trend of this low Reynolds number effect agrees with similar results previously obtained at low speeds when wall conditions are used in the correlating parameter. Examination of the wall-damping effect on the mixing length indicates more validity for evaluating the Van Driest damping scale by using wall conditions than by using local sublayer properties and that the impermeable-wall damping constant may be somewhat greater at hypersonic conditions than the usual low-speed value of 26. In several instances, areas of disagreement occurred between the expected and observed behavior of the data, usually concerning the shape of the published velocity profiles. Indications are that the total-temperature data obtained in hypersonic, low Reynolds number, cold-wall boundary layers may not be suitably corrected for conditions near the wall. There is a clear need for more complete investigations of the mean flow structure of hypersonic turbulent boundary layers, especially at cold-wall conditions.

Langley Research Center,
National Aeronautics and Space Administration,
Hampton, Va., June 30, 1971.

REFERENCES

1. Bushnell, Dennis M.; and Beckwith, Ivan E.: Calculation of Nonequilibrium Hypersonic Turbulent Boundary Layers and Comparisons With Experimental Data. AIAA J., vol. 8, no. 8, Aug. 1970, pp. 1462-1469.

2. Patankar, S. V.; and Spalding, D. B.: Heat and Mass Transfer in Boundary Layers. Morgan-Grampian (London), 1967.

3. Bradshaw, P.; and Ferriss, D. H.: Calculation of Boundary-Layer Development Using the Turbulent Energy Equation. II – Compressible Flow on Adiabatic Walls. NPL Aero Rep. 1217, Brit. A.R.C., Nov. 24, 1966.

4. Noel, François: Calcul par Différences Finies des Couches Limites Laminaires ou Turbulentes Avec ou Sans Injection Pariétale. L'Aéronautique et L'Astronautique, vol. 14, no. 7, 1969, pp. 65-75.

5. Adams, John C., Jr.: Eddy Viscosity-Intermittency Factor Approach to Numerical Calculation of Transitional Heating on Sharp Cones in Hypersonic Flow. AEDC-TR-70-210, U.S. Air Force, Nov. 1970.

6. Herring, H. James; and Mellor, George L.: A Method of Calculating Compressible Turbulent Boundary Layers. NASA CR-1144, 1968.

7. Anderson, Larry W.; and Kendall, Robert M.: A Nonsimilar Solution for Multicomponent Reacting Laminar and Turbulent Boundary Layer Flows Including Transverse Curvature. AFWL-TR-69-106, U.S. Air Force, Mar. 1970. (Available from DDC as AD 867 904.)

8. Lynes, Larry L.; Nielsen, Jack N.; and Kuhn, Gary D.: Calculation of Compressible Turbulent Boundary Layers With Pressure Gradients and Heat Transfer. NASA CR-1303, 1969.

9. Sontowski, J. F.: An Eddy Viscosity Model for Compressible Turbulent Boundary Layers. Tech. Inform. Ser. No. 69SD241, Re-Entry Systems, Gen. Elec. Co., July 1969.

10. Cebeci, Tuncer; Smith, A. M. O.; and Mosinskis, G.: Calculation of Compressible Adiabatic Turbulent Boundary Layers. AIAA Paper No. 69-687, June 1969.

11. Harris, Julius E.: Numerical Solution of the Equations for Compressible Laminar, Transitional, and Turbulent Boundary Layers and Comparisons With Experimental Data. NASA TR R-368, 1971.

12. Maise, George; and McDonald, Henry: Mixing Length and Kinematic Eddy Viscosity in a Compressible Boundary Layer. AIAA J., vol. 6, no. 1, Jan. 1968, pp. 73-80.

13. Clauser, Francis H.: The Turbulent Boundary Layer. Vol. IV of Advances in Applied Mechanics, H. L. Dryden and Th. von Kármán, eds., Academic Press, Inc., 1956, pp. 1-51.

14. Squire, L. C.: A Law of the Wall for Compressible Turbulent Boundary Layers With Air Injection. J. Fluid Mech., vol. 37, pt. 3, 1969, pp. 449-456.

15. Simpson, Roger L.: Characteristics of Turbulent Boundary Layers at Low Reynolds Numbers With and Without Transpiration. J. Fluid Mech., vol. 42, pt. 4, 1970, pp. 769-802.

16. McDonald, H.: Mixing Length and Kinematic Eddy Viscosity in a Low Reynolds Number Boundary Layer. Rep. J214453-1, Res. Lab., United Aircraft Corp., Sept. 1970.

17. Bradshaw, P.: The Response of a Constant-Pressure Turbulent Boundary Layer to the Sudden Application of an Adverse Pressure Gradient. R. & M. No. 3575, Brit. A.R.C., 1969.

18. Martellucci, A.; Rie, H.; and Sontowski, J. F.: Evaluation of Several Eddy Viscosity Models Through Comparison With Measurements in Hypersonic Flows. AIAA Paper 69-688, June 1969.

19. Mayne, Arloe W., Jr.; and Dyer, D. F.: Comparisons of Theory and Experiment for Turbulent Boundary Layers on Simple Shapes at Hypersonic Conditions. Proceedings of the 1970 Heat Transfer and Fluid Mechanics Institute, Turgut Sarpkaya, ed., Stanford Univ. Press, 1970, pp. 168-188.

20. Cebeci, Tuncer: Calculation of Compressible Turbulent Boundary Layers With Heat and Mass Transfer. AIAA Paper No. 70-741, June-July 1970.

21. Fischer, Michael C.; Maddalon, Dal V.; Weinstein, Leonard M.; and Wagner, Richard D., Jr.: Boundary-Layer Surveys on a Nozzle Wall at $M_\infty \approx 20$ Including Hot-Wire Fluctuation Measurements. AIAA Paper No. 70-746, June-July 1970.

22. Meier, H. U.; and Rotta, J. C.: Experimental and Theoretical Investigations of Temperature Distributions in Supersonic Boundary Layers. AIAA Paper No. 70-744, June-July 1970.

23. Spence, D. A.: Distributions of Velocity, Enthalpy and Shear Stress in the Compressible Turbulent Boundary Layer on a Flat Plate. Rep. No. Aero.2631, Brit. R.A.E., Nov. 1959.

24. Poe, Gary G.; and Holsen, James N.: Shear Stress Distributions in Turbulent Compressible Boundary Layers. Tech. Note, Dep. Chem. Eng., Washington Univ., June 15, 1968.

25. Escudier, M. P.: The Distribution of the Mixing Length in Turbulent Flows Near Walls. Rep. No. TWF/TN/1, Mech. Eng. Dep., Imp. Coll. Sci. Technol., Mar. 1965.

26. Bushnell, Dennis M.; Johnson, Charles B.; Harvey, William D.; and Feller, William V.: Comparison of Prediction Methods and Studies of Relaxation in Hypersonic Turbulent Nozzle-Wall Boundary Layers. NASA TN D-5433, 1969.

27. Tetervin, Neal: An Exploratory Theoretical Investigation of the Effect of Longitudinal Surface Curvature on the Turbulent Boundary Layer. NOLTR 69-22, U.S. Navy, Feb. 1969. (Available from DDC as AD 691 419.)

28. Bradshaw, P.: The Analogy Between Streamline Curvature and Buoyancy in Turbulent Shear Flow. NPL Aero Rep. 1231, Brit. A.R.C., May 1, 1967.

29. Van Driest, E. R.: On Turbulent Flow Near a Wall. J. Aeronaut. Sci., vol. 23, no. 11, Nov. 1956, pp. 1007-1011.

30. Jones, Robert A.; and Feller, William V.: Preliminary Surveys of the Wall Boundary Layer in a Mach 6 Axisymmetric Tunnel. NASA TN D-5620, 1970.

31. Perry, J. H.: An Experimental Study of the Turbulent Hypersonic Boundary Layer at High Rates of Wall Heat Transfer. Ph. D. Thesis, Univ. of Southampton, June 1968.

32. Fiore, Anthony W.: Turbulent Boundary Layer Measurements at Hypersonic Mach Numbers. ARL 70-0166, U.S. Air Force, Aug. 1970.

33. Lee, R. E.; Yanta, W. J.; and Leonas, A. C.: Velocity Profile, Skin-Friction Balance and Heat-Transfer Measurements of the Turbulent Boundary Layer at Mach 5 and Zero-Pressure Gradient. NOLTR 69-106, U.S. Navy, June 16, 1969.

34. Adcock, Jerry B.; Peterson, John B., Jr.; and McRee, Donald I.: Experimental Investigation of a Turbulent Boundary Layer at Mach 6, High Reynolds Numbers, and Zero Heat Transfer. NASA TN D-2907, 1965.

35. Samuels, Richard D.; Peterson, John B., Jr.; and Adcock, Jerry B.: Experimental Investigation of the Turbulent Boundary Layer at a Mach Number of 6 With Heat Transfer at High Reynolds Numbers. NASA TN D-3858, 1967.

36. Danberg, James E.: Characteristics of the Turbulent Boundary Layer With Heat and Mass Transfer: Data Tabulation. NOLTR 67-6, U.S. Navy, Jan. 23, 1967. (Available from DDC as AD 650 272.)

37. Johnson, Charles B.; and Bushnell, Dennis M.: Power-Law Velocity-Profile-Exponent Variations With Reynolds Number, Wall Cooling, and Mach Number in a Turbulent Boundary Layer. NASA TN D-5753, 1970.

38. Beckwith, Ivan E.; Harvey, William D.; and Clark, Frank L.: Comparisons of Turbulent-Boundary-Layer Measurements at Mach Number 19.5 With Theory and an Assessment of Probe Errors. NASA TN D-6192, 1971.

39. Cebeci, Tuncer: A Model for Eddy-Conductivity and Turbulent Prandtl Number. Rep. No. MDC-J0747/01, McDonnell Douglas Corp., May 1970.

40. Bradshaw, P.: The Turbulence Structure of Equilibrium Boundary Layers. NPL Aero Rep. 1184, Brit. A.R.C., Jan. 21, 1966.

41. Kemp, Joseph H., Jr.; and Owen, F. K.: Nozzle Wall Boundary Layers at Mach Numbers 20 to 47. AIAA Paper No. 71-161, Jan. 1971.

42. Bradshaw, P.: Special Topics in Turbulent Flows. VKI LS 10,1, Von Karman Inst. Fluid Dyn., Jan. 1969.

43. Coles, D. E.: The Turbulent Boundary Layer in a Compressible Fluid. R-403-PR (Contract No. AF 49(638)-700), RAND Corp., Sept. 1962. (Available from DDC as AD 285 651.)

44. Narayanan, M. A. Badri; and Ramjee, V.: Reverse Transition From Turbulent to Laminar Boundary Layer in a Highly Accelerated Flow. J. Aeronaut. Soc. India, vol. 20, no. 1, Feb. 1968, pp. 39-59.

45. Morkovin, Mark V.: Critical Evaluation of Transition From Laminar to Turbulent Shear Layers With Emphasis on Hypersonically Traveling Bodies. AFFDL-TR-68-149, U.S. Air Force, Mar. 1969. (Available from DDC as AD 686 178.)

46. Patankar, S. V.: Wall-Shear-Stress and Heat-Flux Laws for Turbulent Boundary Layer With a Pressure Gradient: Use of Van Driest's Eddy-Viscosity Hypothesis. Dep. Mech. Eng., Imp. Coll. Sci. Technol., May 1966.

TABLE I.- EDGE AND PROFILE PARAMETERS

Parameter	Profile examined								
	Axisymmetric nozzle wall		Axisymmetric nozzle-wall extension (ref. 30)	Conical nozzle wall (ref. 31)	Two-dimensional nozzle wall (ref. 33)		Hollow cylinder		Flat plate (ref. 36)
	Ref. 21	Ref. 32					Ref. 34	Ref. 35	
$\frac{C_f}{2}$	9.75×10^{-5}	7.50×10^{-4} 4.00×10^{-4}	4.50×10^{-4}	5.25×10^{-4} 2.60×10^{-4}	3.60×10^{-4}	4.3×10^{-4}	3.00×10^{-4}	3.00×10^{-4}	9.5×10^{-4}
R_θ	6.90×10^3	1.12×10^3	8.00×10^3	12.80×10^3	57×10^3	5.0×10^3	1.4×10^4	1.28×10^4	2.53×10^3
M_e	20.0	12.00	5.76	10.65	4.67	4.7	6.02	5.98	6.5
$\left(\frac{\delta}{\rho_e u_e^2}\right)\left(\frac{dp_e}{dx}\right)$	-7.0×10^{-5}	-6.1×10^{-4}	2.2×10^{-4}	-4.7×10^{-4}	0	0	0	0	0
$\frac{d\delta}{dx}$	0.056	0.038	0.017	0.024	0.007	0.0085	0.0116	0.010	0.030
$\frac{T_w}{T_o}$	1.000	0.295	0.730	0.260	0.700	0.700	0.895	0.450	0.480
$\frac{\rho_w}{\rho_e}$	0.007	0.119	0.1787	0.164	0.259	0.275	0.135	0.274	0.218
$\frac{dr_w}{dx}$	0.06	0.052	0	0.0625	0	0	0	0	0
R_{sl}	84.73	125.96 172.48	119.28	176.74 251.15	268.22	252.89	212.13	302.21	151.48
$\frac{\delta}{r_w}$	0.4735	0.4670	0.4400	0.4930	0	0	0.0920	0.0814	0
δ^+	106.5	66.5 48.6	574.0	573.0 404.0	2841.0	323.0	456.0	995.0	295.0
K	0.65	----------	0.445	----------	0.49	----------	0.61	0.51	----------
$\left(\frac{\epsilon}{u_e \delta_i^*}\right)_{max}$	0.060	0.0132	0.023	0.0162	----------	----------	0.0172	0.0135	0.0320
$\left(\frac{l}{\delta}\right)_{max}$	0.2 to 0.3	0.075	0.08	0.081	0.068 to 0.078	0.1 to 0.12	0.06 to 0.08	0.06 to 0.08	0.095
$\frac{\delta^*}{\delta_i^*}$	8.9945	2.8109	3.3905	2.9219	2.5624	2.5484	4.9275	----------	3.9572
$\frac{\delta_i^*}{\delta}$	0.0515	0.1953	0.1077	0.1327	0.1406	0.1420	0.1048	0.0837	0.1056

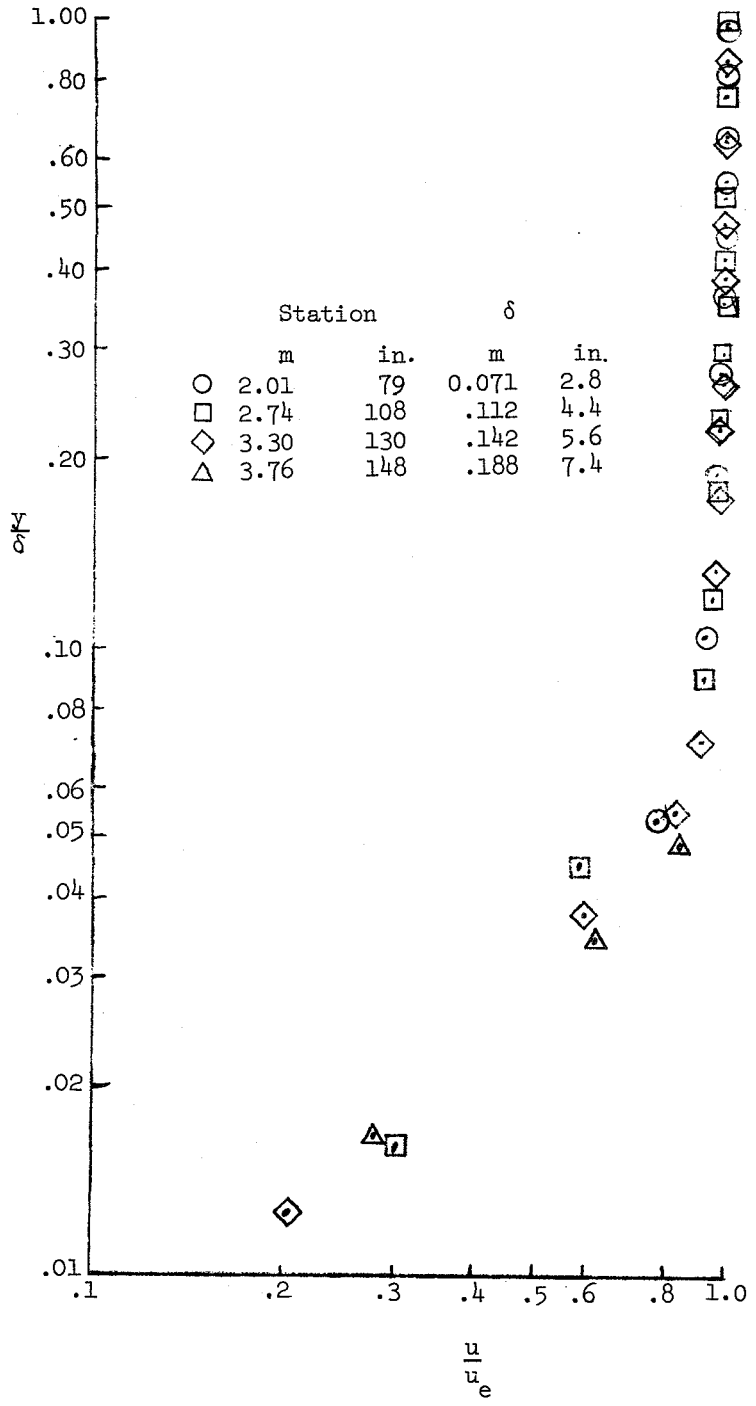

Figure 1.- Velocity profiles from reference 21 at $M_e = 20$ in assumed similarity coordinates. $\frac{T_w}{T_o} = 1.0$; $R_\theta \approx 7 \times 10^3$.

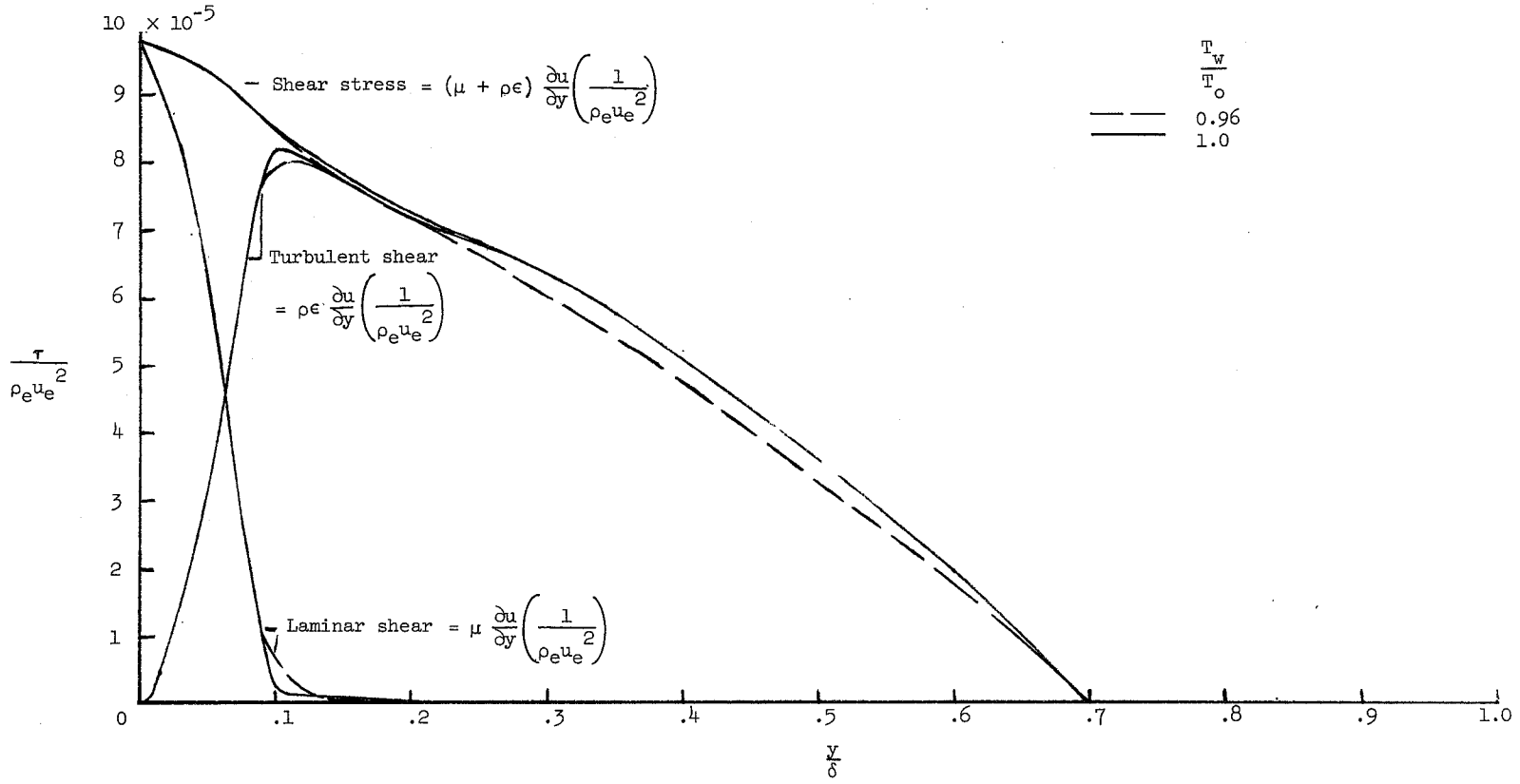

(a) Shear-stress distribution.

Figure 2.- Shear-stress, eddy-viscosity, and mixing-length distributions for a helium nozzle-wall boundary layer at $M_e = 20.8$. Profile data from reference 21; $R_\theta = 6.90 \times 10^3$.

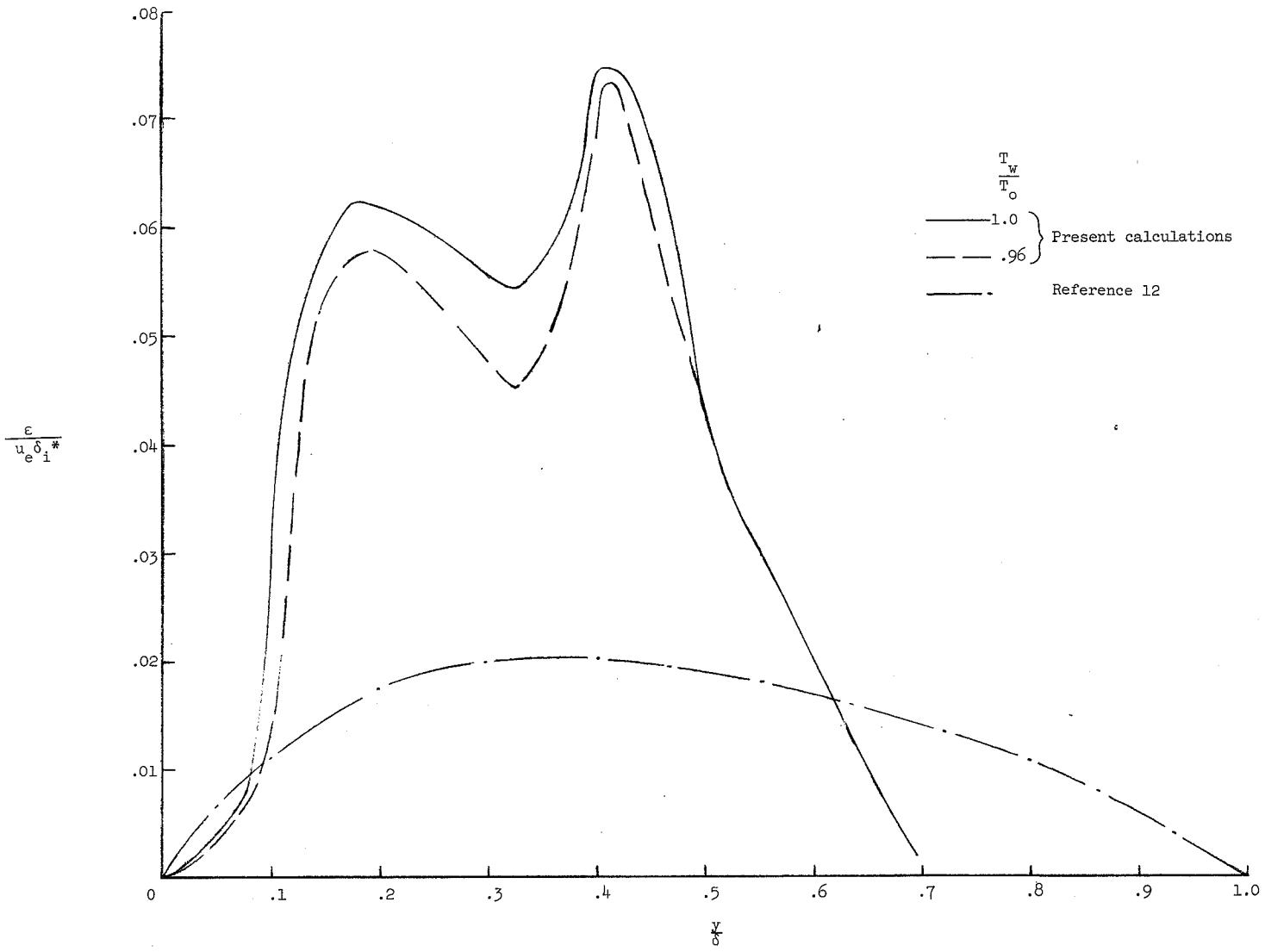

(b) Eddy-viscosity distribution.

Figure 2.- Continued.

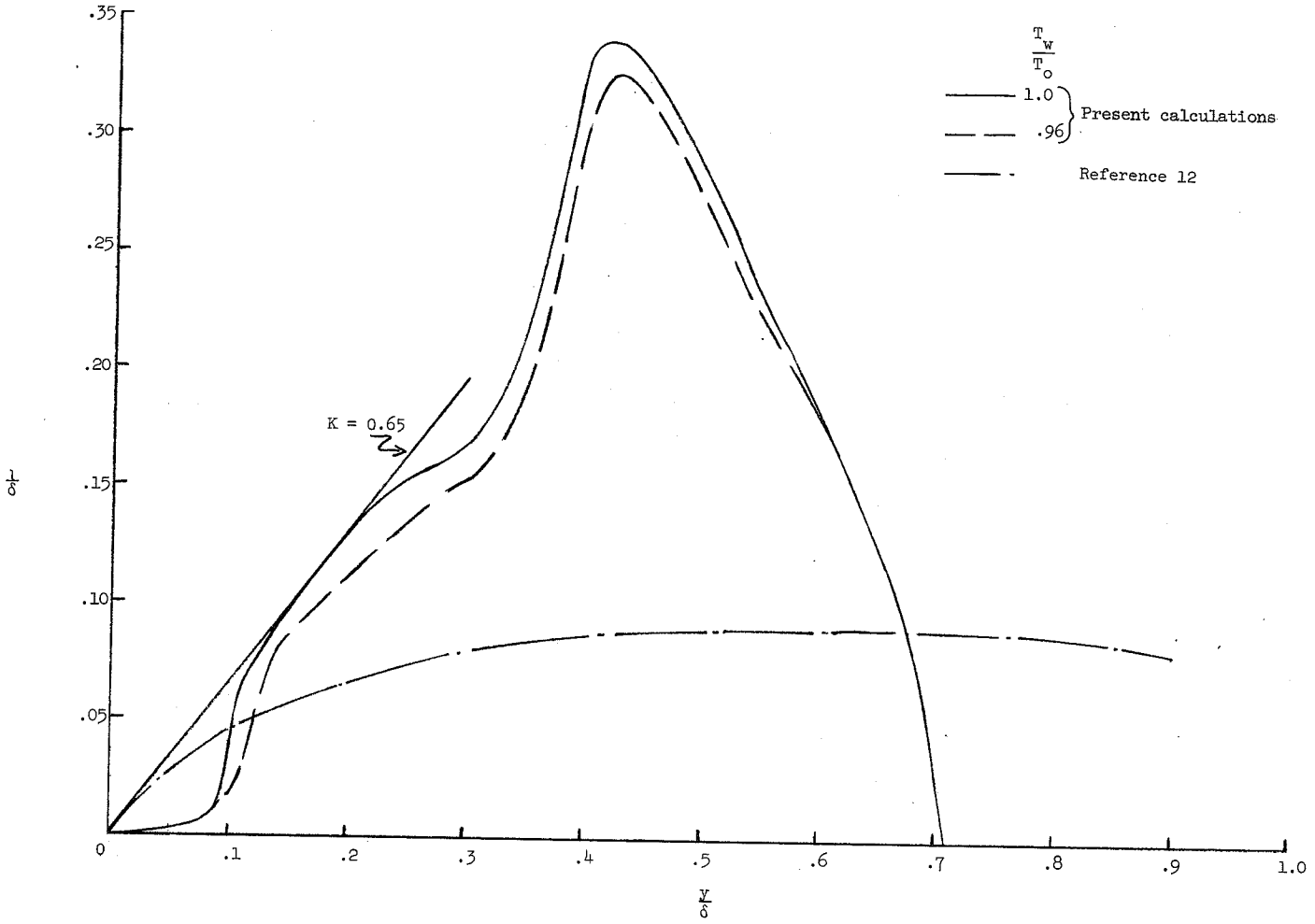

(c) Mixing-length distribution.

Figure 2.- Concluded.

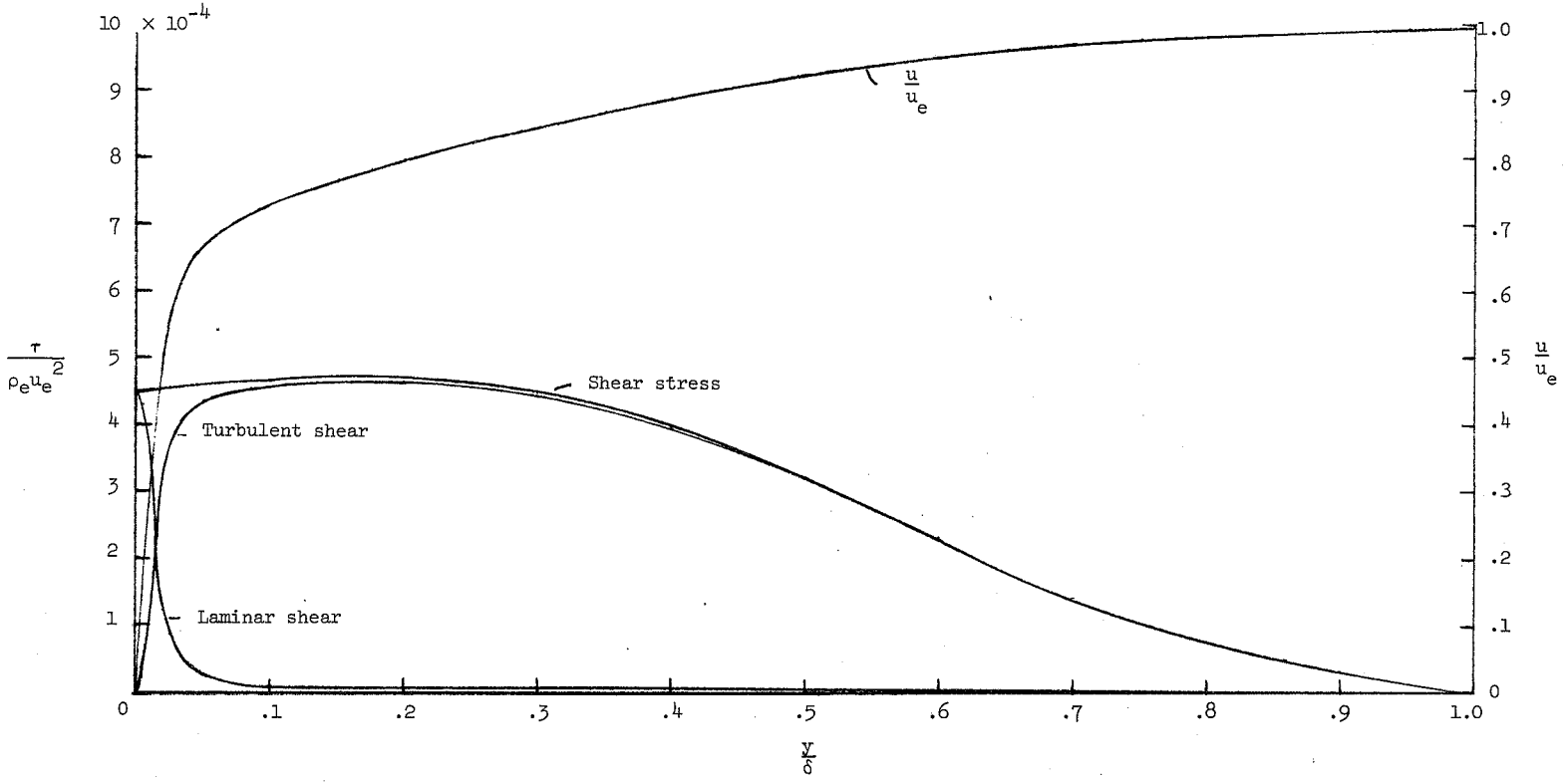

(a) Shear-stress and velocity profile.

Figure 3.- Shear-stress, eddy-viscosity, and mixing-length distributions for an axisymmetric nozzle-wall boundary layer at $M_e = 5.76$. Profile data from reference 30; $R_\theta = 8.00 \times 10^3$.

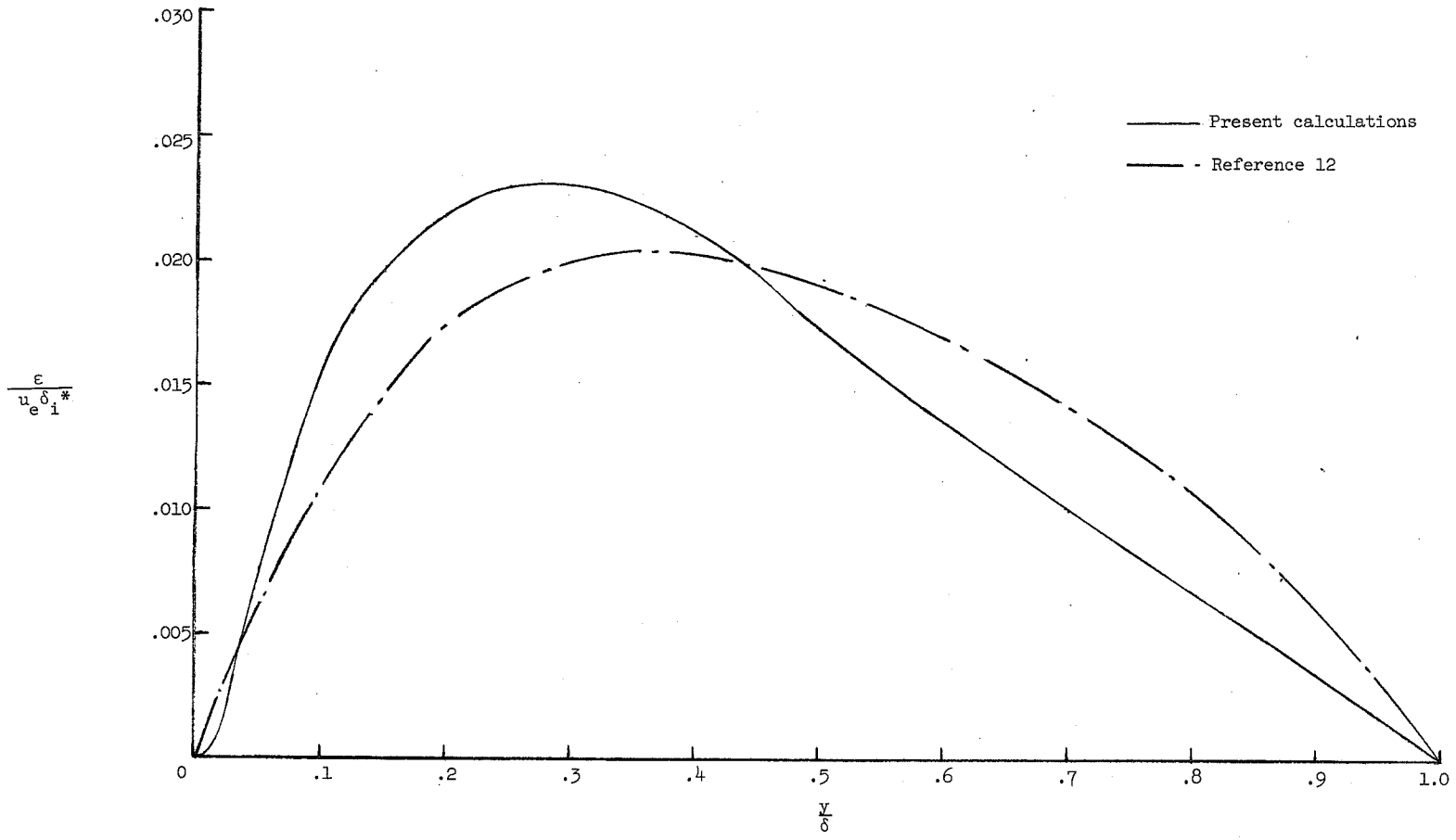

(b) Eddy-viscosity distribution.

Figure 3.- Continued.

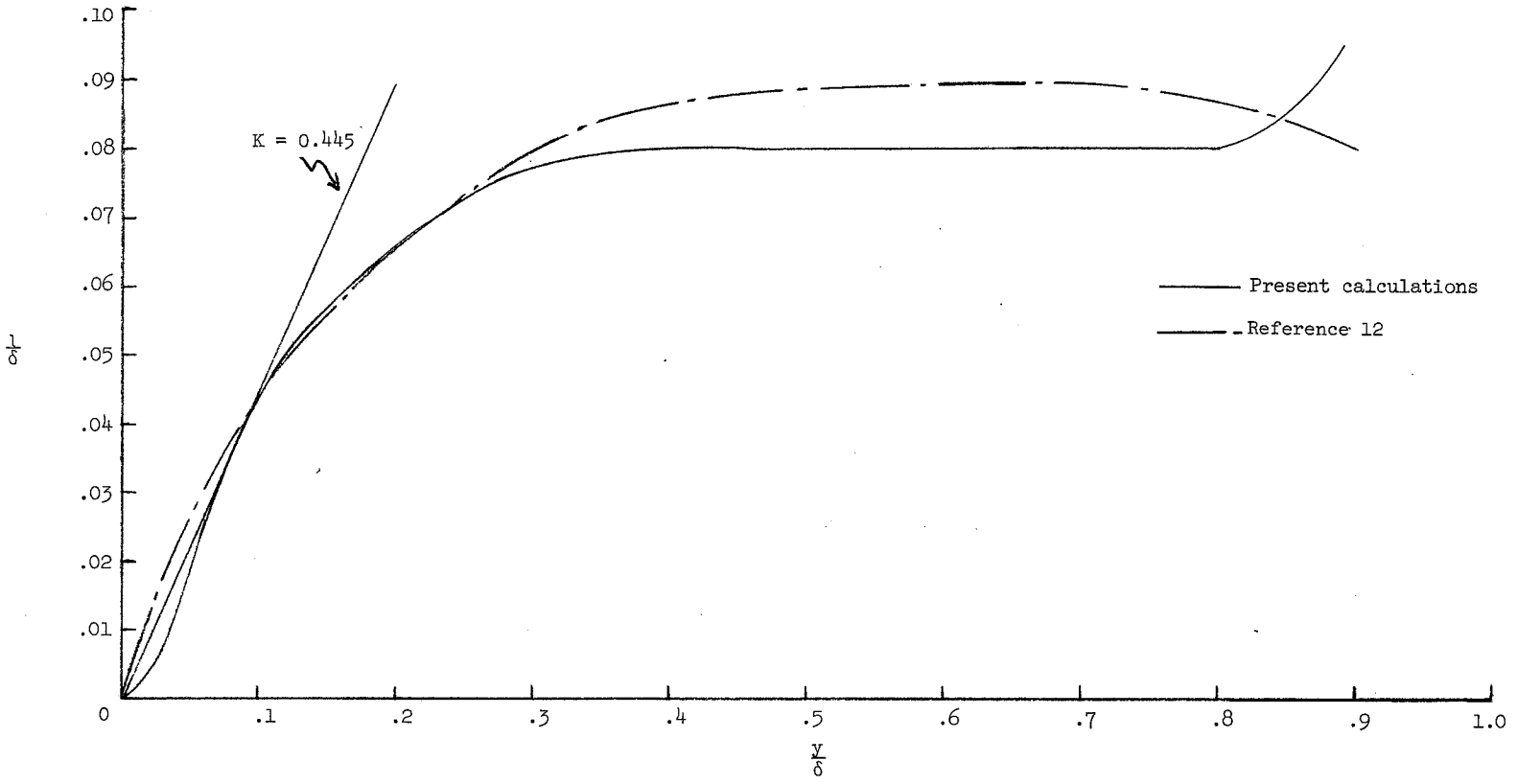

(c) Mixing-length distribution.

Figure 3.- Concluded.

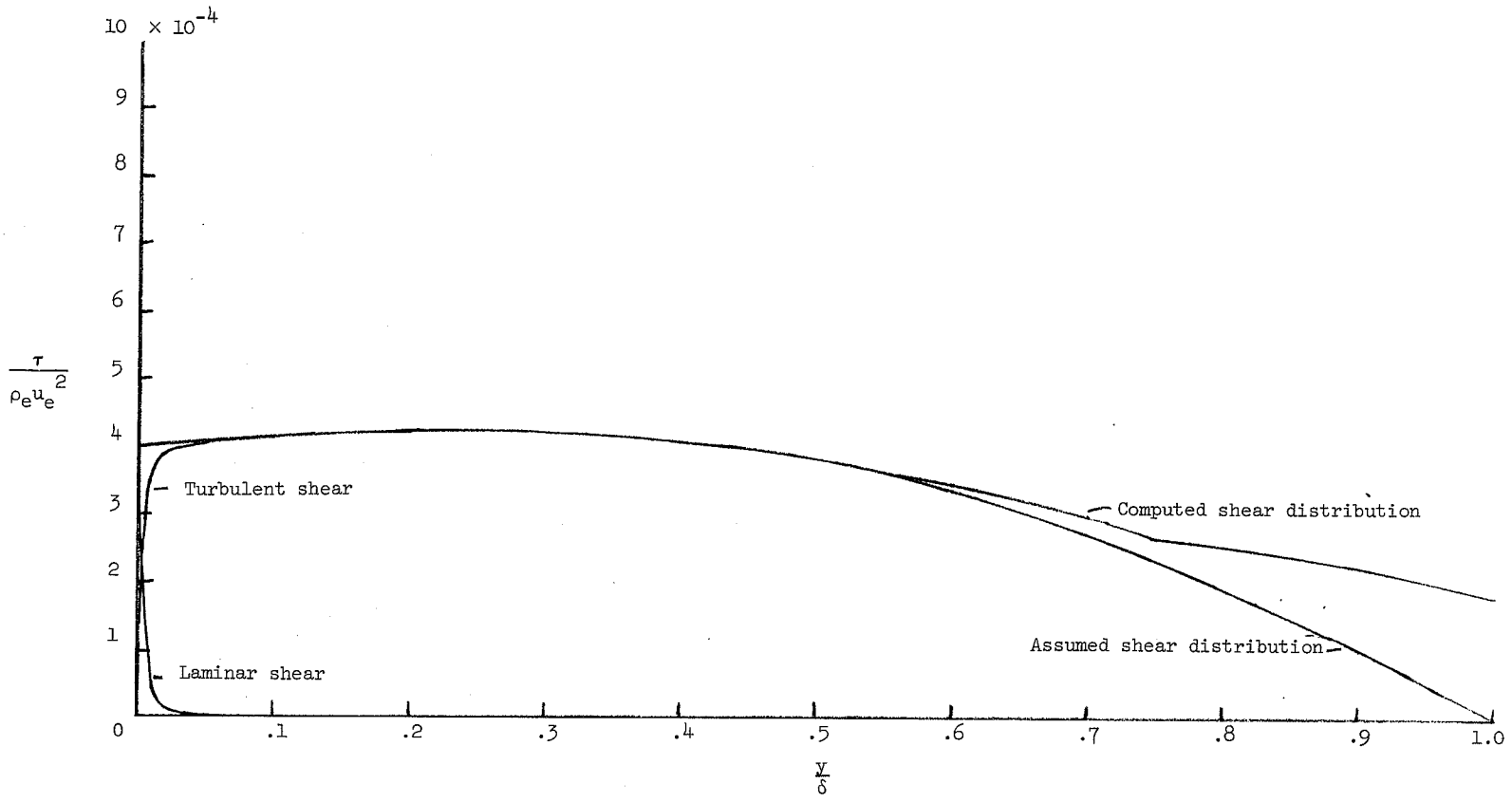

(a) Shear-stress distribution.

Figure 4.- Shear-stress, eddy-viscosity, and mixing-length distributions for an axisymmetric nozzle-wall boundary layer at $M_e = 5.75$. Profile data from reference 30; $R_\theta = 8.00 \times 10^3$.

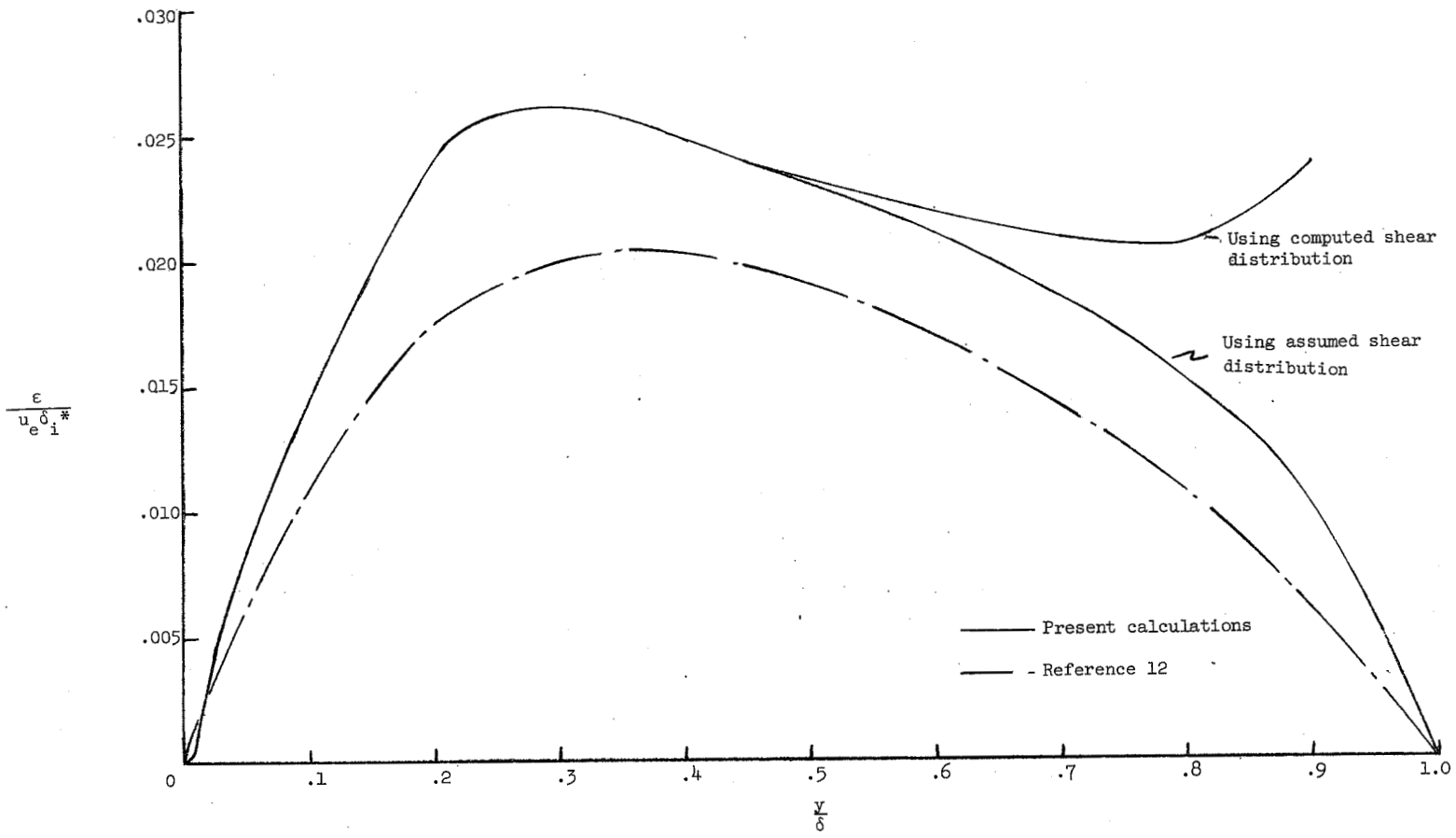

(b) Eddy-viscosity distribution.

Figure 4.- Continued.

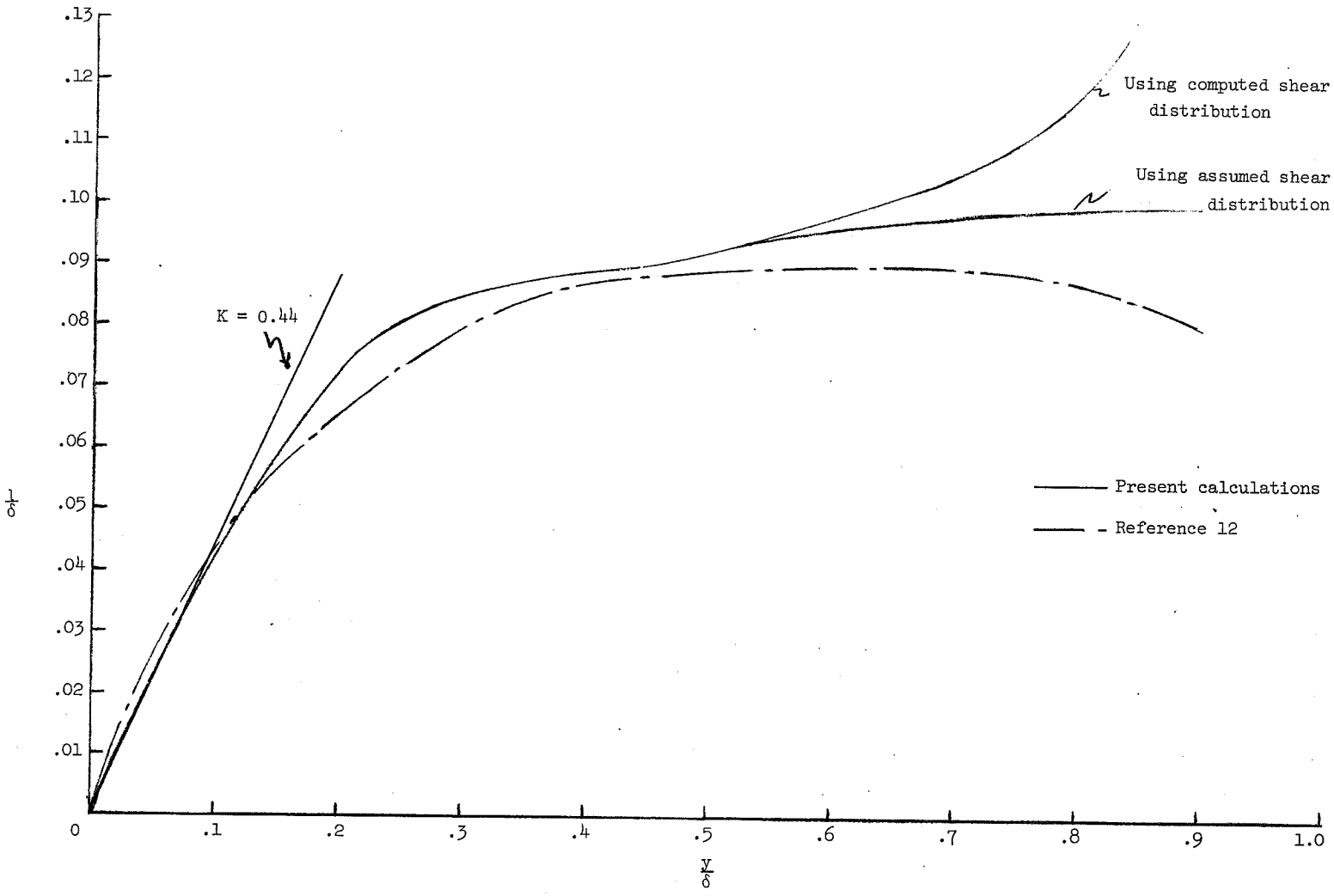

(c) Mixing-length distribution.

Figure 4.- Concluded.

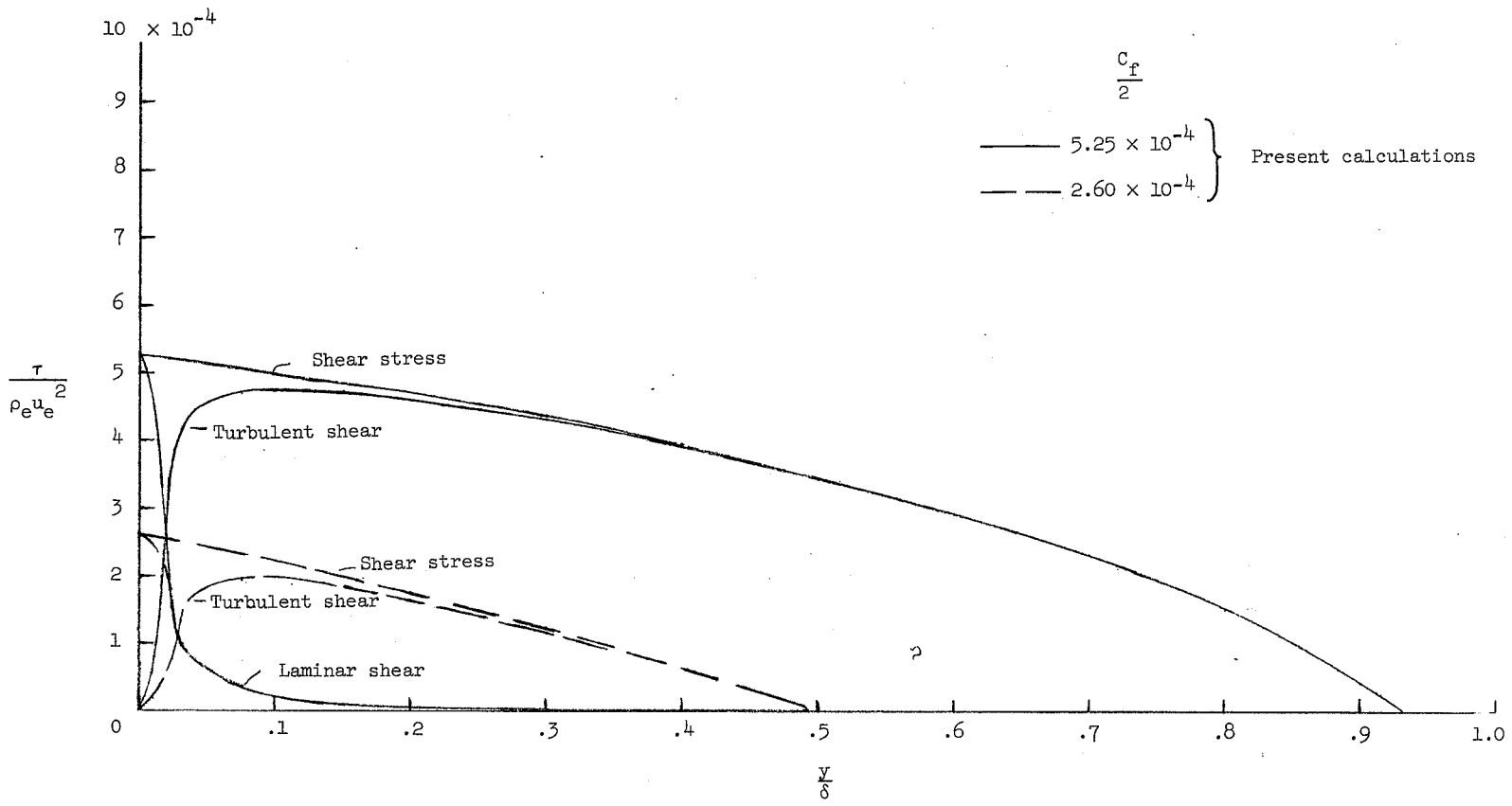

(a) Shear-stress distribution.

Figure 5.- Shear-stress, eddy-viscosity, and mixing-length distributions for a conical nozzle-wall boundary layer at $M_e = 10.65$. Profile data from reference 31; $R_\theta = 12.80 \times 10^3$.

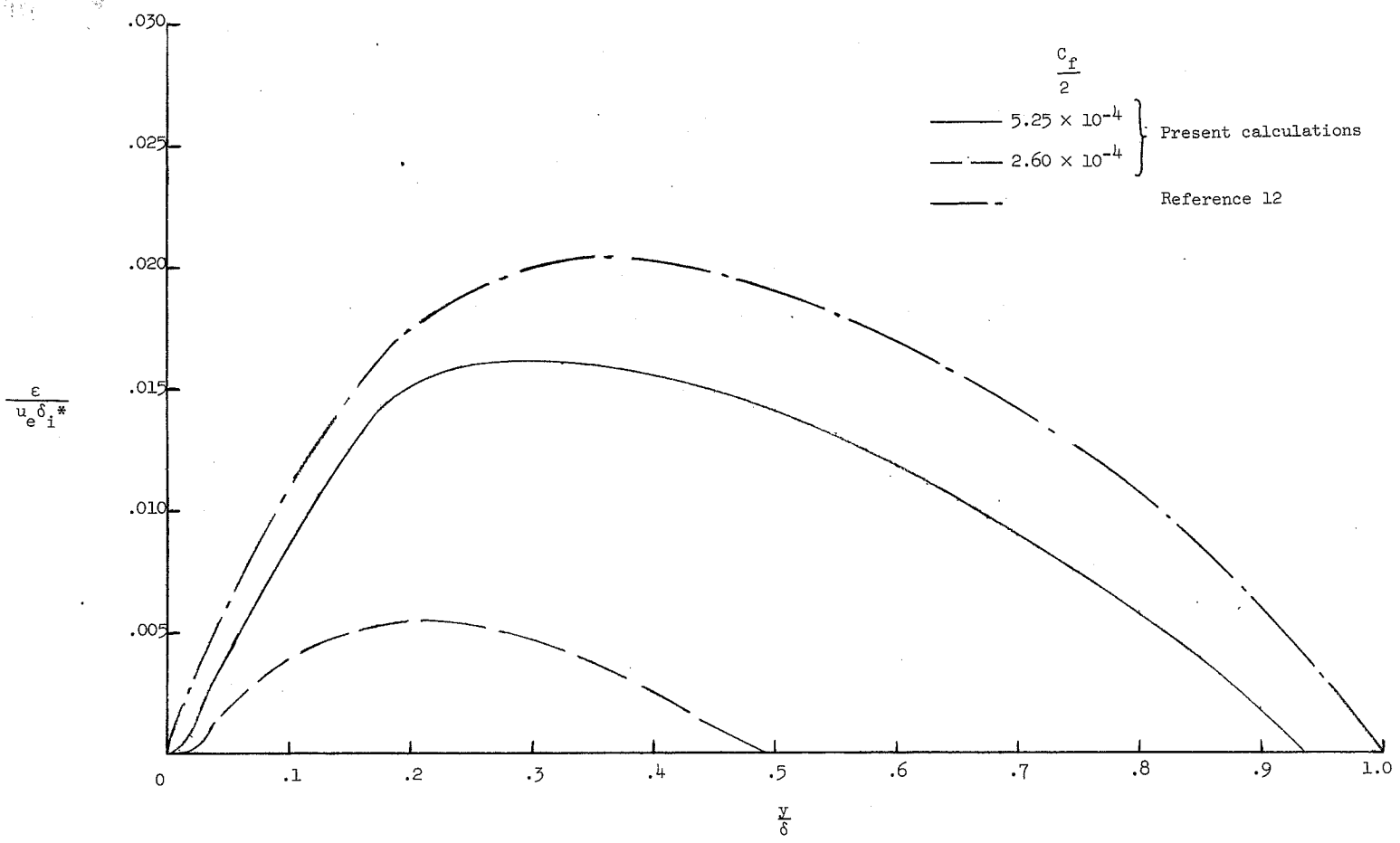

(b) Eddy-viscosity distribution.

Figure 5.- Continued.

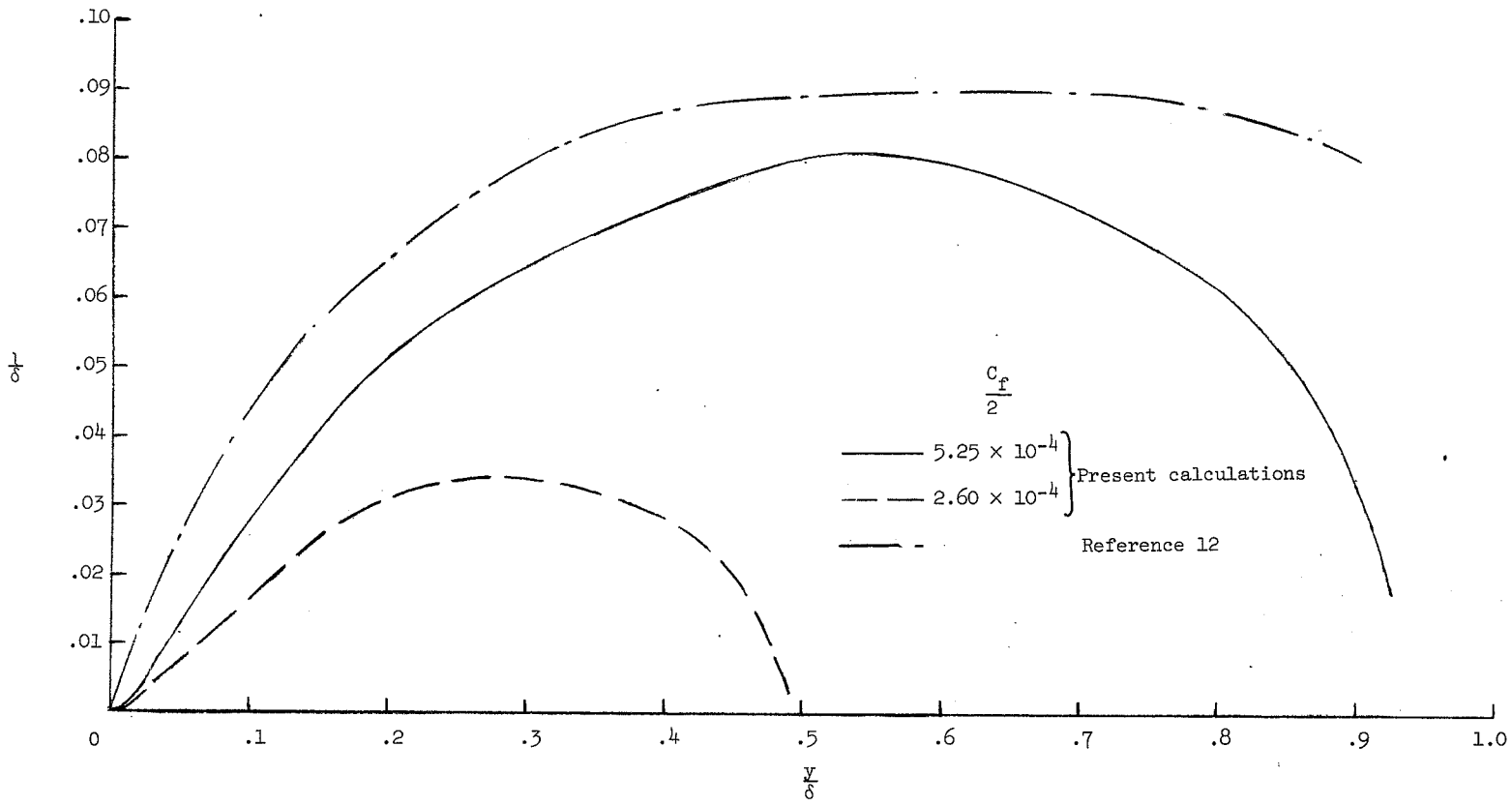

(c) Mixing-length distribution.

Figure 5.- Concluded.

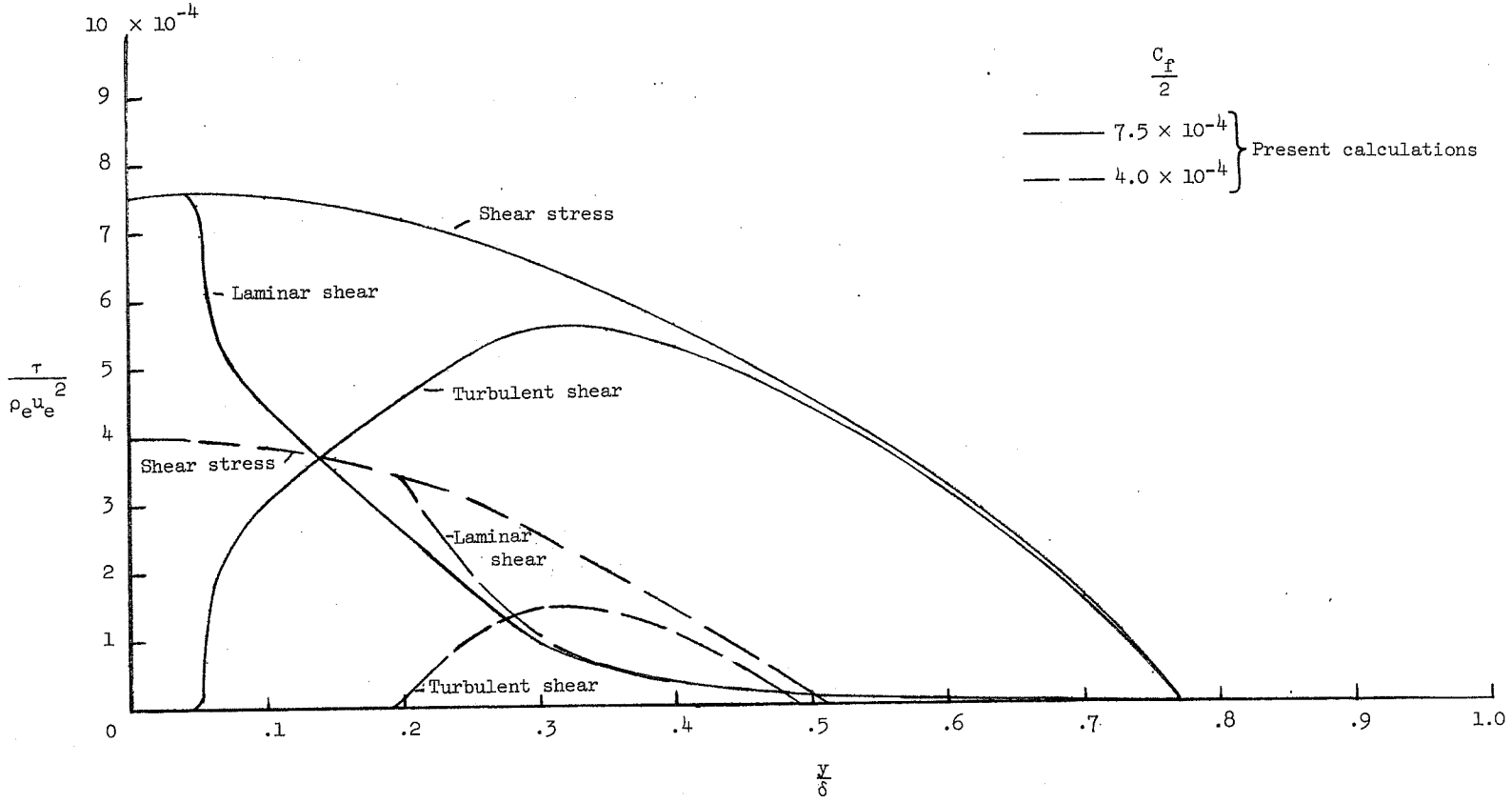

(a) Shear-stress distribution.

Figure 6.- Shear-stress, eddy-viscosity, and mixing-length distributions and velocity-profile data for an axisymmetric nozzle-wall boundary layer at $M_e = 12$. Profile data from reference 32, $R_\theta = 1.12 \times 10^3$.

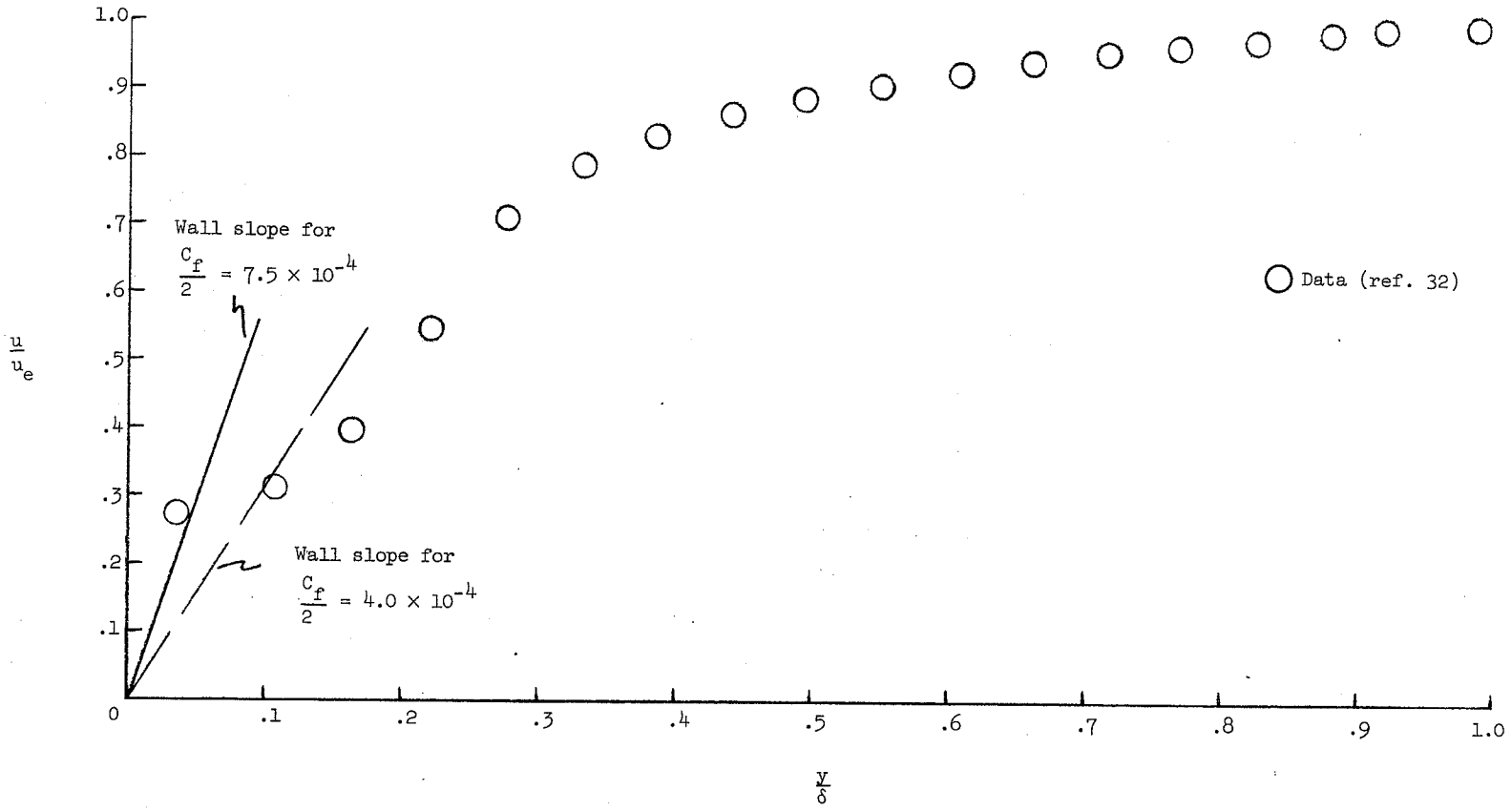

(b) Velocity-profile data.

Figure 6.- Continued.

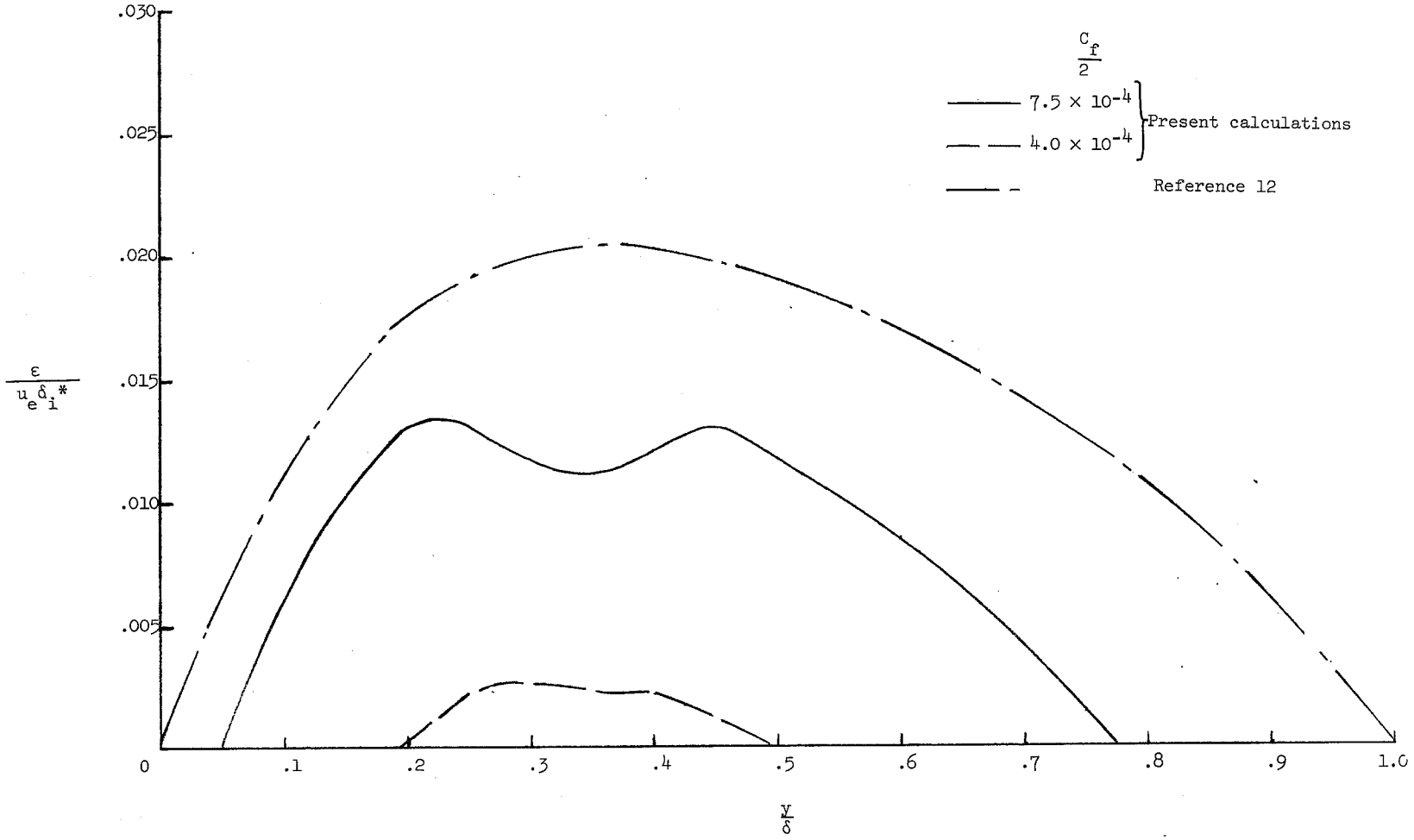

(c) Eddy-viscosity distribution.

Figure 6.- Continued.

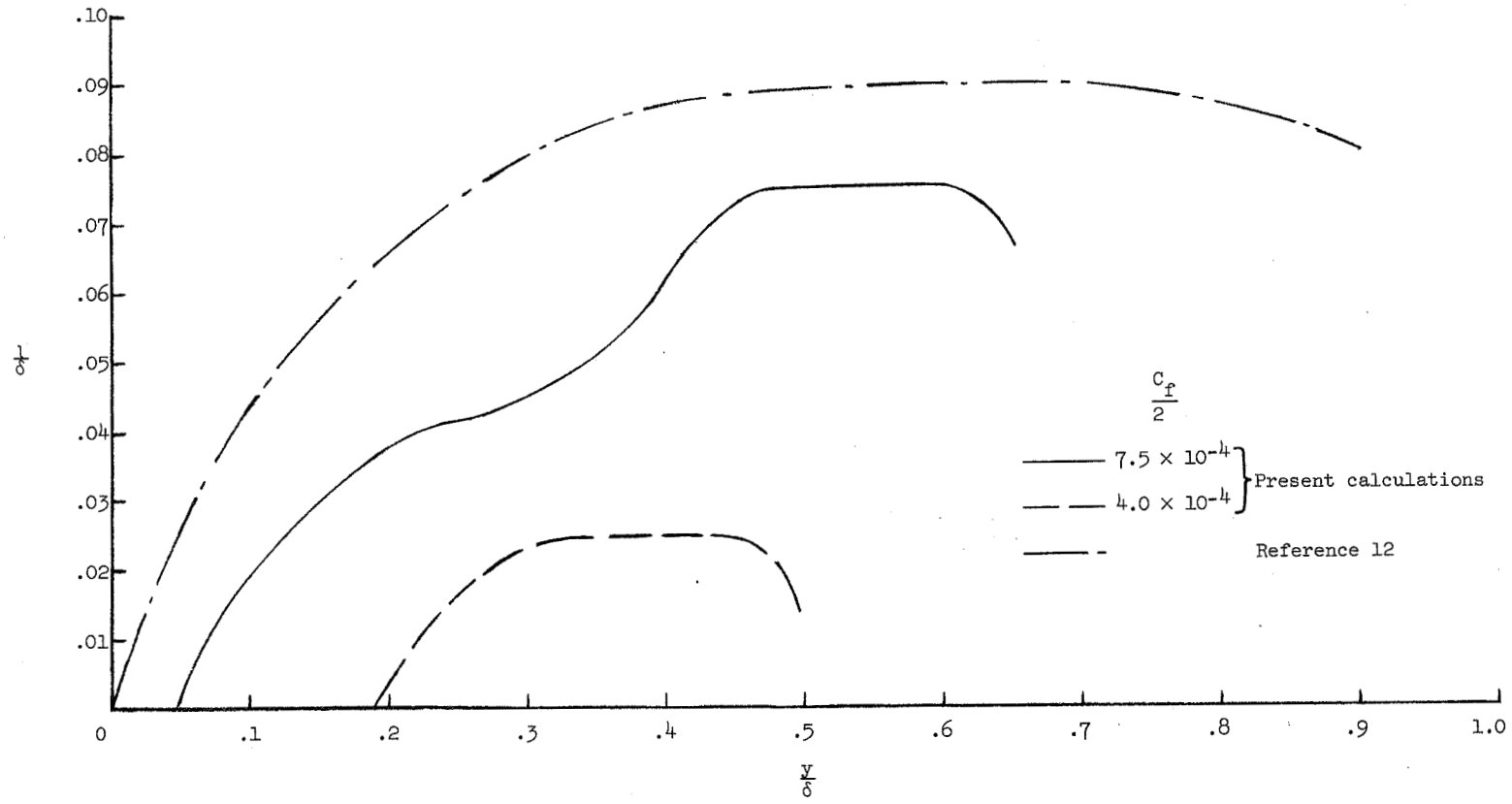

(d) Mixing-length distribution.

Figure 6.- Concluded.

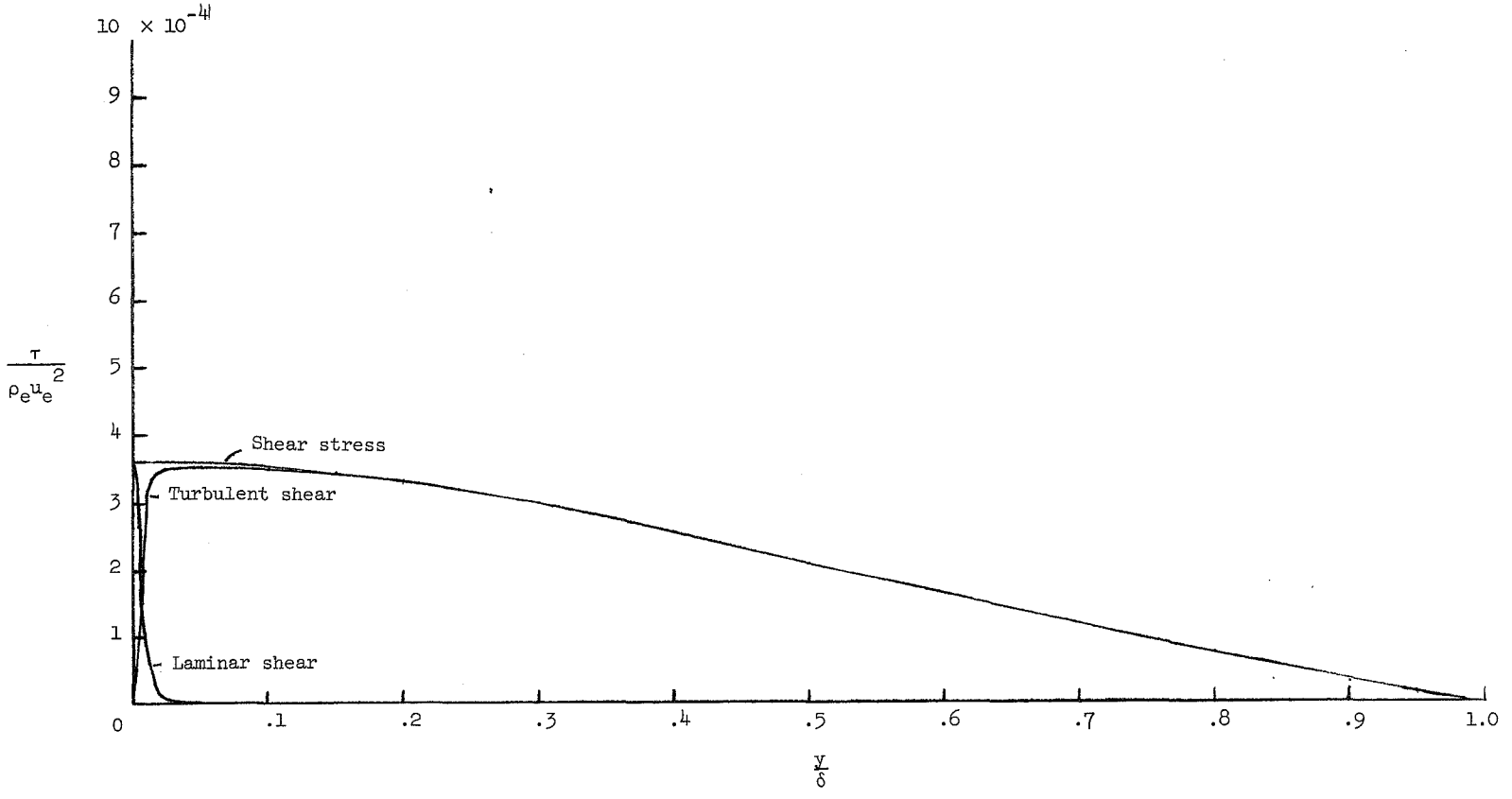

(a) Shear-stress distribution.

Figure 7.- Shear-stress, eddy-viscosity, and mixing-length distributions for a two-dimensional nozzle-wall boundary layer at $M_e = 4.67$. Profile data from reference 33; $R_\theta = 57 \times 10^3$.

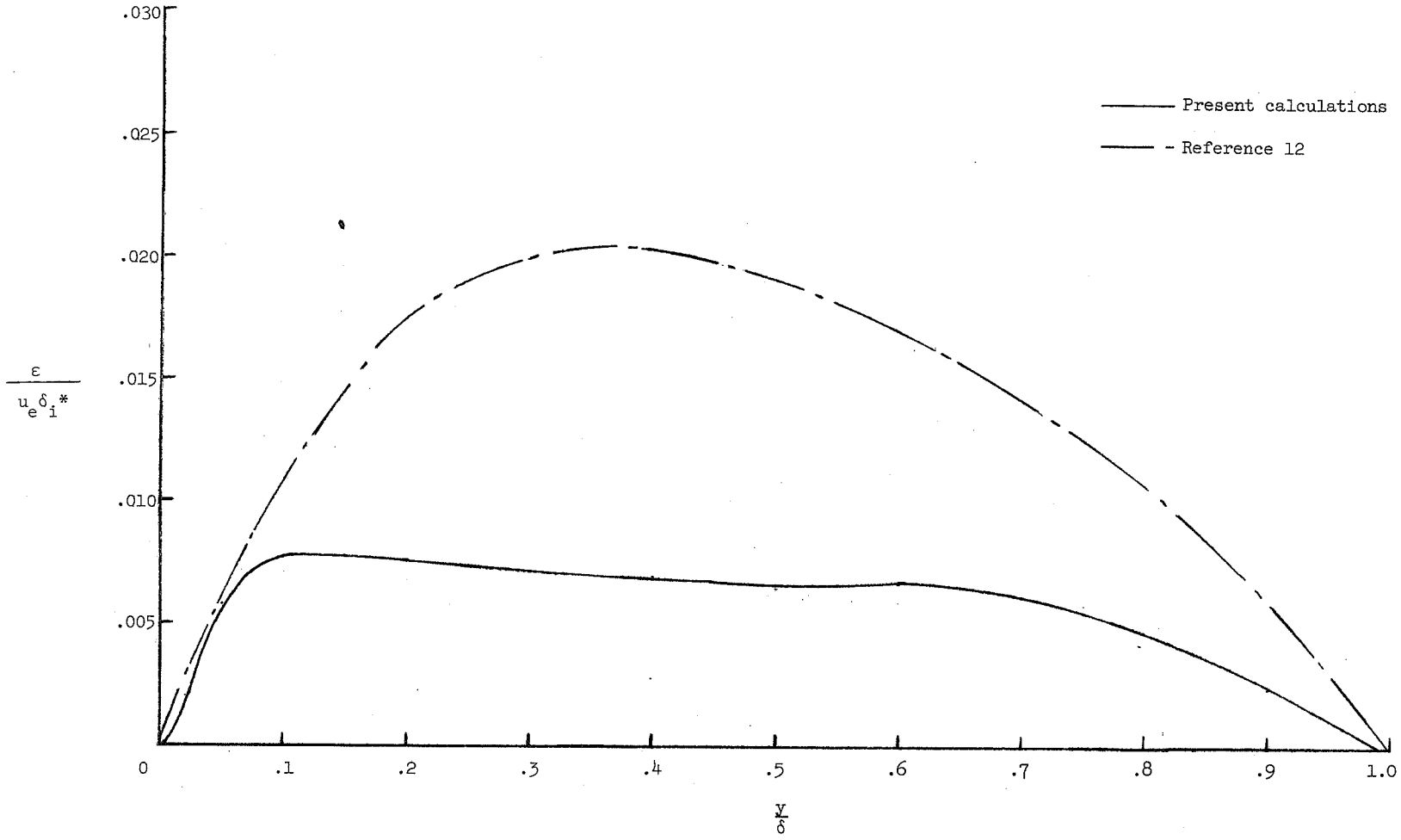

(b) Eddy-viscosity distribution.

Figure 7.- Continued.

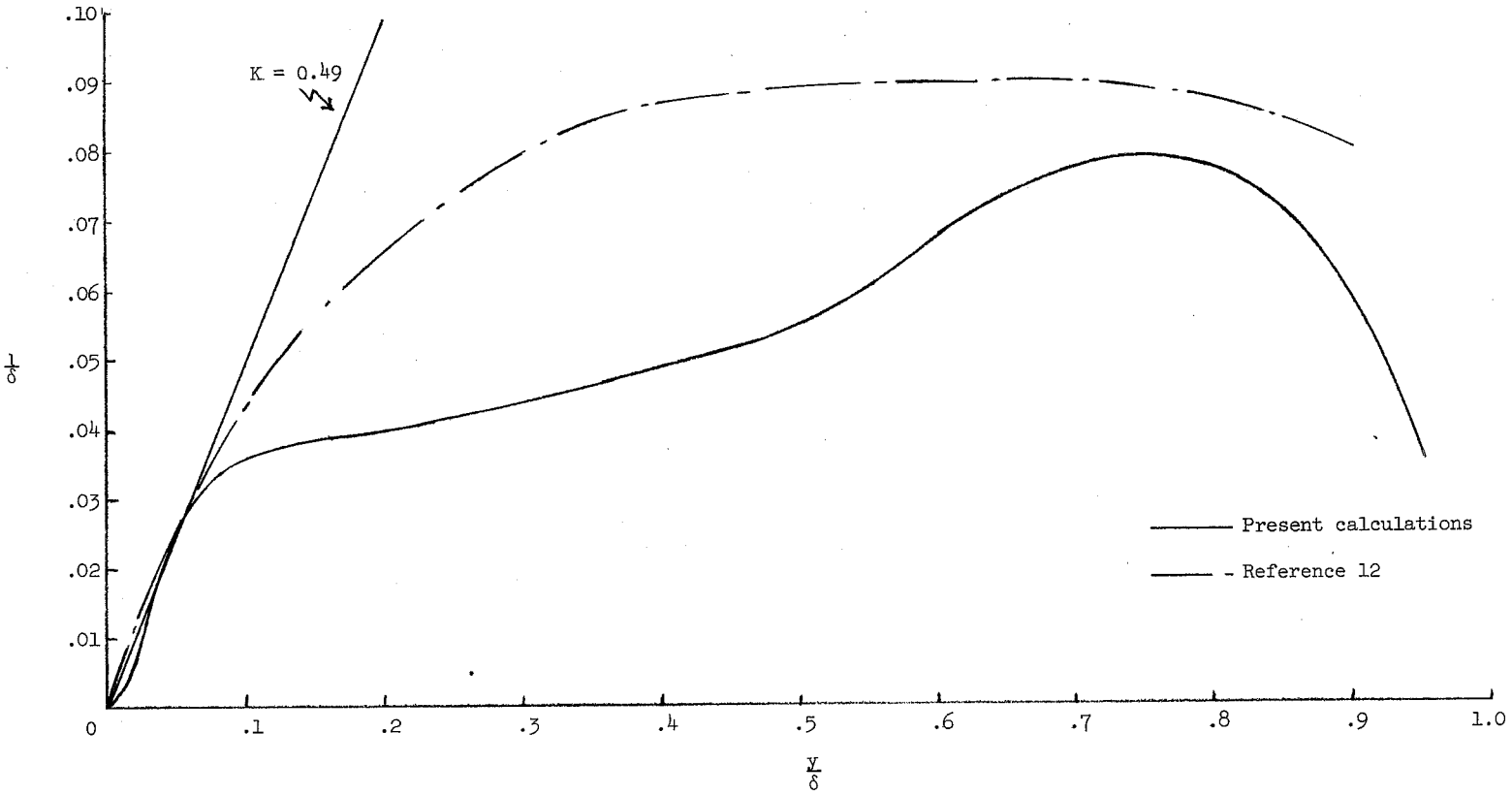

(c) Mixing-length distribution.

Figure 7.- Concluded.

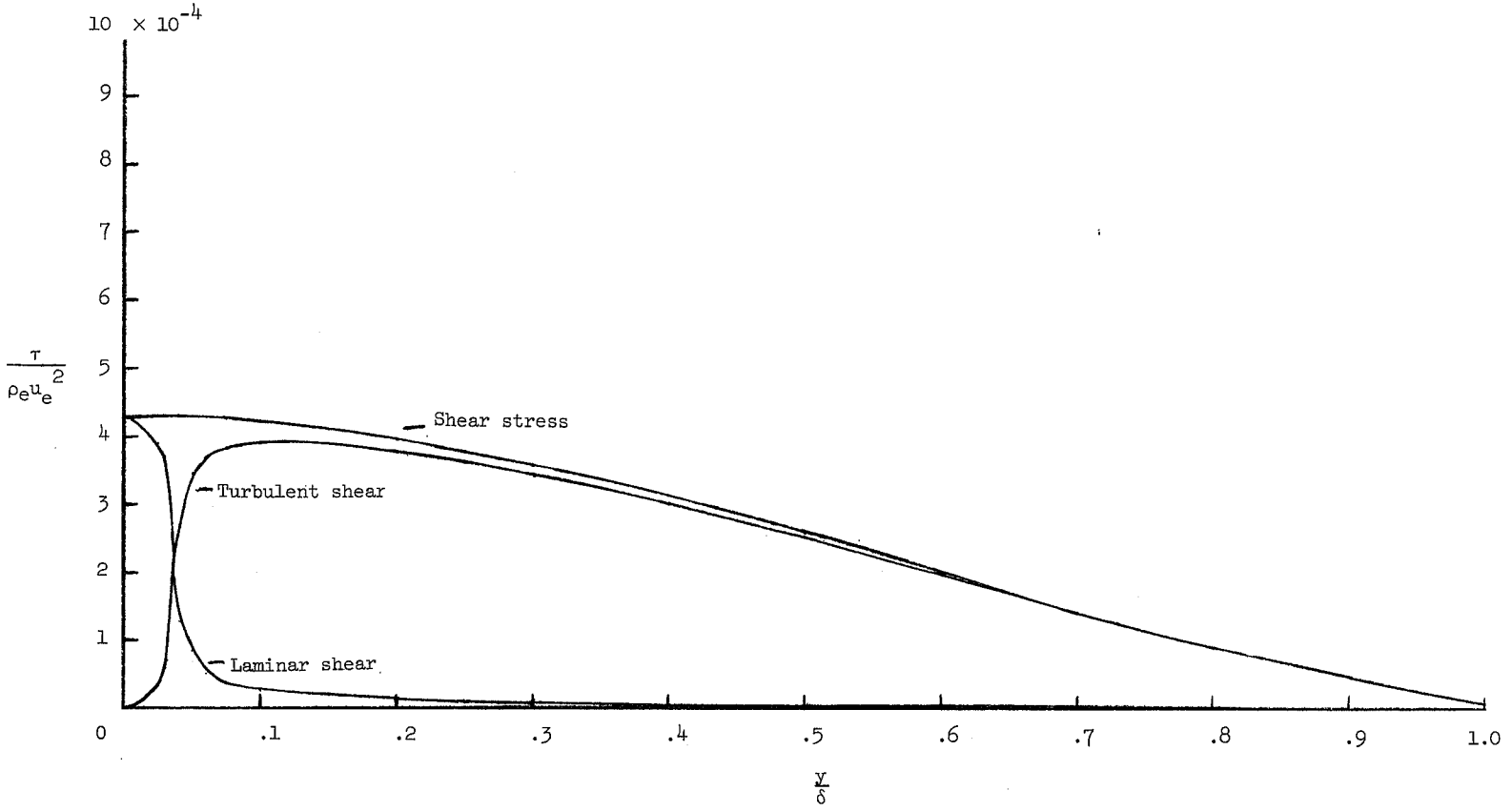

(a) Shear-stress distribution.

Figure 8.- Shear-stress, eddy-viscosity, and mixing-length distributions for a two-dimensional nozzle-wall boundary layer at $M_e = 4.7$. Profile data from reference 33; $R_\theta = 5.0 \times 10^3$.

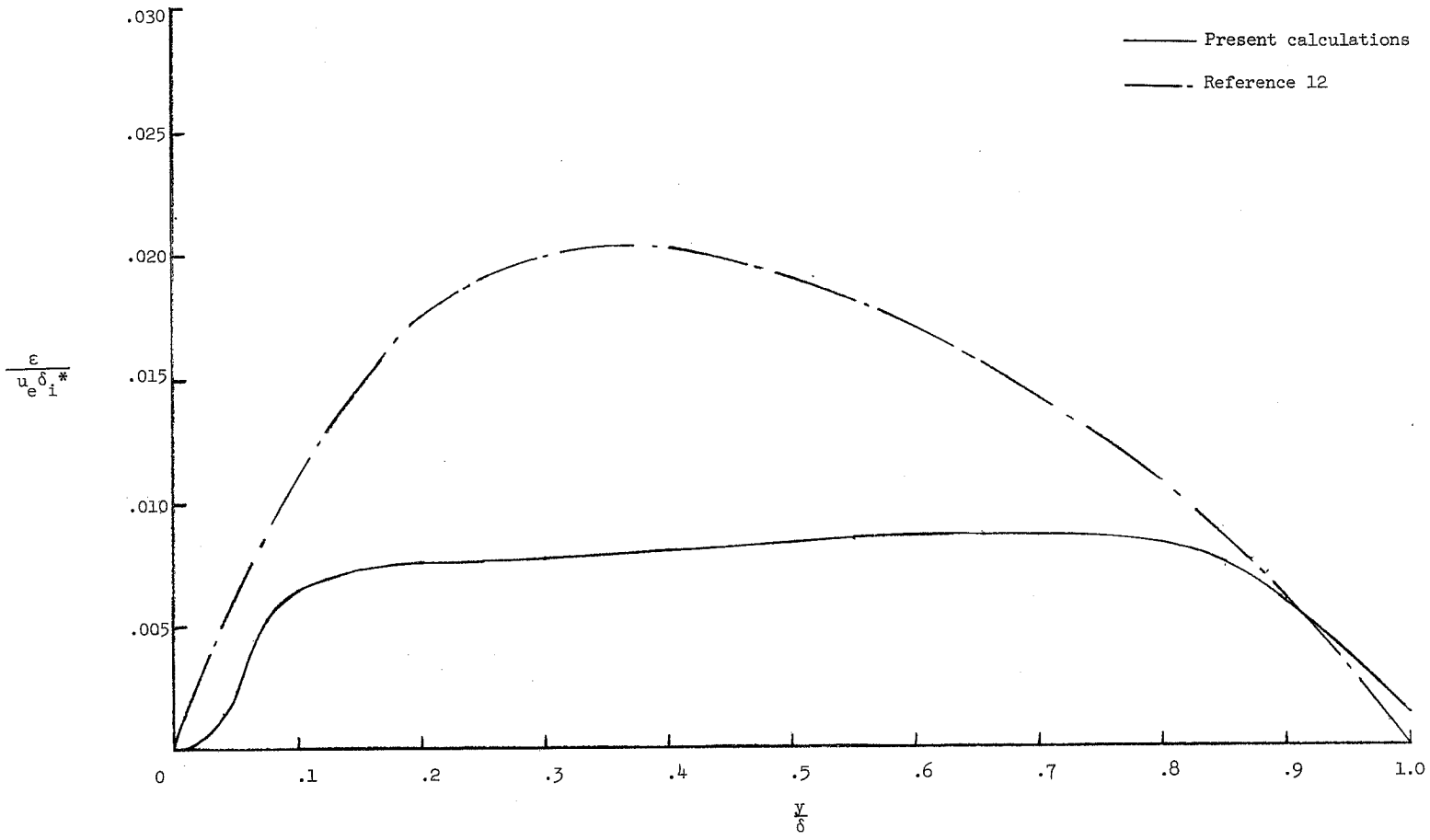

(b) Eddy-viscosity distribution.

Figure 8.- Continued.

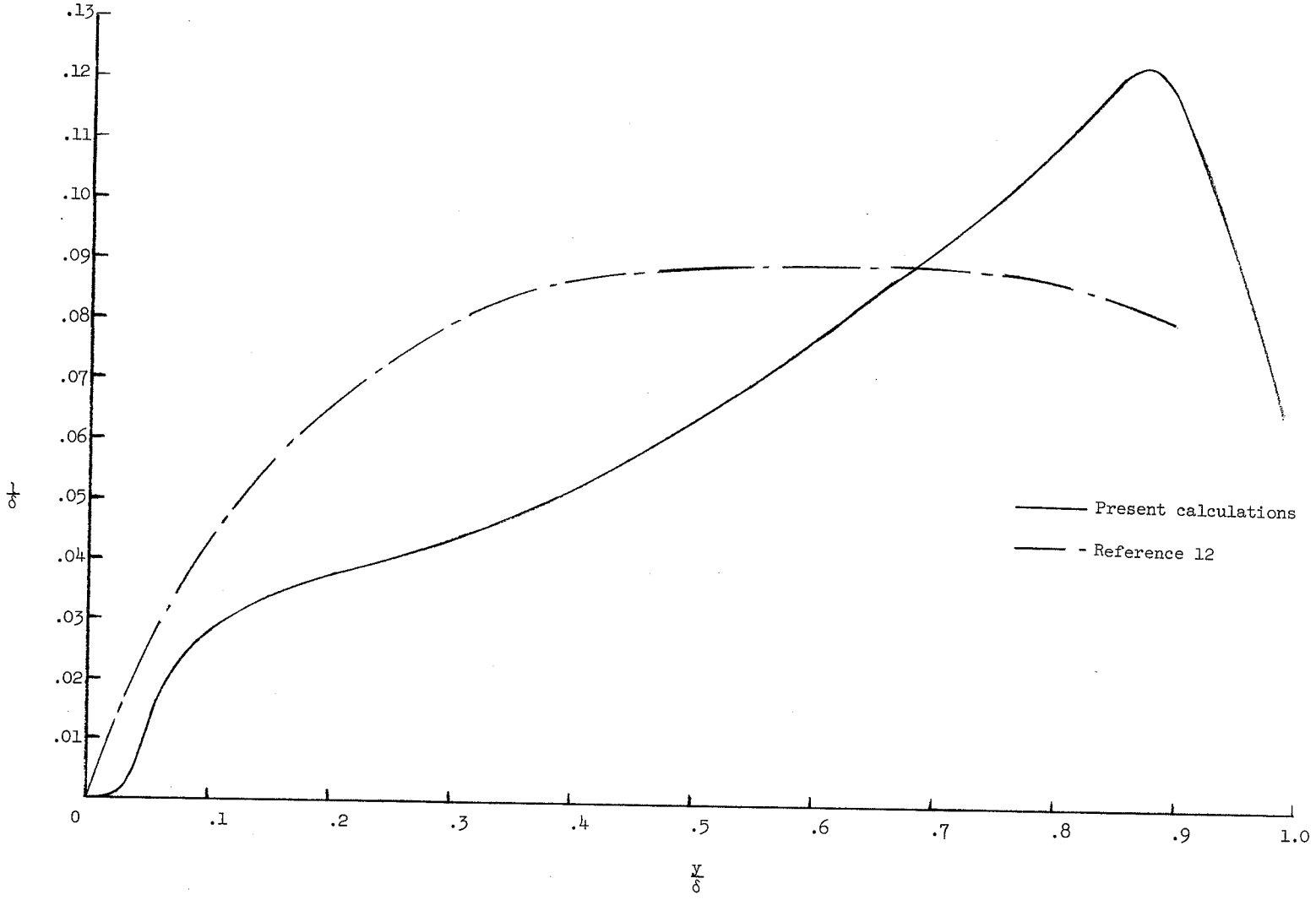

(c) Mixing-length distribution.

Figure 8.- Concluded.

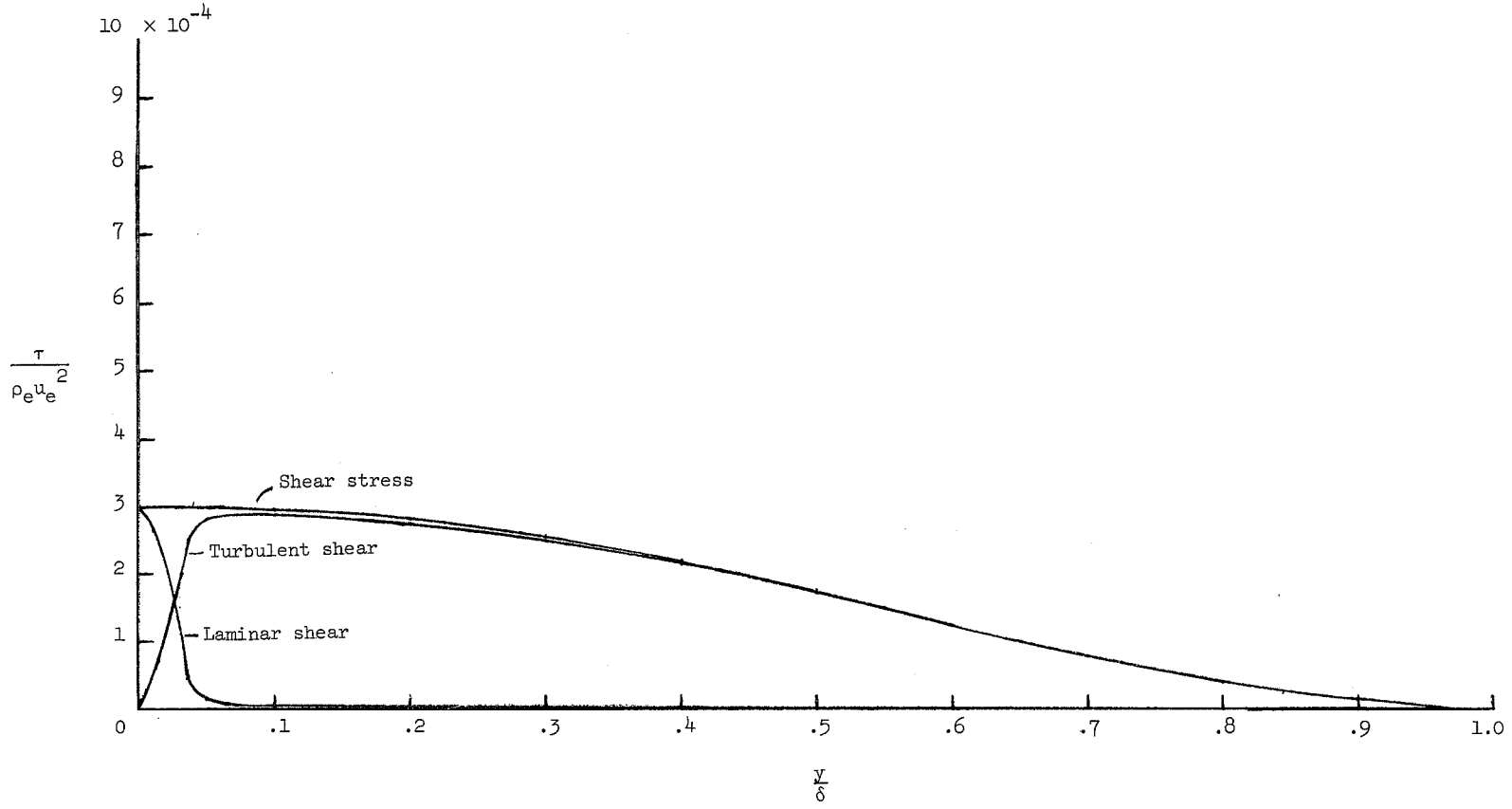

(a) Shear-stress distribution.

Figure 9.- Shear-stress, eddy-viscosity, and mixing-length distributions for a boundary layer on a hollow cylinder at $M_e = 6.02$. Profile data from reference 34; $R_\theta = 1.4 \times 10^4$.

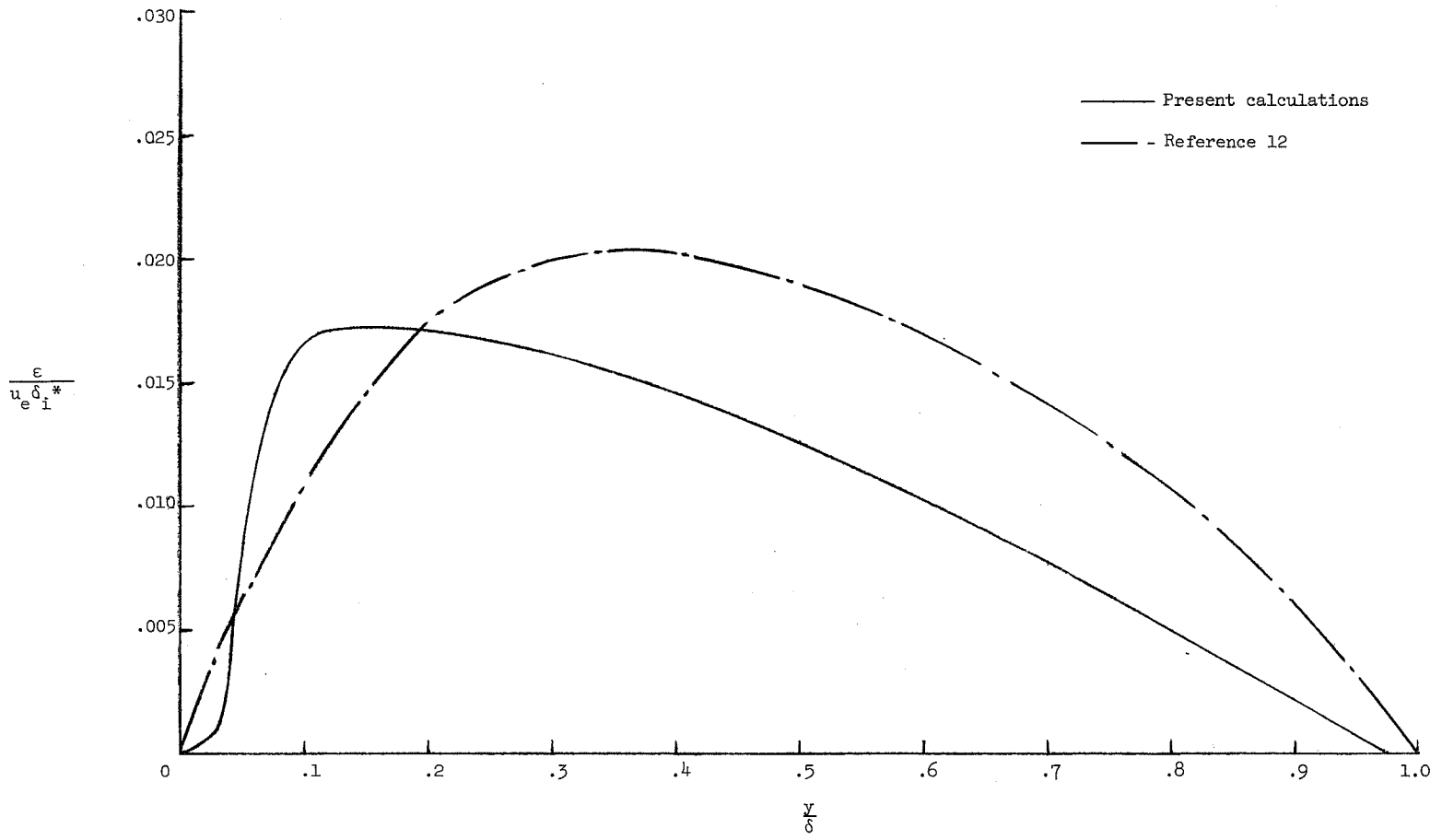

(b) Eddy-viscosity distribution.

Figure 9.- Continued.

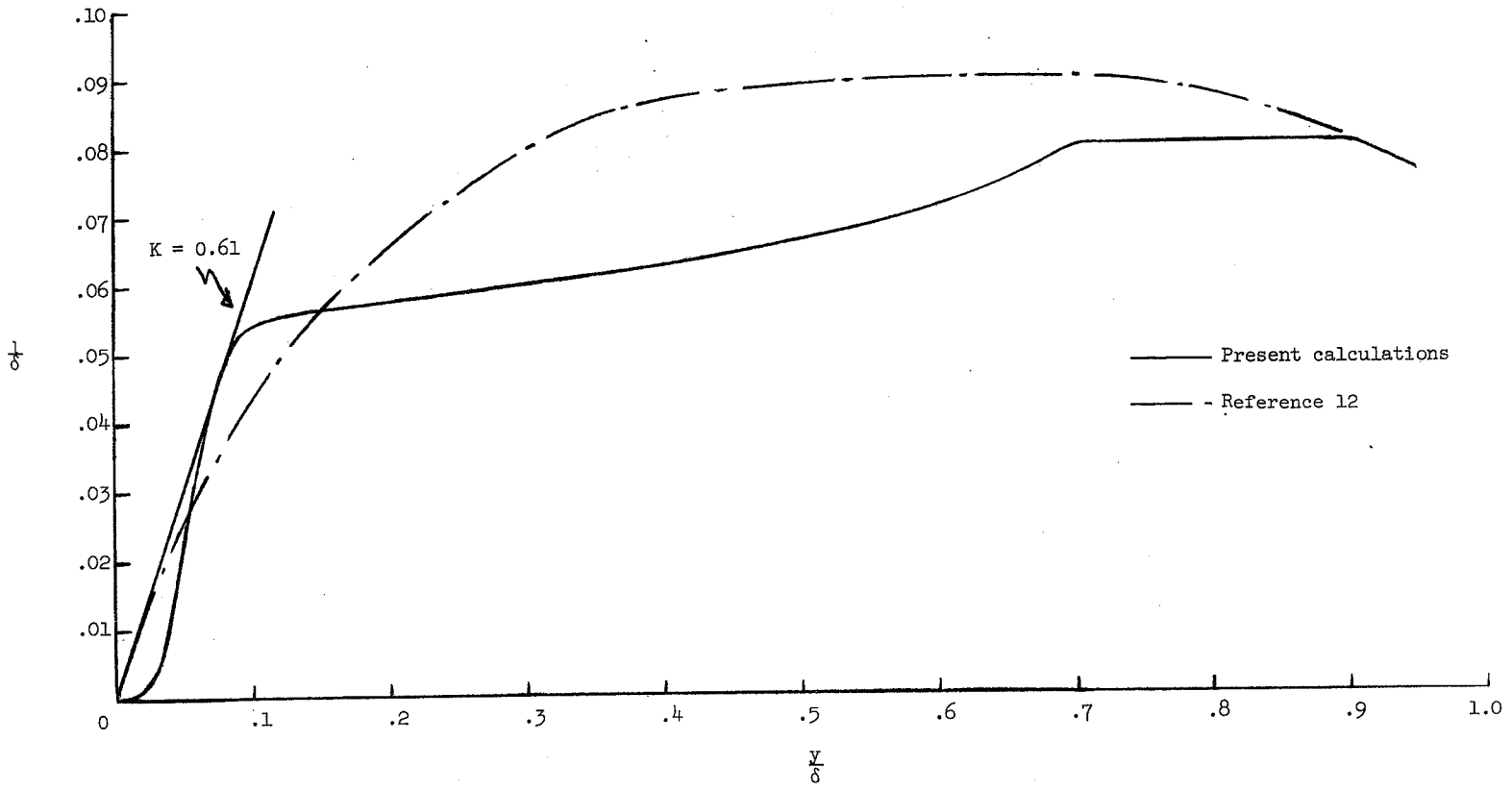

(c) Mixing-length distribution.

Figure 9.- Concluded.

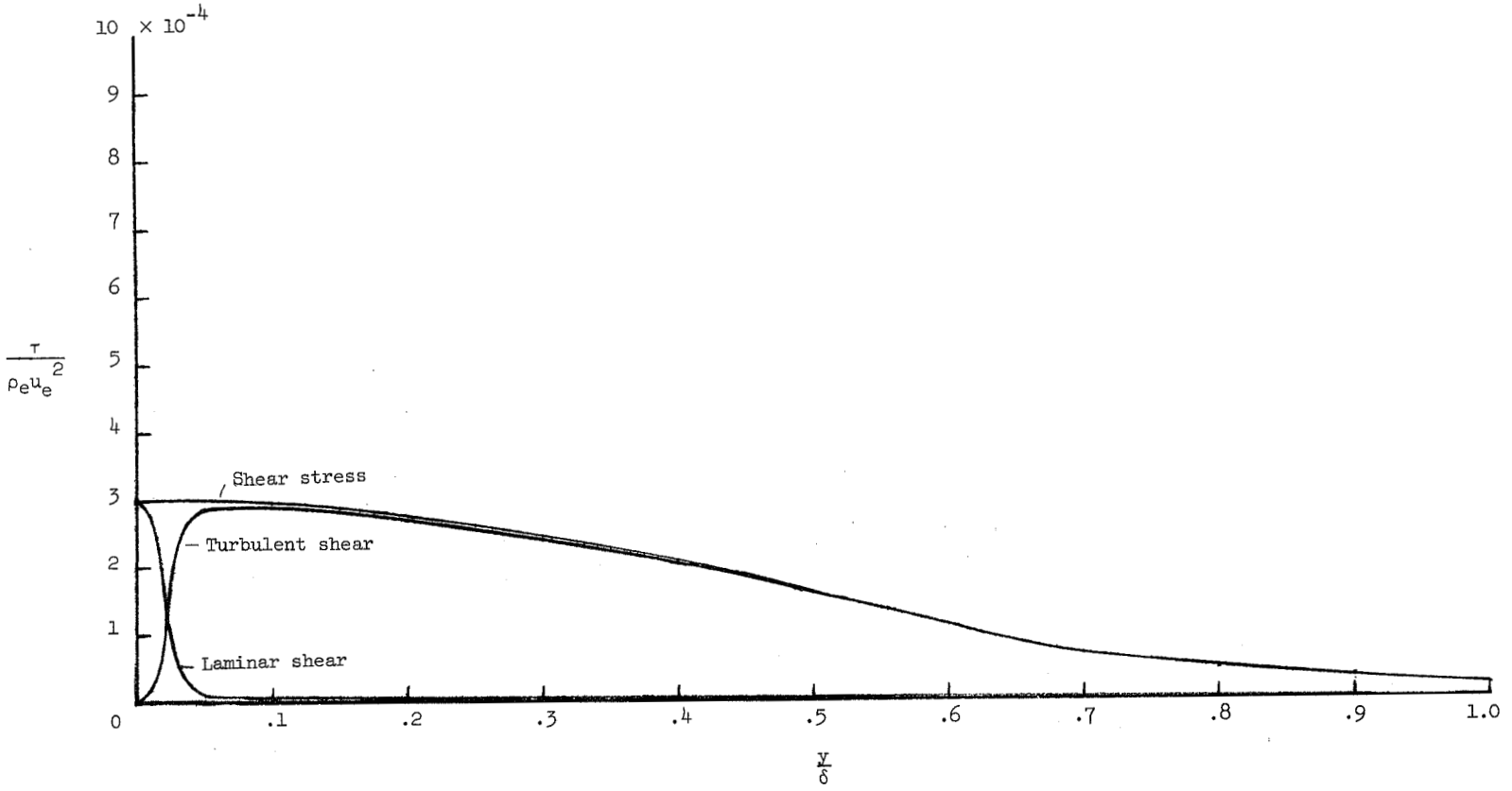

(a) Shear-stress distribution.

Figure 10.- Shear-stress, eddy-viscosity, and mixing-length distributions for a boundary layer on a hollow cylinder at $M_e = 5.98$. Profile data from reference 35; $R_\theta = 1.28 \times 10^4$.

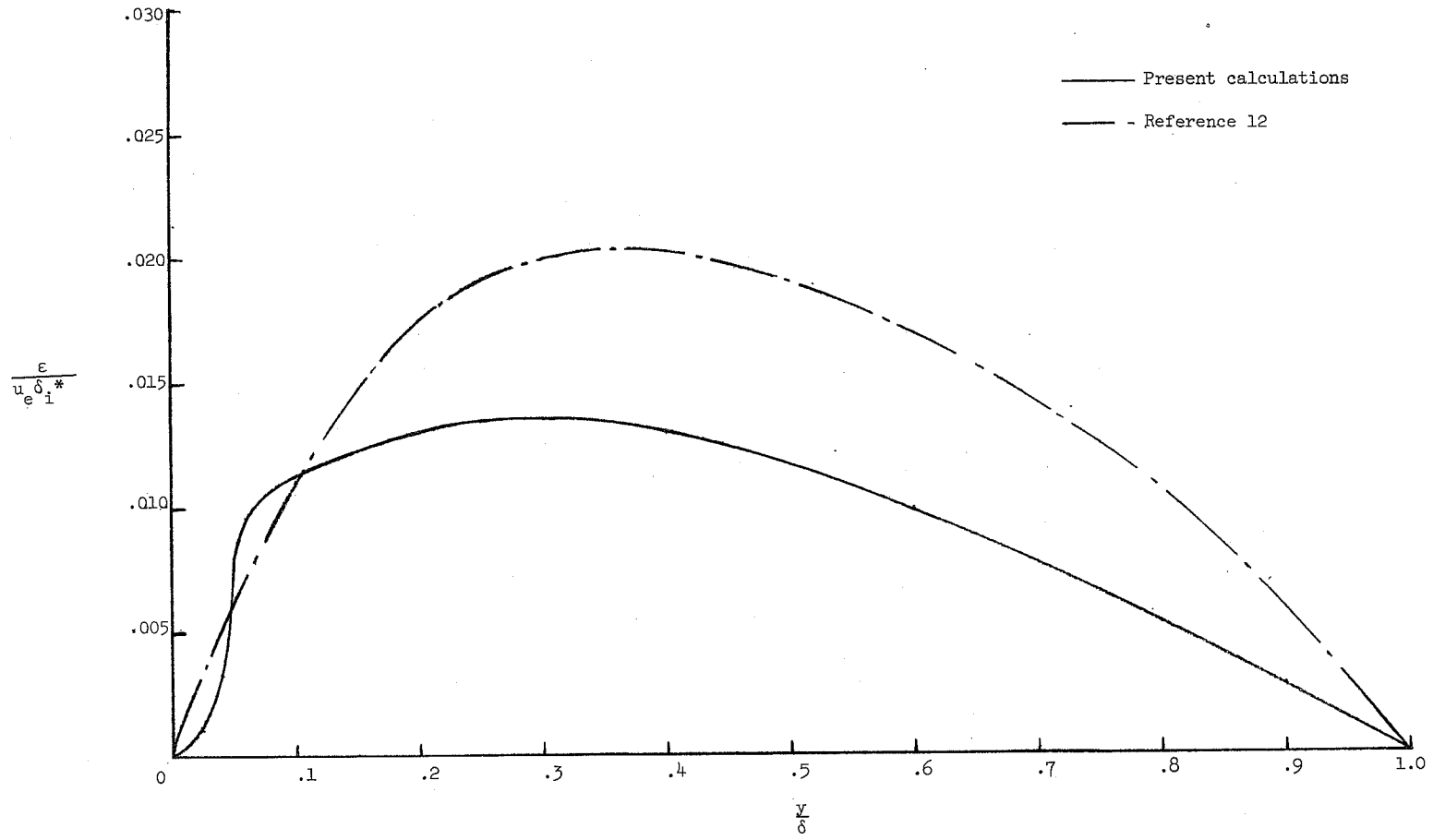

(b) Eddy-viscosity distribution.

Figure 10.- Continued.

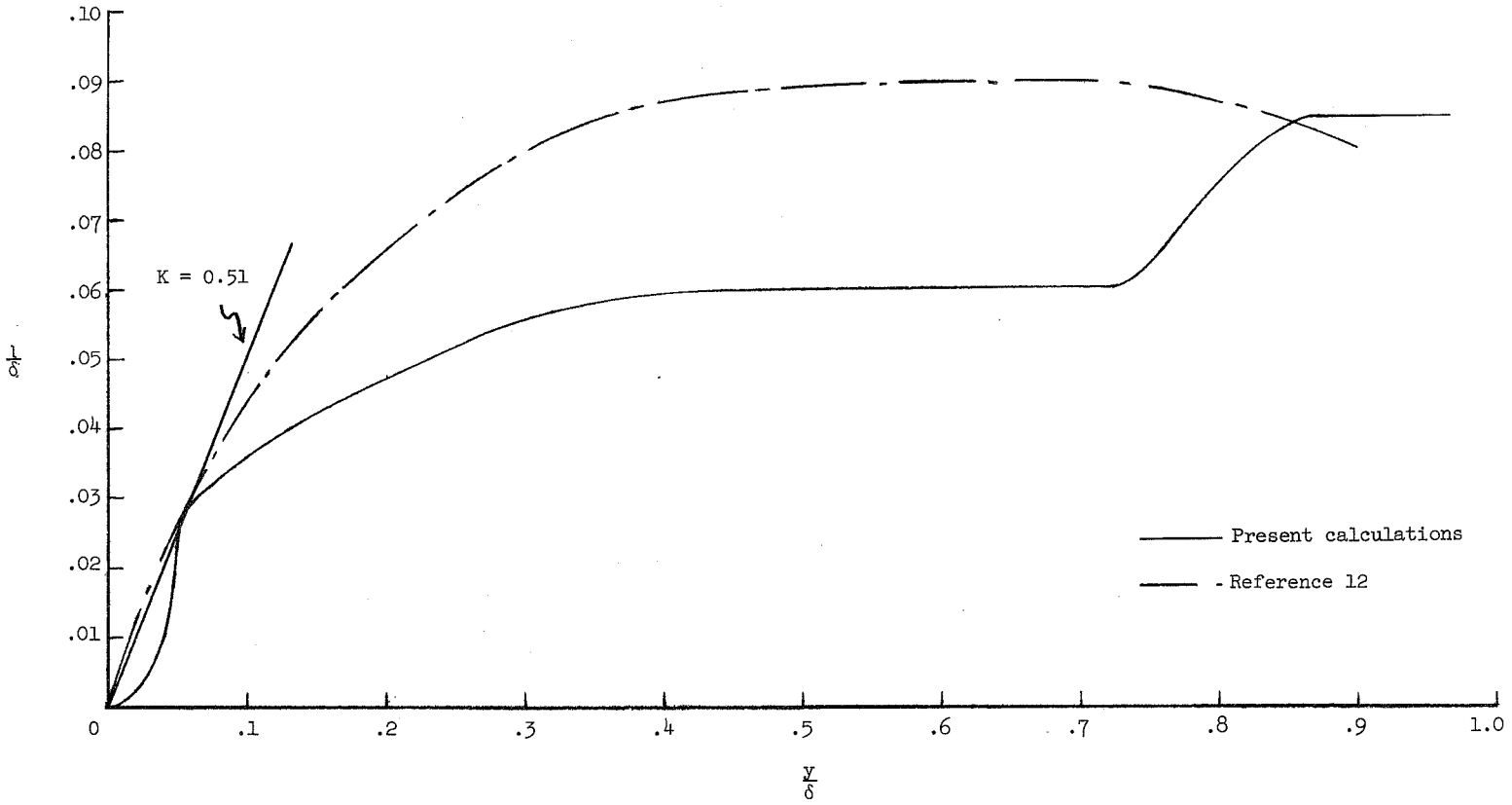

(c) Mixing-length distribution.

Figure 10.- Concluded.

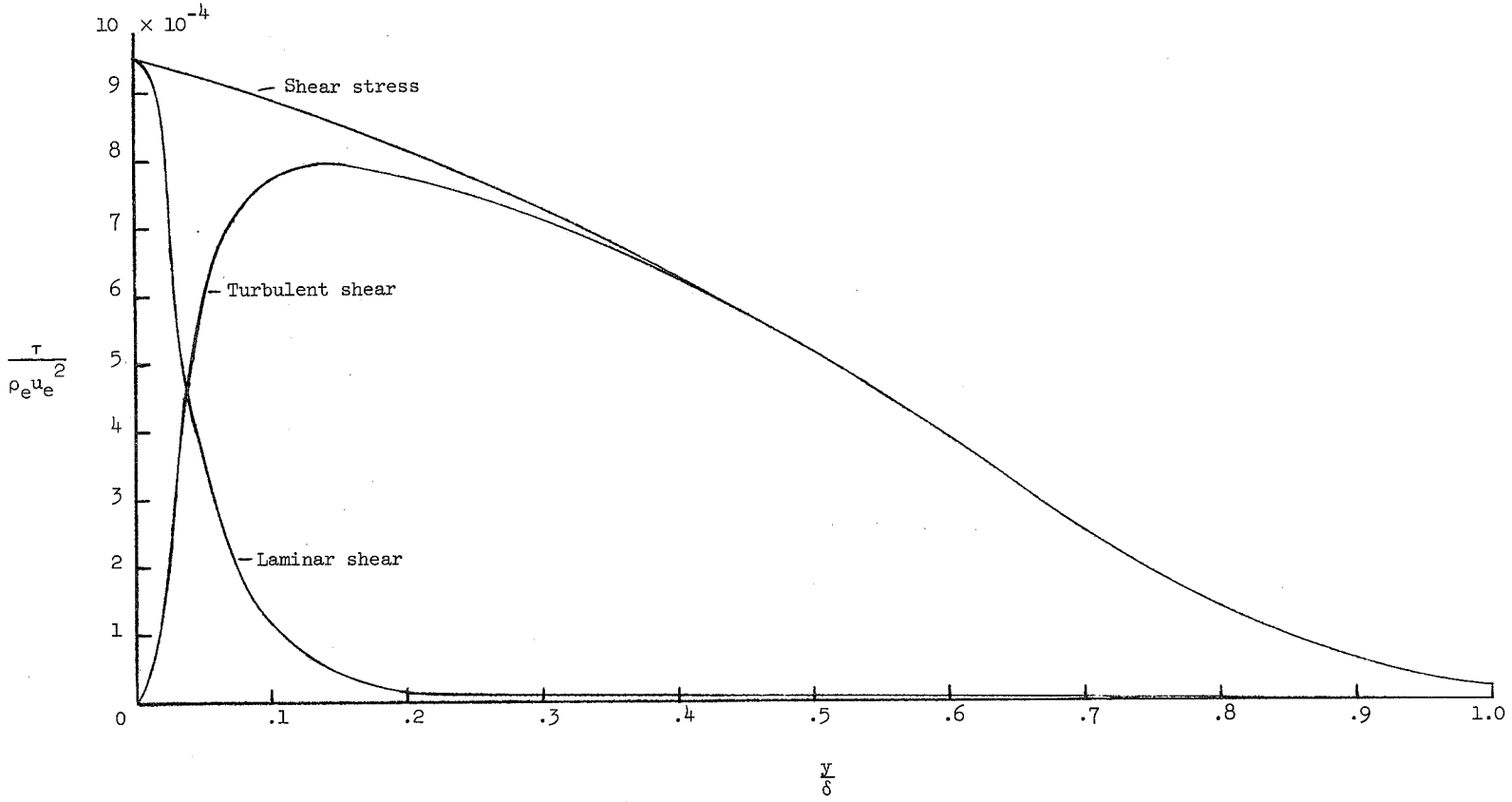

(a) Shear-stress distribution.

Figure 11.- Shear-stress, eddy-viscosity, and mixing-length distributions for a flat-plate boundary layer at $M_e = 6.5$. Profile data from reference 36; $R_\theta = 2.53 \times 10^3$.

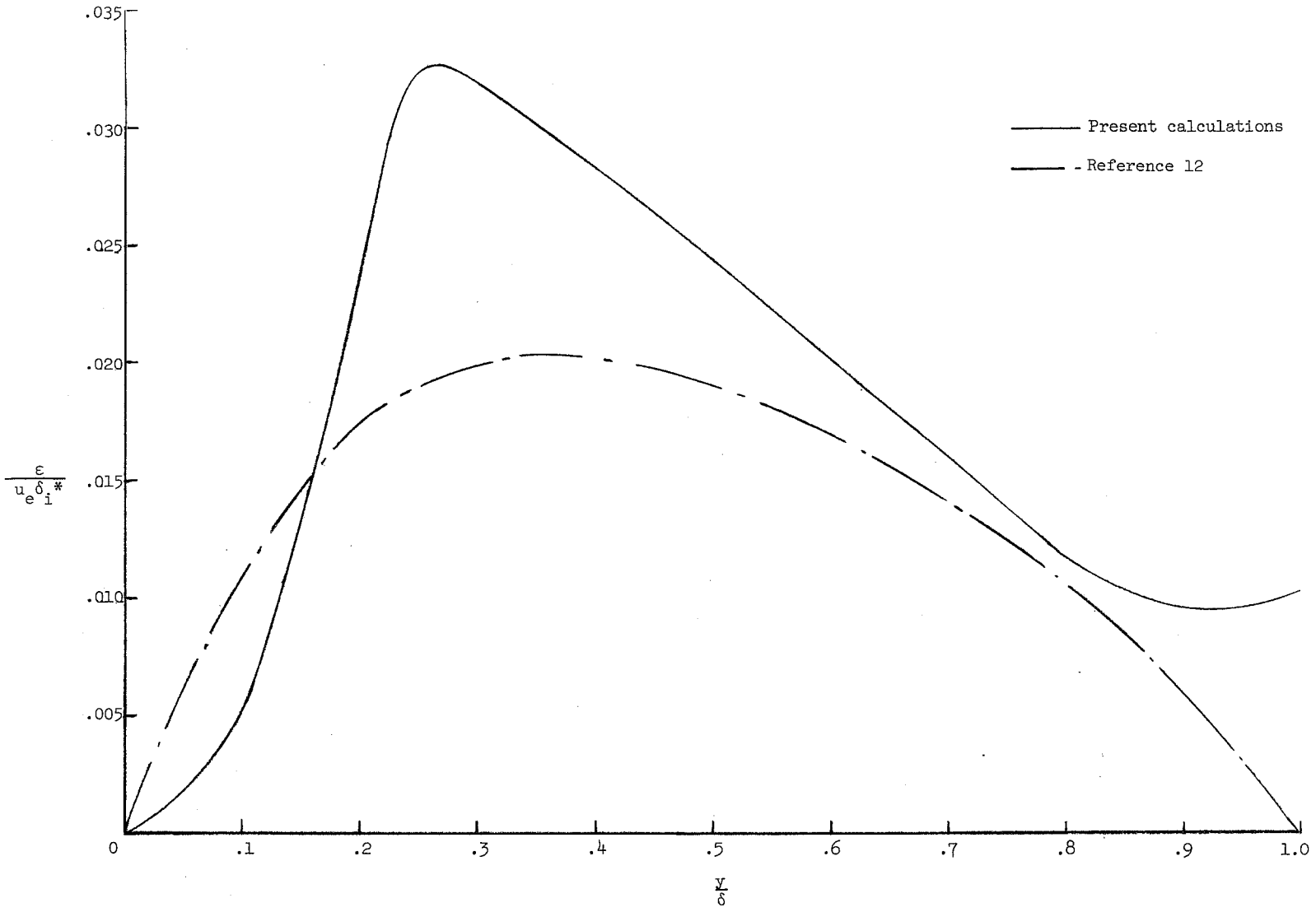

(b) Eddy-viscosity distribution.

Figure 11.- Continued.

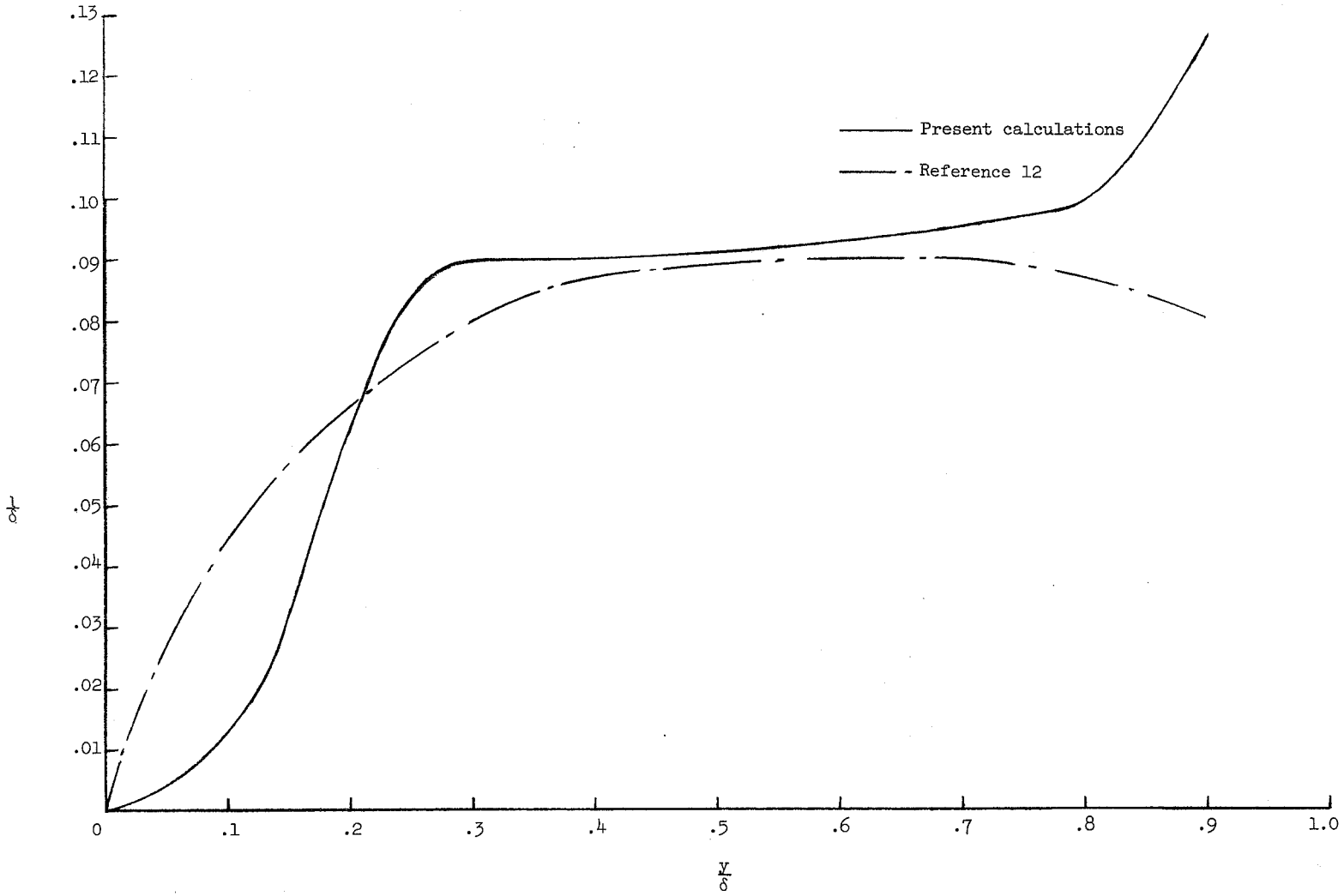

(c) Mixing-length distribution.

Figure 11.- Concluded.

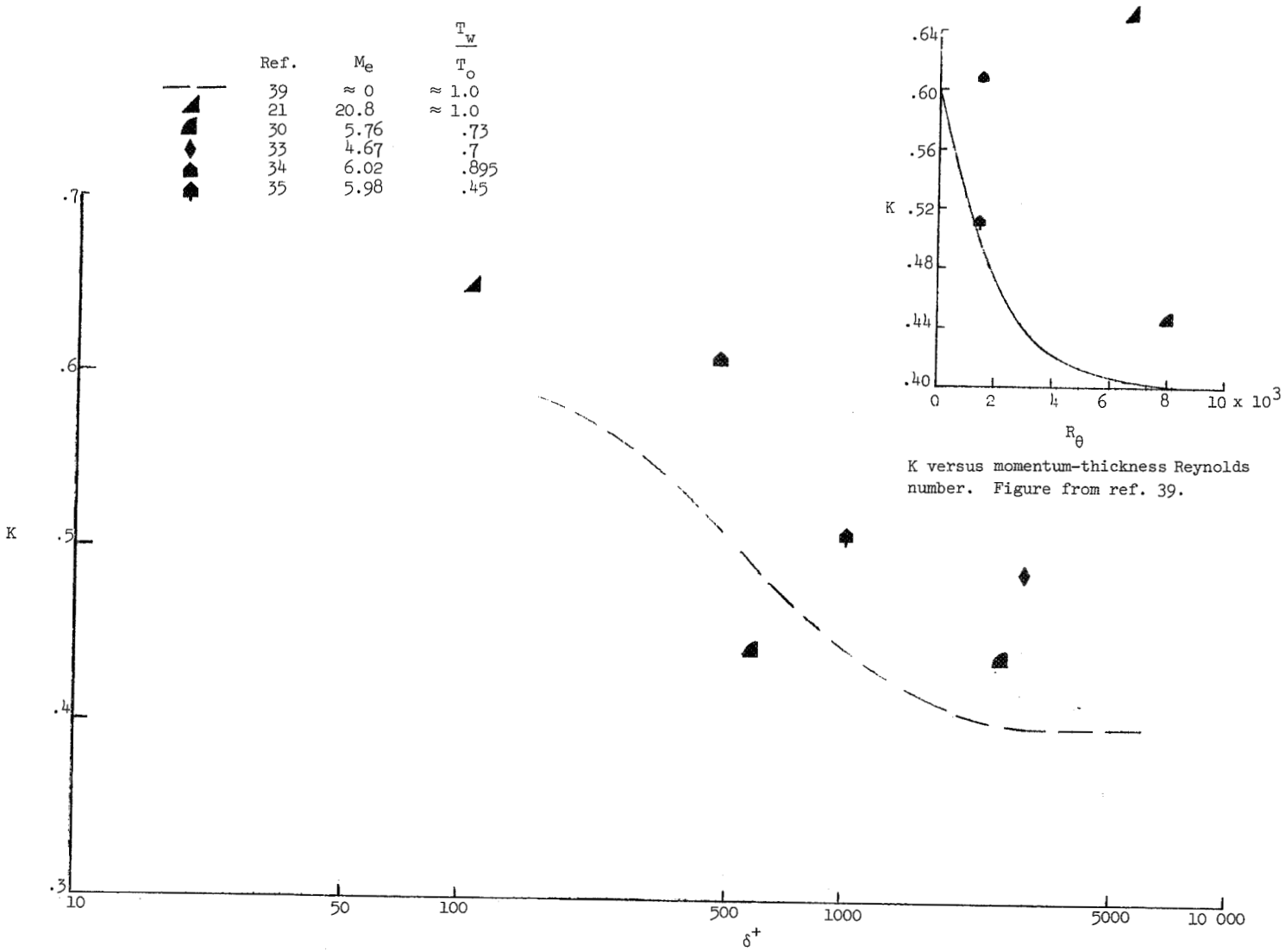

K versus momentum-thickness Reynolds number. Figure from ref. 39.

(a) Mixing-length Prandtl wall slope.

Figure 12.- Correlation of results from present turbulence model with low-speed data on a δ^+ basis.

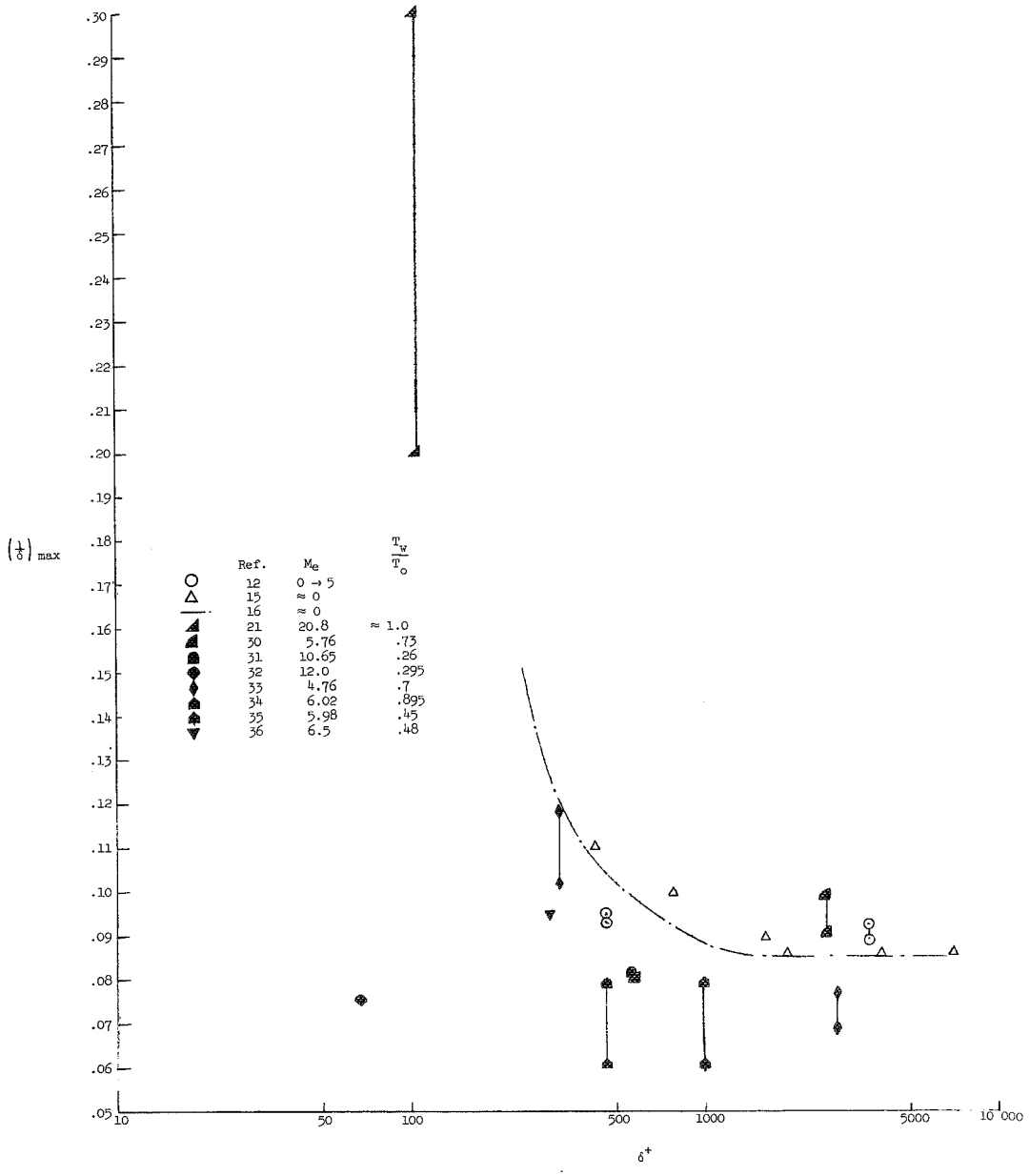

(b) Mixing length in outer region.

Figure 12.- Continued.

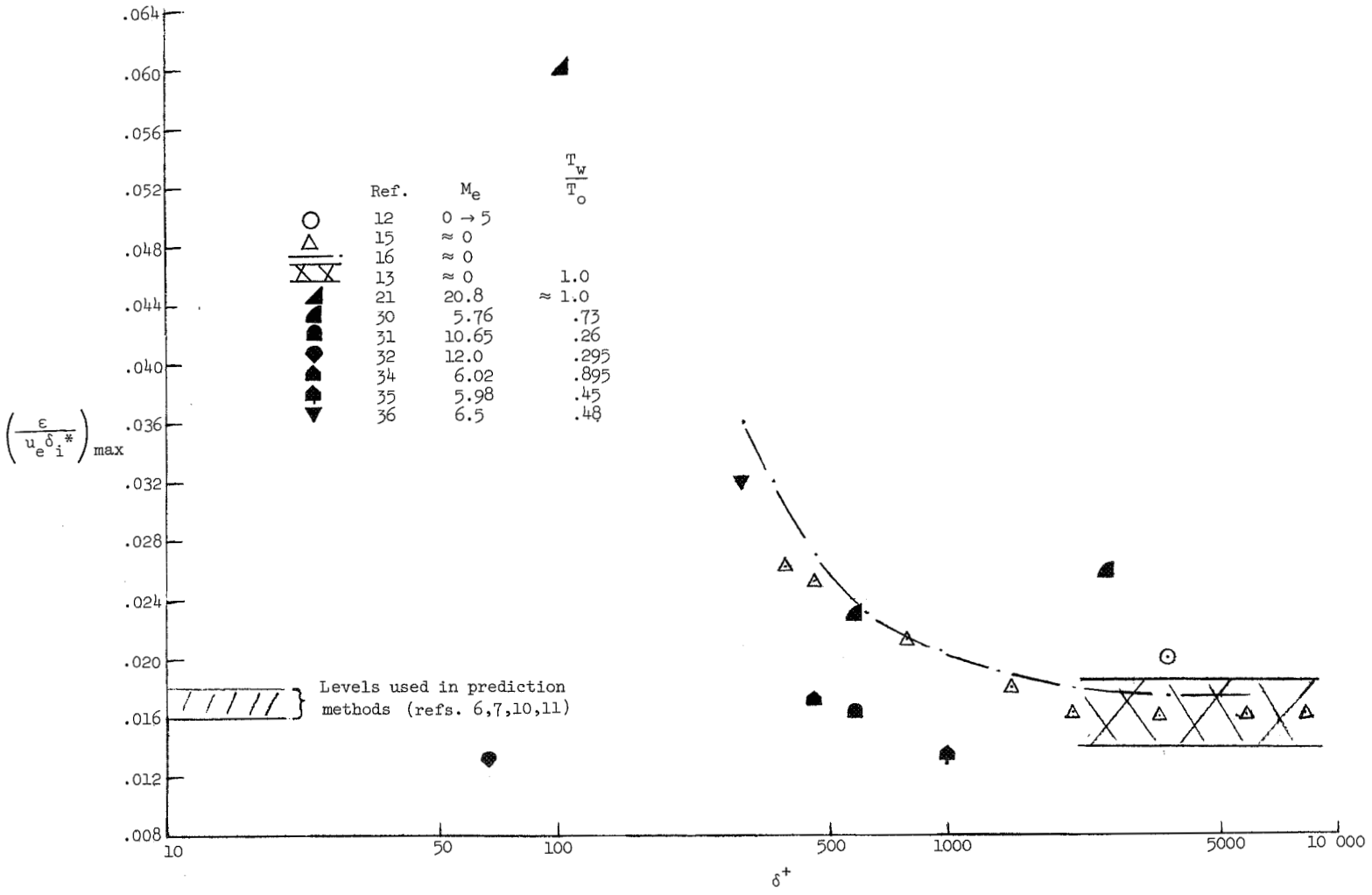

(c) Maximum eddy viscosity.

Figure 12.- Concluded.

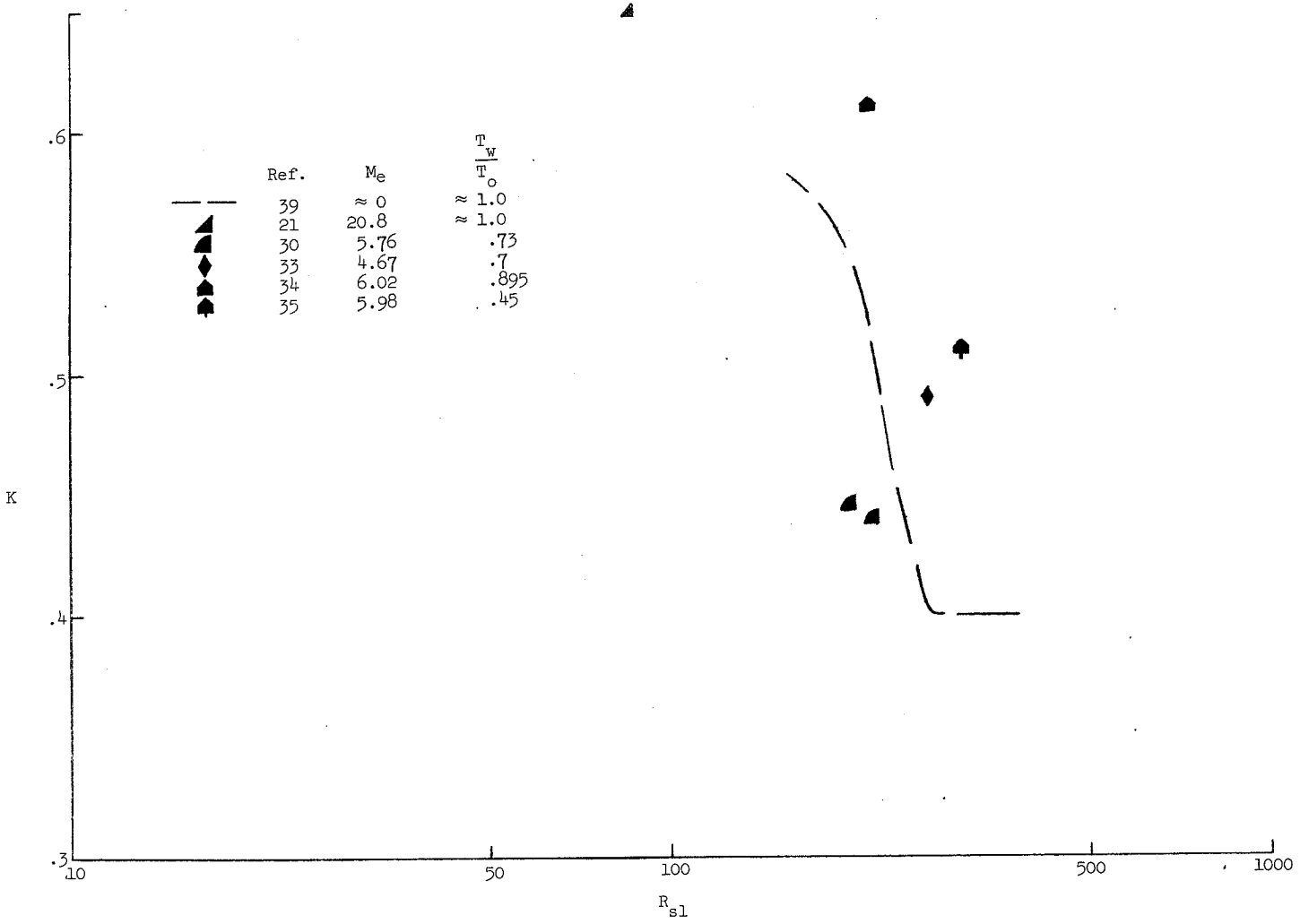

(a) Mixing-length Prandtl wall slope.

Figure 13.- Correlation of results from present turbulence model with low-speed data on an R_{sl} basis.

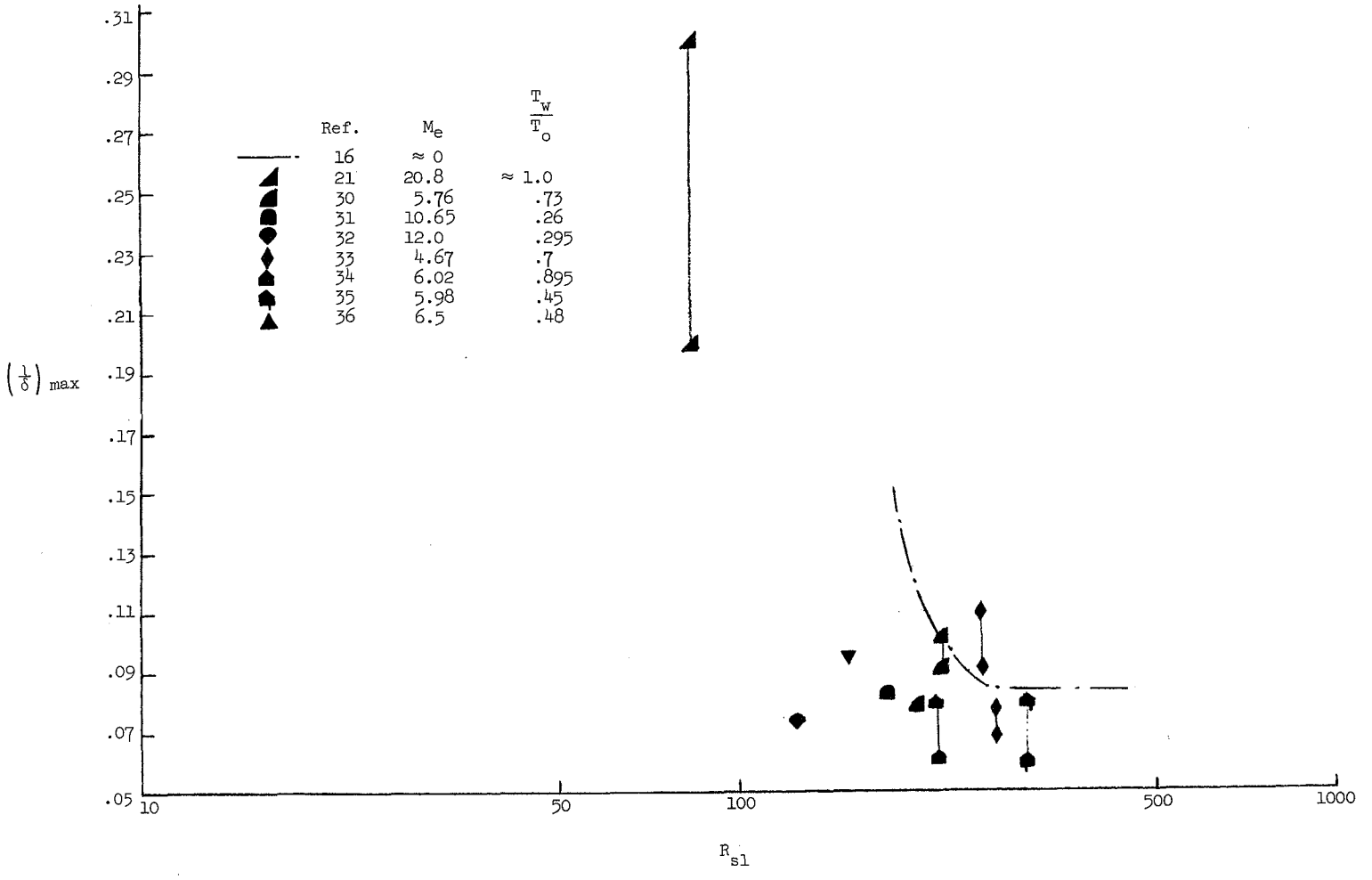

(b) Mixing length in outer region.

Figure 13.- Continued.

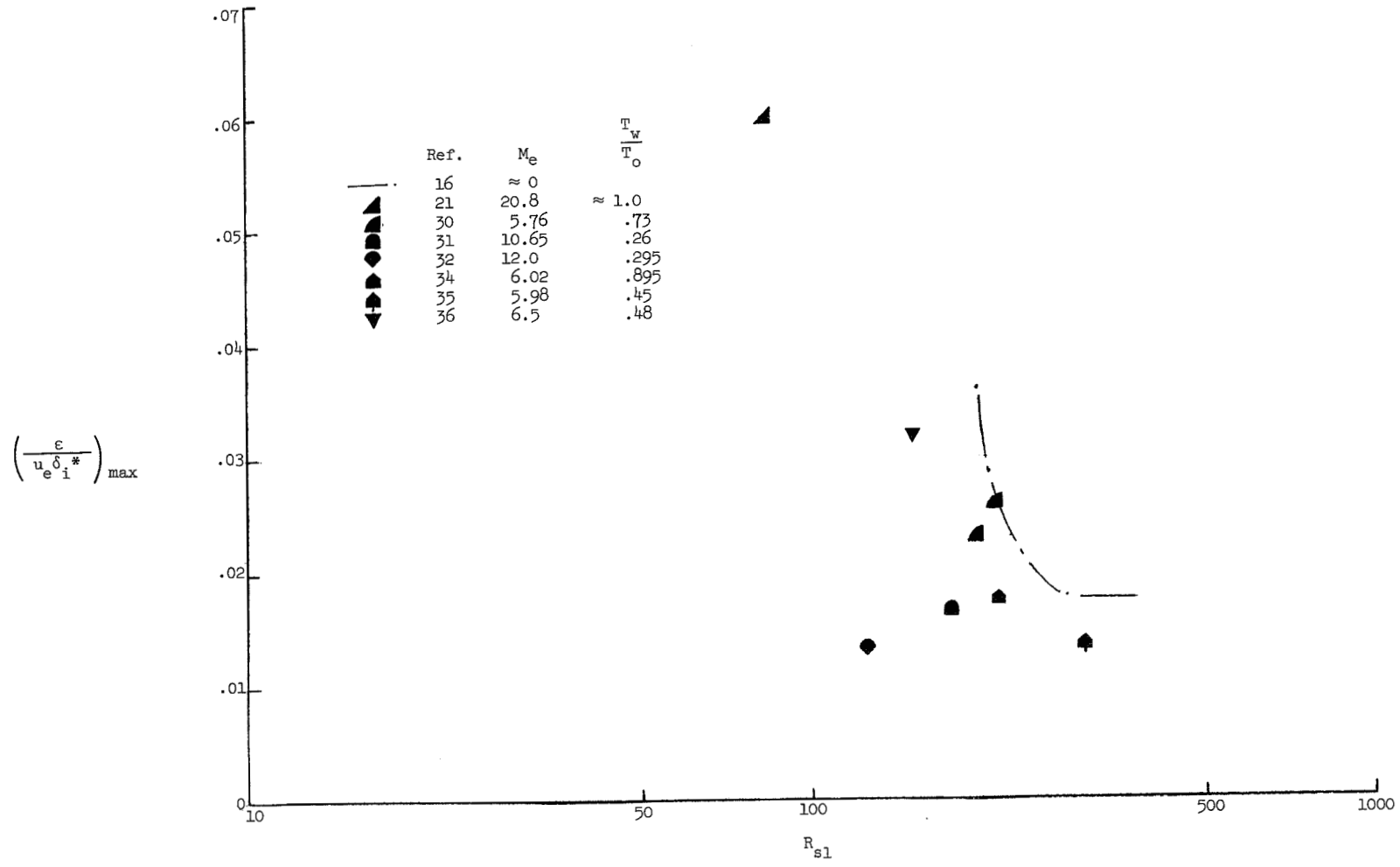

(c) Maximum eddy viscosity.

Figure 13.- Concluded.

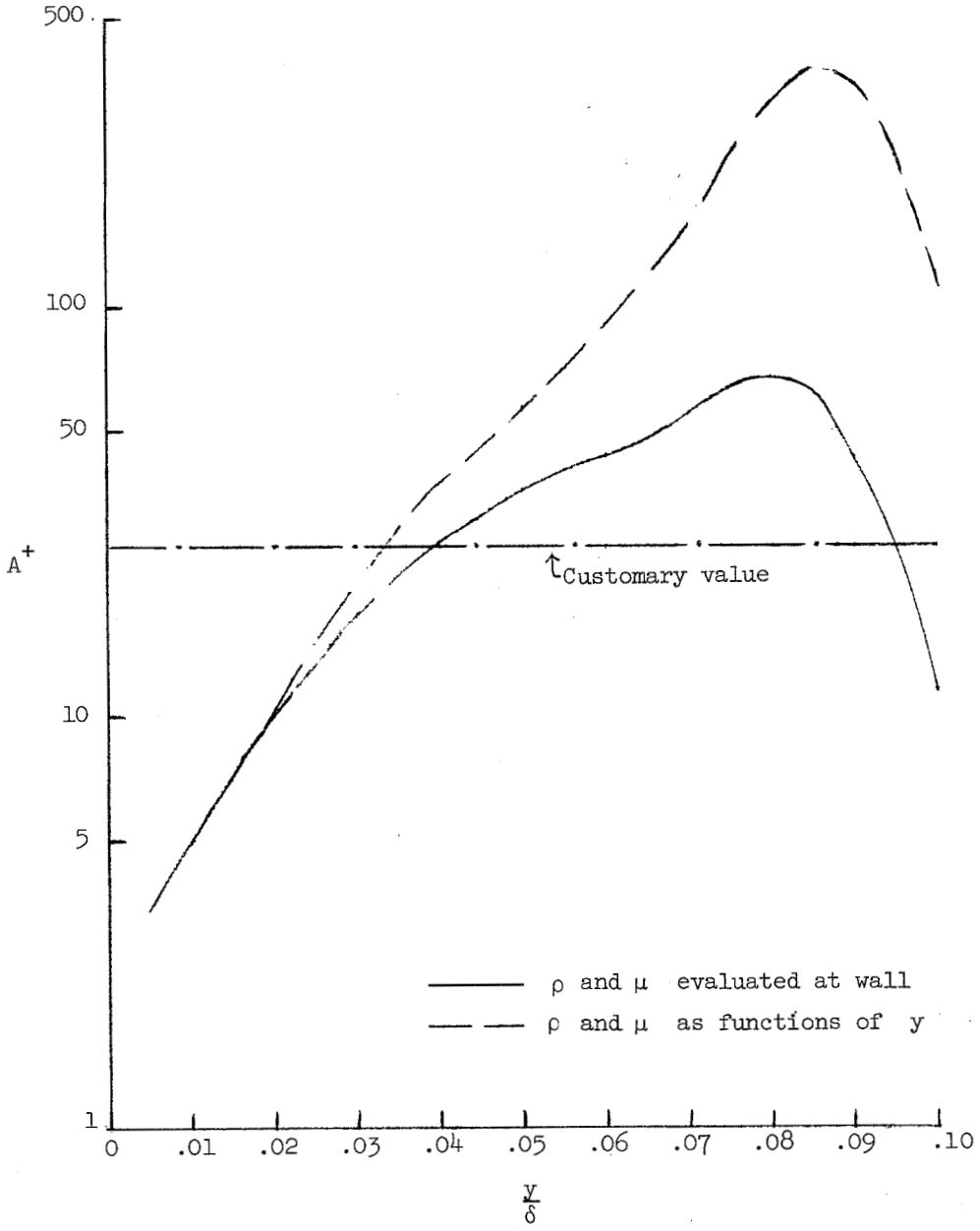

(a) $M_e = 20.8$; $\frac{T_w}{T_o} = 1.0$.

Figure 14.- Variation of damping constant with y/δ.

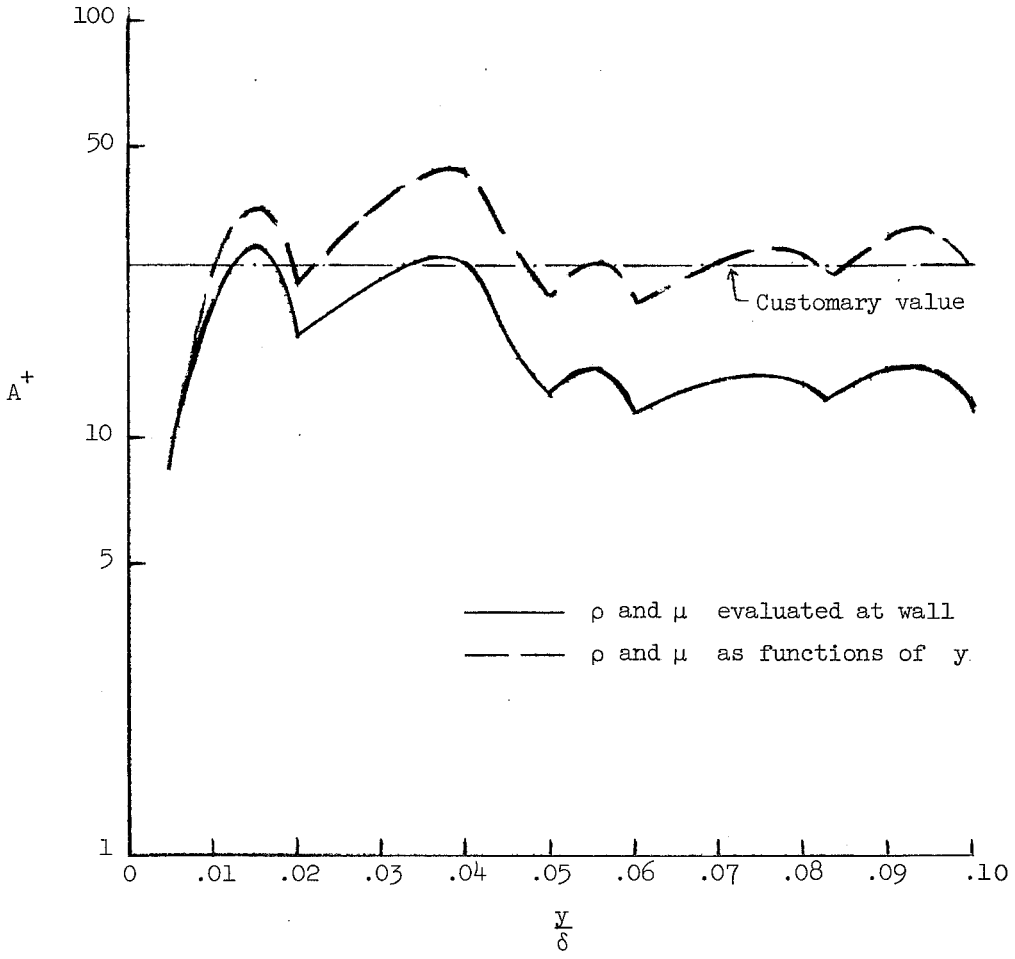

(b) $M_e = 5.76$; $\frac{T_w}{T_o} = 0.73$.

Figure 14.- Continued.

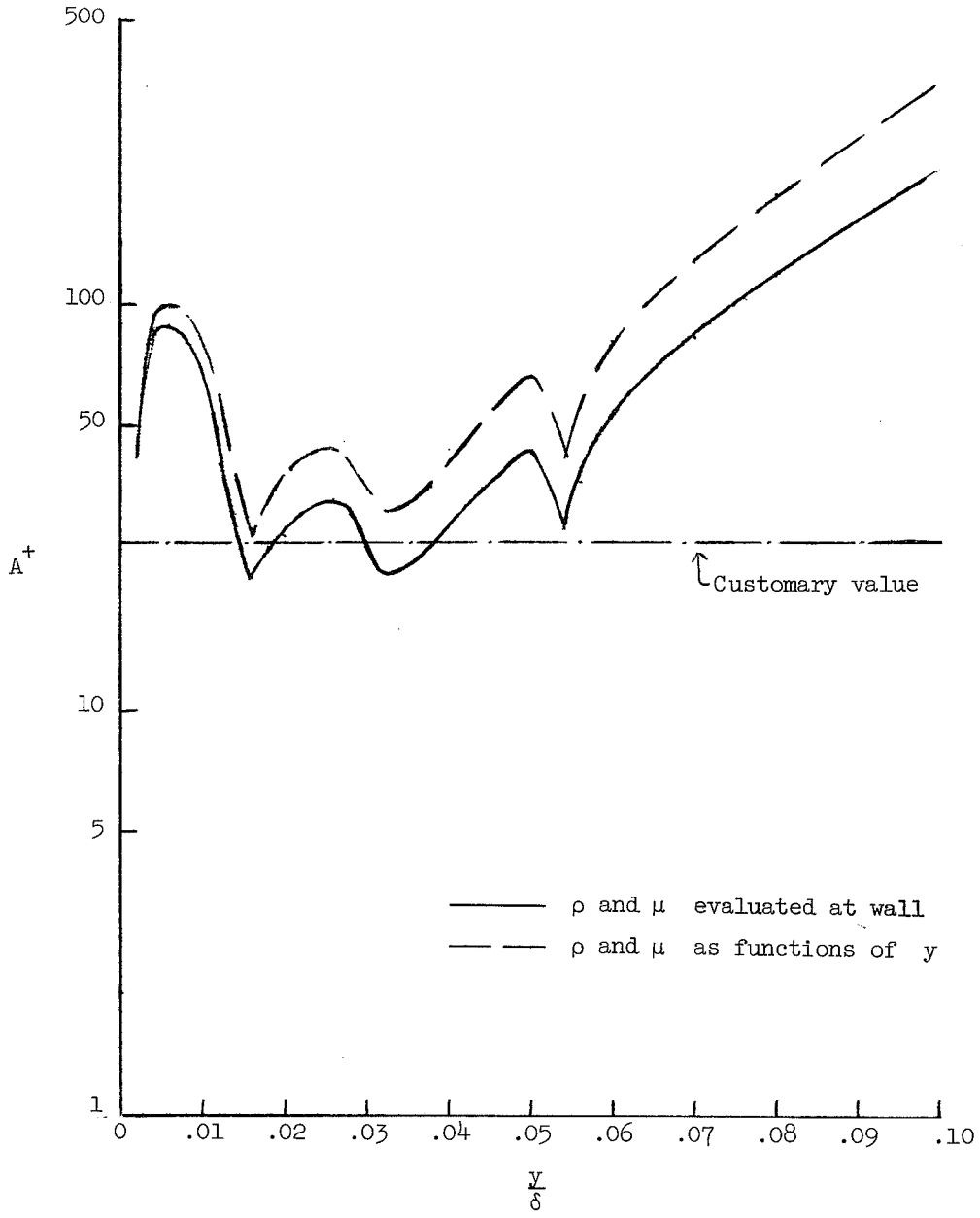

(c) $M_e = 4.67$; $\frac{T_w}{T_o} = 0.7$.

Figure 14.- Continued.

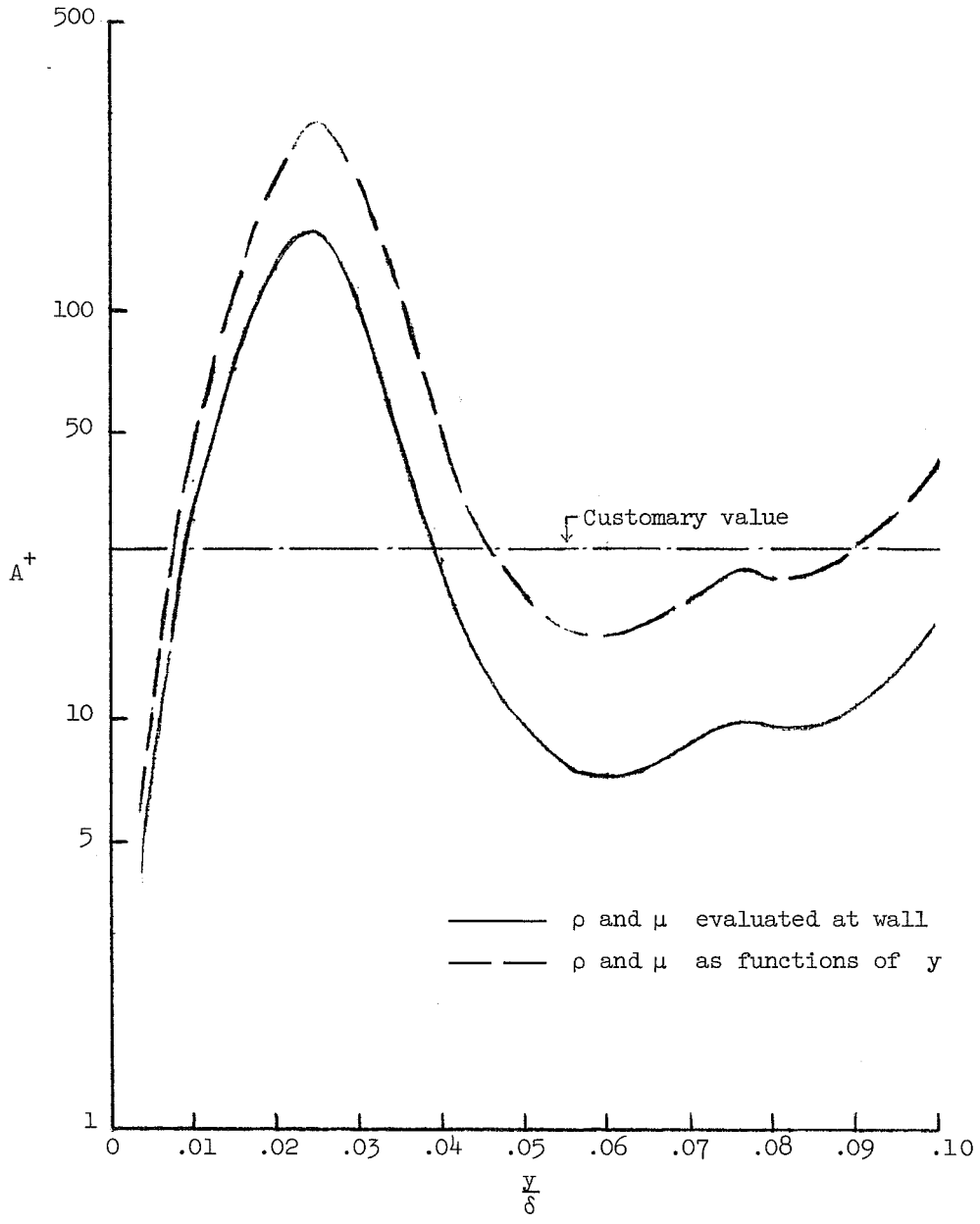

(d) $M_e = 6.02$; $\frac{T_w}{T_o} = 0.895$.

Figure 14.- Continued.

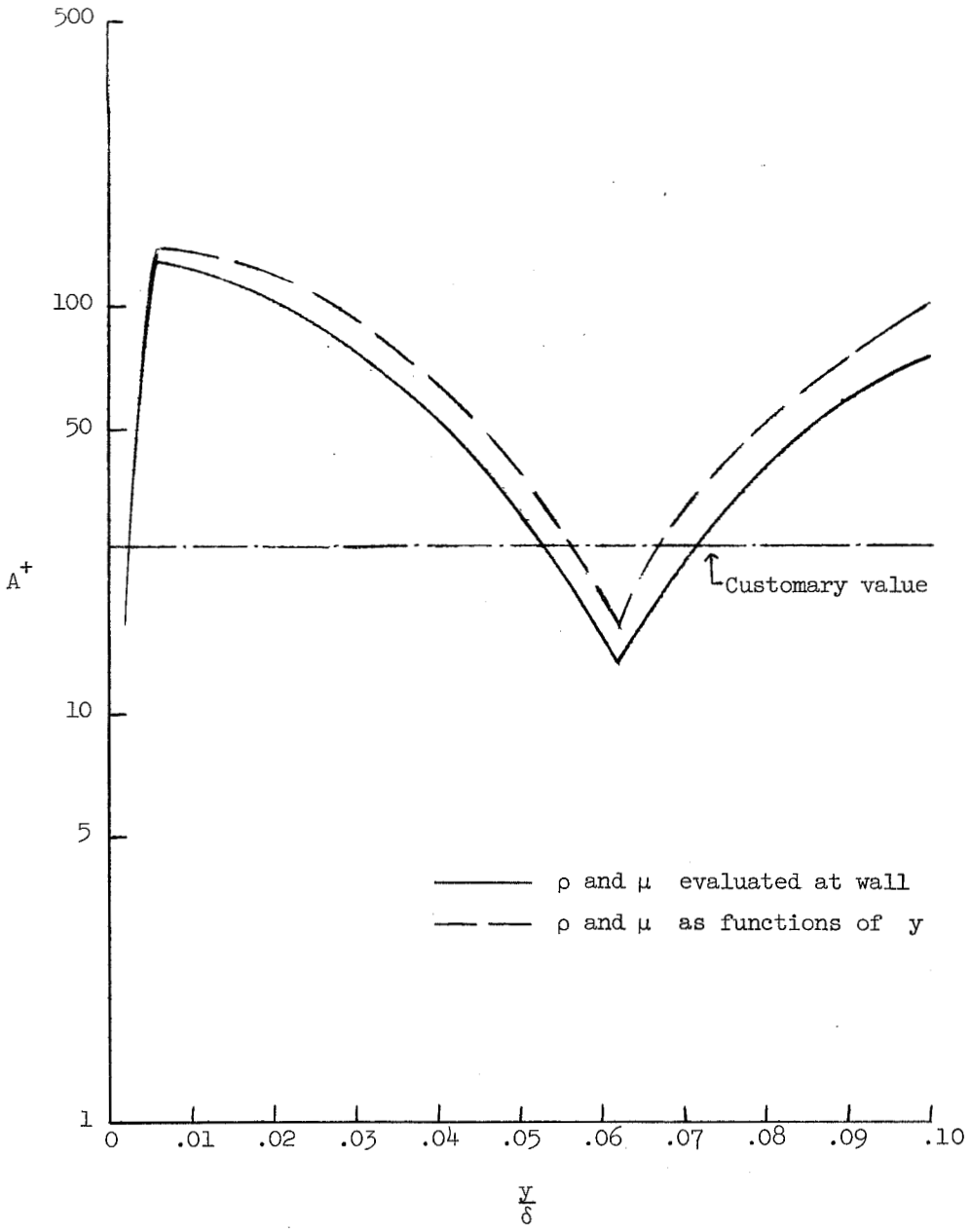

(e) $M_e = 5.98$; $\frac{T_w}{T_o} = 0.45$.

Figure 14.- Concluded.

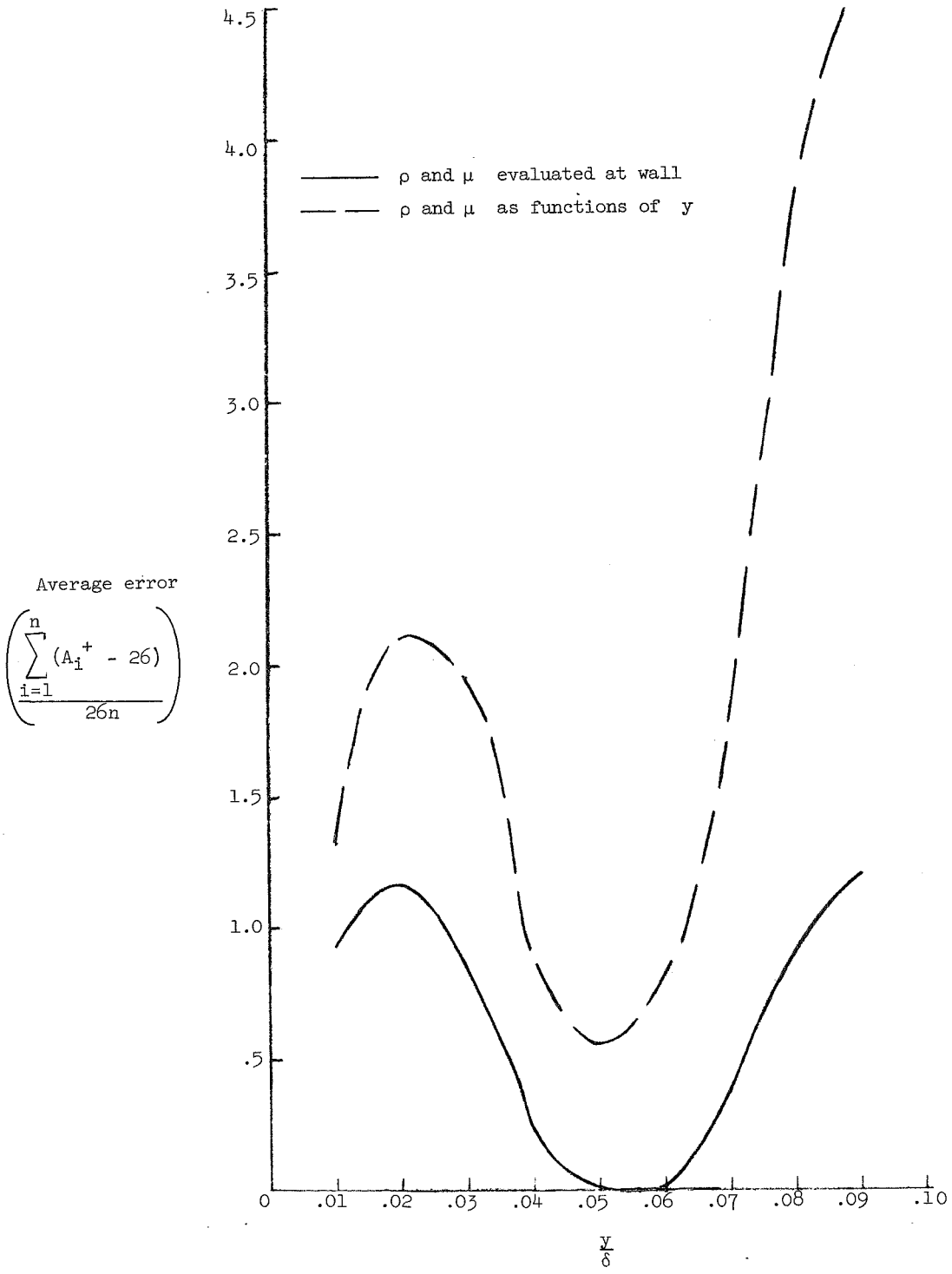

(a) Average error.

Figure 15.- Error between the computed values of A^+ shown in figure 14 and the customary value of 26.

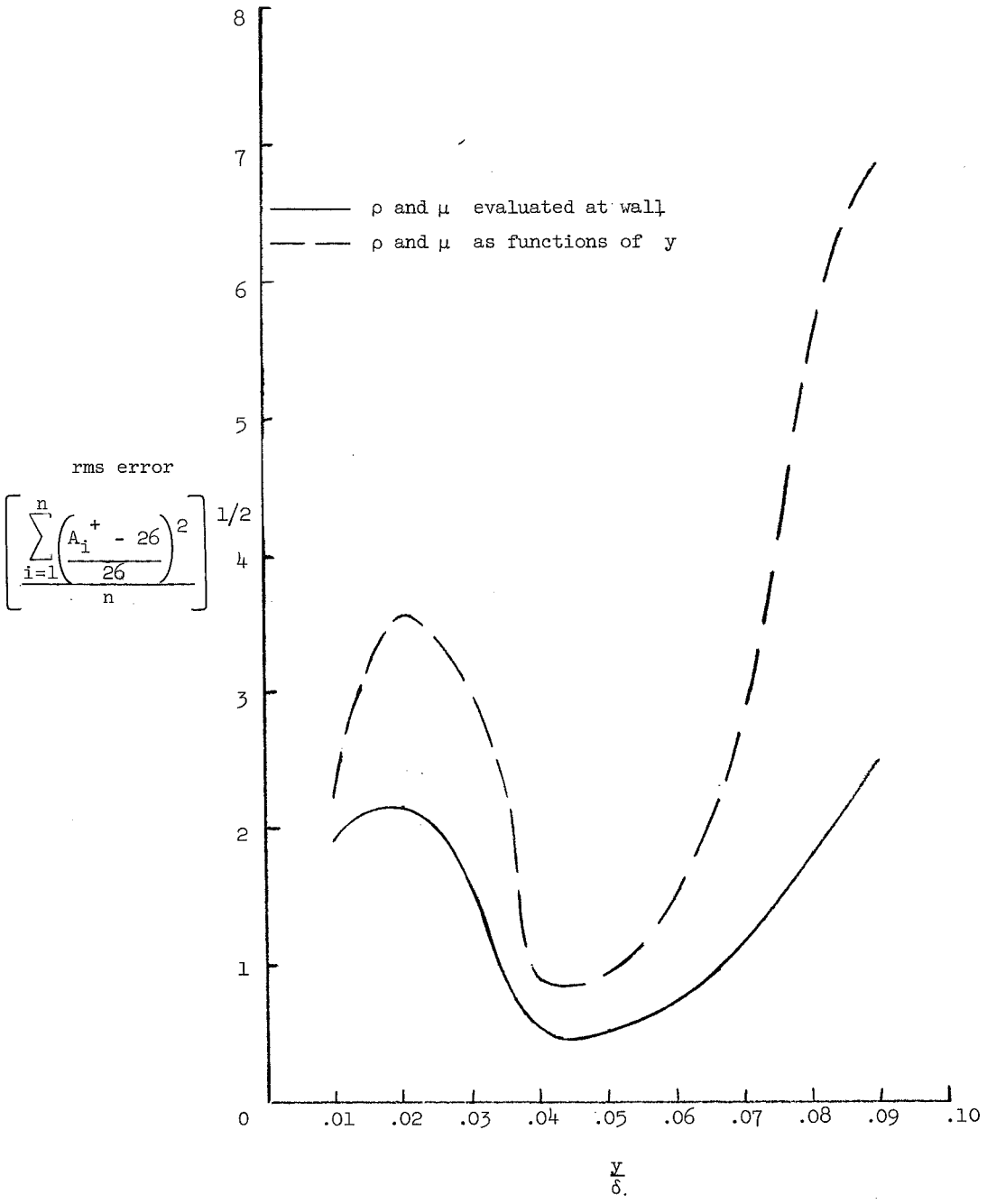

(b) Root-mean-square error.

Figure 15.- Concluded.

NASA-Langley, 1971 — 12 L-7731

NATIONAL AERONAUTICS AND SPACE ADMINISTRATION
WASHINGTON, D. C. 20546

OFFICIAL BUSINESS
PENALTY FOR PRIVATE USE $300

FIRST CLASS MAIL

POSTAGE AND FEES PAID
NATIONAL AERONAUTICS AND
SPACE ADMINISTRATION

POSTMASTER: If Undeliverable (Section 158 Postal Manual) Do Not Return

"The aeronautical and space activities of the United States shall be conducted so as to contribute . . . to the expansion of human knowledge of phenomena in the atmosphere and space. The Administration shall provide for the widest practicable and appropriate dissemination of information concerning its activities and the results thereof."

—NATIONAL AERONAUTICS AND SPACE ACT OF 1958

NASA SCIENTIFIC AND TECHNICAL PUBLICATIONS

TECHNICAL REPORTS: Scientific and technical information considered important, complete, and a lasting contribution to existing knowledge.

TECHNICAL NOTES: Information less broad in scope but nevertheless of importance as a contribution to existing knowledge.

TECHNICAL MEMORANDUMS: Information receiving limited distribution because of preliminary data, security classification, or other reasons.

CONTRACTOR REPORTS: Scientific and technical information generated under a NASA contract or grant and considered an important contribution to existing knowledge.

TECHNICAL TRANSLATIONS: Information published in a foreign language considered to merit NASA distribution in English.

SPECIAL PUBLICATIONS: Information derived from or of value to NASA activities. Publications include conference proceedings, monographs, data compilations, handbooks, sourcebooks, and special bibliographies.

TECHNOLOGY UTILIZATION PUBLICATIONS: Information on technology used by NASA that may be of particular interest in commercial and other non-aerospace applications. Publications include Tech Briefs, Technology Utilization Reports and Technology Surveys.

Details on the availability of these publications may be obtained from:

SCIENTIFIC AND TECHNICAL INFORMATION OFFICE

NATIONAL AERONAUTICS AND SPACE ADMINISTRATION

Washington, D.C. 20546